INFORMATION TO USERS

RICE UNIVERSITY

EXCIMER LASER INDUCED ELECTRICAL CONDUCTIVITY IN POLYIMIDE:
APPLICATIONS TO ENGINEERING, PHYSICS, AND APPLIED SCIENCE

by

ZANE ANDREW BALL

A THESIS SUBMITTED
IN PARTIAL FULFILLMENT OF THE
REQUIREMENTS FOR THE DEGREE
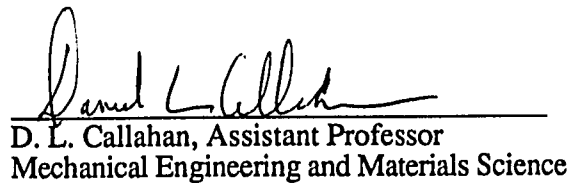
DOCTOR OF PHILOSOPHY

APPROVED, THESIS COMMITTEE:

R. Sauerbrey, Prof.Dr., Chairman
Institut für Optik und Quantenelektronik
Friedrich-Schiller Universität

W. L. Wilson, Jr., Professor
Electrical and Computer Engineering

J. F. Young, Professor
Electrical and Computer Engineering

D. L. Callahan, Assistant Professor
Mechanical Engineering and Materials Science

Houston, Texas

March, 1996

UMI Number: 9631099

UMI

300 North Zeeb Road
Ann Arbor, MI 48103

ABSTRACT

Excimer Laser Induced Electrical Conductivity in Polyimide: Applications to Engineering,

Physics and Applied Science

by

Zane Andrew Ball
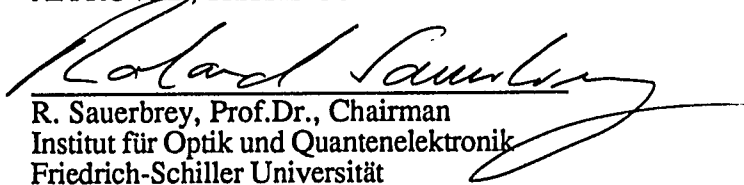
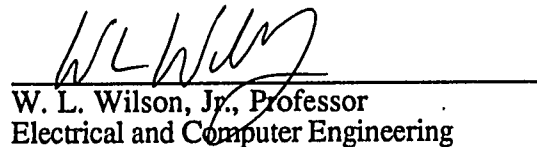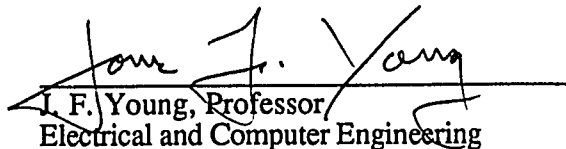Various aspects of the interaction of excimer laser pulses and polyimide were investigated, focusing on low fluences where laser induced electrical conductivity is observed.

Multiple shot excimer ablation of polyimide was investigated, and at fluences between 20 mJ/cm^2 and 260 mJ/cm^2, ablation would cease after a few hundred pulses. This cessation of ablation was found to be the result of a dramatic, fluence dependent increase in surface roughness accompanied by the formation of a conducting, carbonaceous layer on top the laser treated sample. The repetition rate of the laser could affect the electrical conductivity of the layer but had little effect on any other properties, implying that the electronic structure of laser induced conducting layer was highly temperature sensitive.

The optical properties of the laser irradiated surface were also studied with regard to a transient decrease in reflectivity that is observed during and in the first few tens of nanoseconds after irradiation. Pump probe experiments using electronically delayed probe pulses were performed and measurements of reflectivity, transmissivity and scattering were made under identical conditions. The results, a decrease in reflectivity and scattering with a

simultaneous increase in transmissivity, imply a transient refractive index phenomenon during the first 150 ns after excimer irradiation.

A nonlinear current-voltage relation was observed near the critical point of the laser induced metal-insulator transition. The crossover behavior from nonlinear to linear regimes was studied in detail and interpreted in terms of a percolation theory of binary conductor-insulator mixtures. The nonlinearity and the crossover can, for the first time, be described simultaneously in terms of a new theory of space charge limited currents on percolation clusters.

Acknowledgements

My stay in Jena was aided by many but none more than Thomas Feurer, my good friend, collaborator, and roommate. Wolfgang Ziegler showed me enormous kindness and was of crucial help in this research The importance of "Doppelkopf" and my fellow players Klaus Ettrich and Karsten Michelmann to my stay could hardly be overestimated. I am indebted to the many colleagues and friends I met at IOQ including Helmut Schillinger, Roland Häßner, Falk Ronnenberger, Diego Zimare, Cornelius Wülker and Rita Fernsler. Fr. Koss and Fr. Raschelbach were the warriors who conquered German bureaucracy in my behalf for which I am very grateful.

In Houston, many colleagues such as Jan Fure, Harvey Phillips, Paul LeBlanc,Wade Eckhoff, Konstantin Petrov, Angela Wei, Mary Jane Patterson, Vicki Schutter, and Bruce Brinson helped make the last four years enjoyable and interesting. Nora Quiocho helped make the rather complex business of a multinational Ph.D. easy. I also would like to thank my parents for their continued support, the entire Yates family (particularly Chuck who felt slighted by the acknowledgements in the last thesis I wrote), Elva Escochea (who also felt slighted last time), and Rustin Buck.

Finally, I would like to acknowledge the financial support of the National Science Foundation which made such an interesting graduate education possible.

Table of Contents

List of Figures

List of Tables

CHAPTER ONE

GENERAL INTRODUCTION

Since the early 1980's the ability of excimer lasers to precisely manipulate the
surface morphology of various organic materials has been known. The interaction of the
high energy nanosecond pulses of ordinary excimer lasers with highly absorbing materials
such as polyimide results in clean etching with little or no thermal damage or melting and to
spatial resolution limited only by the short uv wavelength of the laser. The exact
mechanisms necessary to explain this interaction have been the subject of research and
controversy for more than ten years while applications in medicine and the microelectronics
industry have grown.

The study of excimer laser ablation in recent years has led to more sophisticated
techniques than simple etching where the surface of the material is modified to produce a
desired property. Laser annealing is a good example where applications from planarization

of metalization layers in semiconductor manufacturing (Wolf, 1990)to crystalization of amorphous silicon thin films or even the production of photoluminescent porous silicon have been developed. Laser processing of materials is attractive for a variety of reasons such as the ability to provide local high temperatures without substracting significantly from a process thermal budget, 100% noncontact processing, and laser processing is also generally more environmentally sound than wet chemical or plasma based technologies. As ultraviolet lasers interact directly with electronic states, they can produce photochemical reactions by direct bondbreaking or promote reactions with an ambient atmosphere in addition to thermal effects.

The interaction of excimer lasers with polymers has received the most attention as 0.25 μm lithography makes use of 248 nm excimer laser steppers. The stringent requirements of deep UV lithography on polymers which serve as resists for 248 nm and also shorter wavelengths have served as a driving force for the study of excimer laser-polymer interactions. Though likely not a candidate as a photolithography system, the use of excimer laser ablation of polyimide has already been implemented in semiconductor manufacturing lines for the production of vias in advanced packaging structures.

One interesting feature of the excimer laser interaction with polyimide is the formation of a layer of carbon organized into small clusters on the sample surface. If the density of these carbon clusters exceeds a critical value then electrical conduction is observed (Schumann, 1990). This effect, first observed in 1990, is the primary subject of this thesis. The importance of this effect is twofold. First it constitutes a new type of metal-insulator transition which, as previous research has shown (Ball, 1994), is well described by percolation theory. As the number of truly percolative systems is quite small, an additional system to experimentally study the unique properties of this kind of disordered matter is naturally of great interest. This system, in addition to allowing comparison with the results of other systems, provides for a much more detailed and accurate study of the

predictions of the percolation theory than previous experiments. The second motivation for this study is the potential for technological application. As polyimide is a popular insulating material in advanced electronic packaging (e.g. multi-chip modules) and a major candidate for interlayer dielectrics in on-chip metallizations, the ability to make conducting patterns to high spatial resolution in polyimide is of clear interest.

The aim of this thesis is to report the results of a detailed experimental program that has concentrated on three areas: i) understanding of the microscopic physical processes involved in conductivity modification ii) understanding of macroscopic properties controlled by the system geometry near the critical point, i.e., properties related to percolation theory , and iii) investigation of possible industrial applications. This work combines two rather disparate fields, percolation theory and laser-materials interactions. A considerable amount of pedagogical material is therefore presented for both subjects since few readers are likely to be familiar both fields.

In chapter two, a general introduction to the physics and principal experimental results of laser processing of materials is presented. Previous investigations into laser ablation of polymers and excimer laser induced conductivity modification are also discussed. These general results explain the physical mechanisms involved and are the result of the many characterization efforts that have been completed with regard to laser processed polyimide.

Chapter three extends the discussion of conductivity modification and ablation to new results dealing with multiple shot processing near the ablation threshold illustrating the crucial roles of substrate temperature, carbon layer formation, and surface morphology. The formation of the carbon layer and its geometry are shown to dominate laser ablation of polyimide for large numbers of pulses and form a self-affine surface. The concept of multiple fluence processing is introduced which results in novel effects for both mechanical and electrical material modification. The approach constitutes a serious departure from

previous methods that look at the results of individual fluences while ignoring that combinations of fluences may produce surfaces with properties not attainable by single fluence processing.

Chapter four approaches the dynamics of the irradiation process through pump probe experiments that relate transient optical properties to both the formation of the the carbon layer responsible for electrical conductivity and material removal. A sharp transient decrease in reflectivity during irradiation which has been observed by many groups is shown to be the result of a transient change in the refractive index profile of the surface. Such experiments provide nanosecond resolution and allow one to follow the interaction step by step.

One of the most promising applications of this technique of conductivity modification of polyimide is the potential to create a high density copper-polyimide interconnect. Copper-polyimide interconnects are desirable since the low dielectric constant of polyimide and the high conductivity of copper combine to make an interconnect with a substantially reduced propogation delay. If such a technology were implemented in an on-chip metalization, propagation delays could be reduced by a factor of 4 (Singer, 1994). The basic idea is to use a copper plating process that selectively deposits copper onto electrically conducting regions formed by laser processing with high spatial resolution. As the creation of vias in polyimide with excimer laser ablation is already a standard industrial process, such a technique is a viable alternative to current methods and offers several advantages in terms of both process simplicity and ultimate product reliability as well. In chapter 5 excimer laser processing is used to control the interface properties of electrolytically deposited copper on polyimide. High spatial resolution is easily obtained and excellent adhesive properties are observed. Again, the advantage of multiple fluence processing is exploited, using high fluences to machine surfaces and low fluences to modify electrical properties for electroless plating. As the national technology roadmap calls for

copper/polyimide interconnections within the next few years for both packaging and all third and higher levels of interconnection on chip these results are particularly timely.

Percolation theory describes the simplest type of phase transition exhibiting critical behavior and is of fundamental interest in physics. The percolation problem is the most important model system for the study of critical phenomena and strongly disordered systems and has been at the heart of developments such as renormalization groups and fractals. Direct applications of percolation theory are as vast as they are diverse. The theory has been used to model flow in porous media for oil exploration studies, epidemiology, forest fires, combustion synthesis reactions, and many random composite materials, particularly carbon/polymer composites that are now standard engineering materials. In this thesis the experimental results obtained with excimer laser irradiated polyimide are related to the specific theoretical results for transport on percolation clusters. A broad explanation of percolation theory is thus presented in chapter six concentrating on percolation as a model for electrical conduction in binary disordered systems such as conductor-insulator mixtures.

In chapter seven, results of experiments dealing with the nonlinear *I-V* characteristics observed in excimer laser irradiated polyimide are presented. These results combined with those from other systems also associated with percolation systems are described by a new theory for nonlinear conduction on percolation clusters. The new theory is the geometric analogue to the Space Charge Limited Currents (SCLC) observed in many insulators and explains both the form and the scaling of the nonlinearity simultaneously.

Finally a summary and discussion of potential future invesitgations is presented in chapter 8. Possibilities for independent verification of the SCLC theory are discussed as well as ideas for further investigation of the conduction mechanism near threshold.

The majority of the original results in this thesis have been published previously elsewhere (Ball et al., 1995a, 1995b, 1996; Ball and Sauerbrey, 1996) while the pedagogical material in chapter 6 is adapted from various sources and does not represent original research. Chapter 2 is drawn from "Surface Modification with Lasers" (Sauerbrey and Ball, 1996) from a forthcoming volume of the series Methods in Experimental Physics: Laser Ablation and Desorption.

CHAPTER TWO

OVERVIEW OF LASER-MATERIALS INTERACTIONS AND MATERIALS

PROCESSING WITH LASERS

2.1 Introduction

Over the last decade, materials processing with lasers has taken on increased

sophistication and now offers tremendous promise for applications. Laser processing of

materials can produce many changes to a surface including novel microstructures and

alloys, micromachined morphology, chemical reactions, and spontaneous periodic

structures. To meet stringent engineering requirements it is desirable for surface and bulk to

have contrasting properties where it would either be impossible to use a single material or

incur unreasonable costs to do so. Traditionally simple coating through electroplating and

other means has allowed inexpensive materials to acquire the properties of rare and

expensive materials for corrosion resistance or catalysis. Using lasers, a whole new level

of ability to modify the surface is becoming available, particularly in microelectronics

where tight thermal budgets prevent or limit the use of traditional modification techniques.

As laser pulses allow for high local temperatures with low energy and operation at

wavelengths that allow control over chemistry as well, it is easy to see that laser processing offers many advantages. The many combinations of materials and laser sources in various intensity regimes produce a truly vast range of novel effects that can be exploited for industrial or scientific application.

We will first examine the laser sources commonly used in surface modification techniques, the absorption of an intense laser pulse, and explore the possible pathways through which the surface returns to equilibrium. In the second section we divide the effects of the laser pulse into two categories, physical and chemical. Physical effects include surface wave optical phenomena, shock waves, phase transitions and thermal diffusion while chemical reactions include thermally activated processes, photochemical bondbreaking, and charge transfer reactions. Specific examples of laser processing will then be discussed including the role of laser induced surface modification in lithography, laser crystallization of amorphous silicon (a-Si) for flat panel displays, laser induced diffusion and alloying, as well as surface modification of fluoropolymers. Finally we will turn our attention to laser induced electrical conductivity in polyimide. The principal results accomplished previously will be presented and will focus on microscopic properties and basic experimental facts related to this phenomenon. The conduction mechanism, microstructure, spatial resolution and dependence on irradiation parameters will all be discussed.

2.2 Laser Sources for Surface Modification

Though a great amount of research has been performed with cw lasers such as Ar^+ lasers and CO_2 lasers (Bäuerle, 1986) we will constrict ourselves here to pulsed laser systems which form the core of the most active research areas today.

The traditional pulsed laser source for materials applications is the Nd:YAG laser because of its reliability and high output energy. At 1.06 μm these lasers couple to a

material through vibrational excitation in free molecules and phonons in solids. Through harmonic generation wavelengths as short as 213 nm (fifth harmonic) can be produced with substantial energies. The laser can be operated CW, Q-switched for nanosecond pulses, and mode-locked for sub-ns pulses. For processes where the 1.06 μm fundamental wavelength is acceptable the Nd:YAG laser is almost always the laser of choice, and it has therefore been widely used in industrial environments (Chester and Geusie, 1972). Microsecond pulsed CO_2 lasers (10.6 μm) have also traditionally been used in high power materials applications for laser welding and other industrial processes, though most newer effects that will be discussed here benefit from shorter wavelengths and shorter pulse widths. The primary advantages of CO_2 lasers are their high average power and commonplace use in industrial environments.

Great progress has been made in recent years with excimer laser technology such that excimers can now operate profitably in an industrial environment. The most common excimer lasers (ArF, 193 nm; KrF, 248 nm; and XeCl, 308 nm) provide pulses with energies of up to 1 J in pulses of 10 to 30 ns in length (Lacour et al., 1994). Modern excimer lasers can operate at repetition rates as high as 1 kHz and for up to a billion pulses on a single gas fill. These short wavelengths are absorbed by direct electronic transitions and therefore allow for manipulation of the target through photochemistry as well as thermal effects with very high spatial resolution. It is the opportunity for increased spatial resolution in photolithography that has provided a prime motivation for major improvements in excimer technology. Other applications have also appeared, such as in opthamology (Pettit, 1990) and via creation in electronics packaging (Lankard and Wobold, 1992). Specialized excimer systems even allow for the production of sub-picosecond pulses with peak intensities as high as 10^{19} W/cm^2.

Newly available Ti:Sapphire lasers may find great application in surface modification as well. These lasers exhibit tunability over a wide wavelength range (720 nm

to 1080 nm) and can generate picosecond and femtosecond pulses at a number of wavelengths through a combination of harmonic generation and various cavity configurations. Pulse width can also be controlled over many orders of magnitude as well using pulse compression techniques which allow for investigation of intensity dependence of laser materials interactions (Pronko et al., 1995). Like the Nd:YAG laser and other solid state systems, Ti:Sapphire lasers have reliability advantages over gas lasers.

2.3 Absorption of Laser Pulses at Moderate Intensities

Most laser-based materials processing techniques are a result of the energy density produced in a surface layer of the target material. Explosive thermal decomposition, shock waves, and phase transitions are all directly related to the deposited energy density as are many thermally induced chemical reactions. The energy balance is governed by two considerations: the amount of energy deposited and the volume in which it is deposited. Although the former may at first appear to be a simple laboratory measurement, changes in optical properties during irradiation can significantly alter the amount of energy that is actually absorbed. The depth in which the energy is absorbed is the quantity that is most dependent on material properties however. The determination of the absorption depth is certainly nontrivial and is essential in understanding any light matter interaction. The small signal absorption coefficient which is readily measured serves as only a starting point to understanding the interaction.

Different intensity regimes are dominated by different processes. At low intensities the small signal absorption coefficient and Beer's Law provide an accurate measure. At moderate intensities such as those used in nanosecond excimer laser ablation, saturation of the ground state and excited state absorption may play a role (Pettit et al., 1994). In the case of chemically complex materials such as polymers, chemical reactions may occur during irradiation that alter absorption properties. Even in simpler species such as metals or

semiconductors phase transitions can change materials properties remarkably, particularly reflectivity (Auston et al., 1978). At high intensities, plasma physics must be employed as entirely different absorption mechanisms become important (Ginsburg, 1970; Kruer, 1988). At the highest intensities with ultrashort pulses, effects such as resonance absorption of p-polarized light have been observed (Sauerbrey et al., 1994). Here we focus on the absorption of moderate intensity pulses commonly associated with nanosecond laser ablation. As pulsewidths of 15 to 30 ns are almost universal in practical commercial laser systems effects are often discussed in terms of the laser fluence. Typical fluences used in laser ablation of a wide variety of materials vary from 50 mJ/cm^2 to 100 J/cm^2, corresponding to intensities ranging from 1 MW/cm^2 to 10 GW/cm^2 .

2.3.1 Absorption in Polymers

Taking the most conservative end of this intensity range as a numerical example, we consider a 30 ns excimer pulse at a fluence of 50 mJ/cm^2 incident on polyimide (an important thermopolymer that is a popular insulating material in the microelectronics industry) where the small signal absorption coefficient is 10^5 cm^{-1} (Pettit et al., 1994) producing a substantial energy density of 5000 J/cm^3. This situation is depicted in Fig. 2.1. Such an energy density is large enough to cause some material removal and certainly thermal decomposition though many effects such as plasma formation are reserved for much higher intensities. If we consider the KrF excimer laser (a common source for polyimide ablation) which emits 5 eV photons (248 nm) then this energy density corresponds to 6x10^{21} photons/cm^3 delivered in a 30 ns time frame (an intensity of 1 MW/cm^2). The possibility exists, then, that the number of ground state electrons promoted to an excited state has become large enough to limit absorption from the depleted ground state. In such an instance the absorption depth would no longer be governed simply by the small signal absorption coefficient and the laser energy will then propagate to a considerably greater depth. As the fluence is increased, the importance of the effect grows
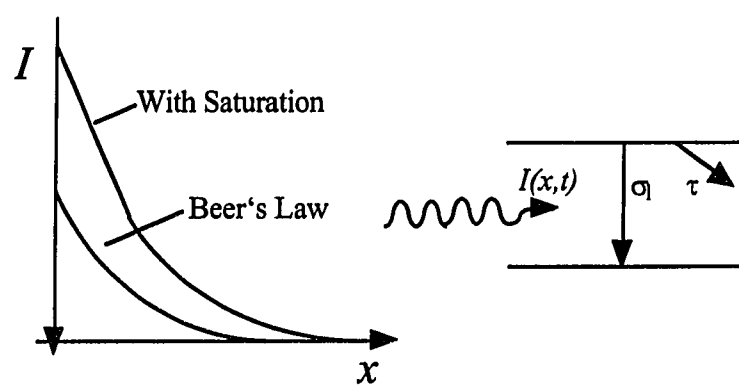
Fig. 2.1. Model for radiation transport in polymers.

and an effective fluence dependent absorption depth must be defined in order arrive at the correct deposited energy density. If the excited state has a large absorption crossection for the irradiating wavelength, excited state absorption must also be considered.

A rate equation model is commonly used to approximate the situation. Following the method of Petiit et al. (1994). we consider the simple two level system depicted in Fig. 2.1 where the crossection for stimulated emission and absorption is defined in the usual way and rate equations for the photon density and ground state population are written as:

$$\frac{\partial \rho_1}{\partial t} = -\frac{\partial \rho_0}{\partial t} = \sigma_1 \rho_0(x,t) I(x,t)$$

$$\frac{\partial I}{\partial x} = -\sigma_1 [\rho_0(x,t) - \rho_1(x,t)] I(x,t).$$

(2.1)

Here $I(x,t)$ is the photon flux from the laser pulse as a function of depth into the material and time, ρ_0 the ground state population density, ρ_1 the upper state population density with σ_1 representing the stimulated emission or absorption cross-section. Equation (2.1) is similar to a two level laser, the important difference being that relaxation is through non-radiative processes rather than emission. The model assumes that the absorption cross-section remains constant through irradiation even though chemical and structural changes are occurring at the fluences where saturation is important. The model also neglects absorption in the excited state and assumes that the lifetime of the upper state is long compared to the laser pulse. These latter two can be easily incorporated into equation (2.1) with additional terms, though their addition necessitates numerical solutions. To specify the solution of equation (2.1) we impose the conditions that $\rho_0(x,0) = \rho$, and $\rho_1(x,t) = 0$ which is simply to say that initially all of the population is in the ground state. $I(0,t)$ is just the incident photon flux. The first equation of equations (2.1) can then be integrated directly:

$$\rho_0(x,t) = \rho \cdot \exp\left[-\int\limits_0^t \sigma_1 I(x,t')dt'\right]. \qquad (2.2)$$

Substituting equation (2.2) into the second of equations (2.1) we obtain an expression for I(x,t).

$$\frac{\partial I}{\partial x} = -\sigma_1\rho\left\{2 \cdot \exp\left[-\int\limits_0^t \sigma_1 I(x,t')dt'\right] - 1\right\}I(x,t). \qquad (2.3)$$

Now if we consider the total photon flux S(x) which is just the integral of I(x,t) over time we find,

$$\frac{\partial S}{\partial x} = \int\limits_0^\infty \frac{\partial I(x,t')}{\partial x}dt' \qquad (2.4)$$

Employing equation (2.4) with equation (2.3) we can then write the dependence of the total photon flux on depth:

$$\frac{\partial S}{\partial x} = -\frac{\rho}{2}\left[1 - \exp\{-2\sigma_1 S(x)\}\right] \qquad (2.5)$$

Which reduces to the familiar form of Beer's law when S(x) << $1/\sigma_1$ and the exponential can be developed:

$$\frac{\partial S}{\partial x} = -\sigma_1\rho S(x) \qquad (2.6)$$

Clearly such a result cannot be relied upon in all situations, but with suitable modifications to equation (2.1) based on detailed knowledge of the target material, numerical solutions yield a reliable picture of light absorption at these intensities. For many systems, including

248 nm KrF irradiation of polyimide, equation (2.5) can be used directly. Complex molecules such as polyimide monomers may have more than one absorption site or chromophore each with a different absorption crossection. A straightforward averaging process can be applied in such a case to give an effective crossection for use in a simple two or three level model. Such a model likewise ignores the absorptive properties of the upper state. These can be easily implemented into the same framework, but only if some information about the crossection and lifetime of the upper state is known. In some cases, absorption is dominated by two photon processes such as in sub-picosecond ablation of Teflon and equation (2.1) with suitable modifications yields excellent agreement to experimental results (Pettit et al., 1994).

In Fig. 2.2 a schematic of the energy pathways present in ultraviolet processing of polymers is shown and it is clear from the figure that as polymer ablation and modification involves actual chemical tranformation of the material, absorption can change with laser processing. Some polymers initially only lightly absorbing become absorbing after the first few laser pulses and ablation does not begin until this 'incubation' is accomplished.

2.3.2 Metals and Semiconductors

In metals an effectively infinite supply of electrons is available for absorption such that the penetration depth will be dominated by the plasma frequency until the intensity is high enough that plasma is formed. Absorption is then dominated by the physics of the laser produced plasma. Absorption in semiconductors comes from electron-hole pair creation for excitation above the bandgap though below the bandgap a whole host of effects depending on the doping and defects are dominant (Haglund and Kelly, 1993; Boyd, 1987). Crossections for two photon absorption in semiconductors can be quite large and two photon absorption is observed in some cases. The large temperature dependence in semiconductors necessitates detailed thermal modeling to understand the exact absorption properties (Boyd, 1987).
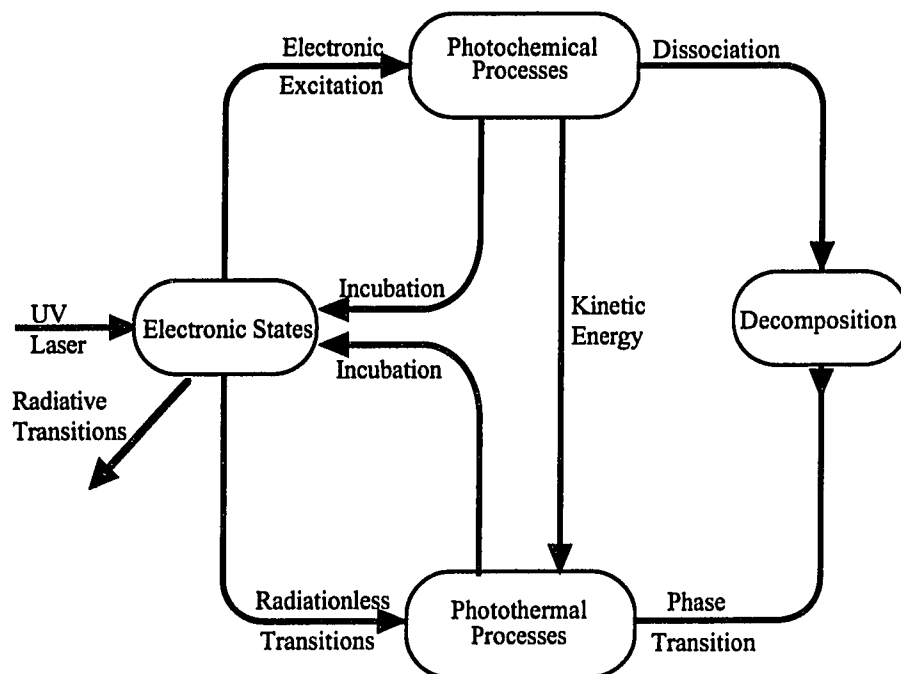
Fig. 2.2. Schematic of energy pathways in laser processing of materials.

2.3.3 Other Absorption Mechanisms

In many systems the nature of absorption may be completely different from the simple situation described by equation (2.1). In particular defects may become the major source of absorption and thus give a lateral spatial distribution to absorption. Such effects are most notably observed in systems with a wide bandgap such as MgO (Dickinson et al., 1993). In such a case a cleaved surface will always have much higher ablation threshold than a cut surface due to the greater defect density of the cut surface. In PMMA for example absorption at 248 nm is much smaller than in a polymer such as polyimide. After a small number of preliminary or 'incubation' pulses, the absorption of PMMA increases dramatically and ablation begins (Srinivasan, 1989). Another interesting system is diamond for which the bandgap is almost equal to the energy of the 248 nm photons (5eV). In this case the small signal absorption at 248 nm is strongly temperature dependent. Ablation, however, is largely temperature *independent* (Patterson et al., 1995). The reason is that surface states absorb initially and cause a phase transformation into graphite of a thin surface layer which serves to couple the laser light into the diamond on subsequent laser pulses, making the small signal absorption properties completely irrelevant for laser ablation.

Understanding of radiation transport in a system alone can explain many experimental observations. For example, the rather large variation in ablation thresholds for different materials and wavelengths can be understood when the different absorptive properties are considered. Smaller absorption depths lead to higher energy densities and thus lower ablation thresholds, though the depth of material ablated per pulse will then be small. For situations with large absorption depths, a higher fluence is necessary to produce the high energy density necessary for ablation, however once the ablation threshold is reached the etch rates will be higher. If surface defects are determined to dominate absorption, irregular ablation in patches and a strong dependence on surface preparation are

explained immediately. In order to understand the effects of laser irradiation in any material, the details of the absorption process must be known. From this point temperature modeling and other considerations can be used to understand the wide variety of effects that can be induced by laser processing

2.4 Physical and Chemical Effects of Laser Irradiation

Once the absorptive properties of a material are understood for the appropriate wavelength and intensity, the energy density produced can be calculated. In the case of excimer ablation where the source photons are in the ultraviolet, this energy is absorbed into electronic states. The excited electronic state can result in bond cleavage, chemical reaction, or the energy is converted to heat, usually on timescales much shorter than the nanosecond pump pulses. Infrared pulses interact with the target on a vibrational level either localized or delocalized. Thus we normally view the ablating pulse as essentially a process of instantaneous heating that follows the intensity profile of the incident pulse. However, the purely thermal picture is not always appropriate, particularly for deep uv pulses such as with ArF (193 nm) or F_2 (157 nm) lasers where photochemical reactions can occur directly. In the case of polymer ablation there has been a great deal of discussion over the role of direct photochemical bond breaking in the ablation process. In the case of metals or semiconductors, excitation of localized lattice modes can produce anomalous effects, namely desorbed atoms with energies well beyond those accounted for by uniform temperature distributions (Haglund and Kelly, 1993). Also, many surface modification effects with semiconductors involve laser stimulated interactions with a chemically reactive ambient.

Physical effects fall into two categories, those concerned with optical phenomena and those concerned with thermal phenomenon. Turning first to optical effects there are two primary phenomena that are of great importance and are also related: laser speckle (of crucial concern for lithography) and laser induced periodic surface structures or LIPSS.

Both are wave optical in nature and create an imhomogeneous spatial intensity distribution across the sample, however, speckle occurs with a single pulse while LIPSS build up over a number of pulses. Changes in optical properties of the surface (i.e. the complex refractive index) also effect energy absorption through reflectivity changes.

2.4.1 Laser Speckle and LIPSS

Lasers typically emit light with a high degree of spatial coherence because of the properties of modes of an optical cavity. In continuous wave single mode operation, spatial coherence is virtually perfect, such that a Young's two slit experiment will yield clear fringes even as the slit separation is made larger than the beam waist (Miloni and Eberly, 1988). Such a high degree of spatial coherence allows scattered light from random irregularities in a surface to interfere even when those irregularities are far from one another. The resulting pattern is known as speckle. In laser ablation the speckle pattern can be faithfully reproduced in the etched surface and thus constitutes a serious problem when any sort of patterning is desired (Jain, 1990). In lithography applications speckle is a major concern in the move to laser based techniques. Excimer lasers, fortunately, have poor spatial coherence compared to most other lasers, though still considerably more than incoherent sources. This is due to the high gain and consequently small number of passes in the resonator. In excimer lasers the gain lifetime is only about 20 ns which in turn requires a large output coupling for optimum energy extraction (Sauerbrey and Ball, 1993). Methods of eliminating speckle will be discussed in detail in the last section on lithography.

Similar to speckle, LIPSS occur from the interference of scattered light from a rough surface with the incident laser beam. The exact solutions to Maxwell's equations from which the LIPSS phenomenon are derived have been termed "radiation remnants" and have proved an interesting physical problem (Sipe et al., 1983; van Driel et al., 1982). If the intensity of the light is high enough, the interference from the "radiation remnants" and the incident beam will be etched into the target surface. On the first pulse this is a random

roughening of the surface. However, subsequent pulses then create intensity distributions that are in response to the modified surface. This positive feedback then results in periodic ripples in the surface after a sufficient number of pulses. The structures come in three types and have been given the designation S+, S- and c type fringes which correspond types of remnants found from the solution of Maxwell's equations. As they are an interference phenomenon, the ripple structures have a definite period related to the wavelength of the incident light and have a direction related to the polarization of the light. The S+ and S- type fringes appear perpendicular to the polarization and have a period given by the following formula:

$$\Lambda_\pm = \frac{\lambda}{1 \pm \sin(\theta)}. \qquad (2.7)$$

Where Λ is the fringe period, θ the angle of incidence and λ the laser wavelength. The S-is usually dominant in experiments. A rarer form of LIPSS is the c type fringes which run parallel to the polarization and have a period given by

$$\Lambda_c = \frac{\lambda}{\cos(\theta)}. \qquad (2.8)$$

The phenomenon of LIPSS is really quite general and has been observed in all types of materials and with many laser sources.

The key difference between laser speckle and LIPSS is that speckle is a function of the spatial coherence of the laser and comes from interference effects on the surface regardless of whether the light intensity is strong enough to modify the surface. LIPSS, in contrast, only form when the light can modify the surface and when successive pulses continue to modify the surface with positive feedback. The surface modification need not be direct ablation and can come from photochemical etching or any other process that modifies the surface in response to the spatial intensity distribution present at the surface (Kumagi et al., 1991). If the ultimate surface morphology is dominated by effects that do

not exactly follow the light intensity distribution at the surface, LIPSS will not be observed. Holographic irradiation has also been shown to suppress LIPSS formation by imposing an external periodicity on the surface which breaks down the necessary positive feedback (Heitz et al., 1994).

2.4.2 Reflectivity

The extreme conditions produced by laser irradiation can affect the refractive index and roughness of the surface. The melting transition in metals and semiconductors causes a drastic change in reflectivity. In most metals reflectivity is sharply reduced and in silicon the reflectivity sharply increases (Walters and Clauer, 1978; Chun and Rose, 1970). In excimer laser ablation of polyimide a transient change in refractive index results in strong reduction in reflectivity and will be discussed at length in chapter 4 while plasma formation can produce a 'mirror' effect where reflectivity is greatly increased (Bor et al., 1995).

2.4.3 Thermal Phenomena

The primary effect of an intense laser pulse absorbed into a target material is to heat the surface layer to relatively high temperatures in only a few nanoseconds. The heating rates are typically on the order of 10^{11} Kelvins/s. These are extreme thermodynamic conditions and produce extreme results. One of the principle problems with a theoretical understanding of laser material interaction is that the system is very far from thermodynamic equilibrium when all interesting effects are occurring. Phase transitions, decomposition temperatures, and physical constants which are well understood close to equilibrium should be viewed only as estimates and be correlated with experimental results from a variety of characterization techniques.

The most important parameter in understanding thermal effects is of course the temperature distribution in the material and its development in time. Reasonable estimates of the subsurface temperature distribution can be made from solutions to the thermal diffusion equation. Such solutions suffer from their reliance on physical parameters that are

determined from equilibrium experiments, and often room temperature constants are used

with temperature dependent parameters being implemented in only in cases where the effect

under study requires detailed knowledge of the temperature dependence. Surprisingly,

good agreement between experiment and calculation is obtained with such models. As a

starting point we consider the thermal diffusion length $l(t)$ which gives an estimate of the

length heat will diffuse in a time t,

$$l(t) = \sqrt{\frac{\kappa t}{\rho c}}, \qquad (2.9)$$

where κ is the thermal conductivity, ρ the density, and c the specific heat. Equation (2.9)

allows one to estimate in a very simple way how far a significant amount of heat should

diffuse during a given amount of time. Of great importance is the diffusion length over the

time of the laser pulse as this can affect the energy density if the length is greater than the

absorption depth. In thermally conductive targets such as metals and semiconductors,

thermal diffusion is of demonstrated importance. For example, the ablation threshold of

many metals can be decreased by two orders of magnitude in fluence if an ultra-short pulse

(< 1 ps) laser source is used where thermal diffusion during the pulse is negligible. During

the course of a nanosecond laser pulse, heat can diffuse to many times the absorption depth

in these materials and is thus the dominant factor in determining the absorbed energy

density and, thus, the maximum subsurface temperature. In table 2.1 we have listed

thermal diffusion lengths of a variety of materials calculated from equation (2.9) together

with their room temperature physical constants. Noting the large differences in values for

the thermally insulating polymers compared to the conductive metals and semiconductors,

we see that thermal diffusion during the pulse is less important in polymer ablation but

crucial in metals and semiconductors. This is due to both the shorter diffusion length *and*

Table 2.1

MATERIAL	ρ (g/cm^3)	c (J/gK)	κ (W/mK)	$1/\alpha$ (nm)[*]	l(t=15ns) nm
aluminum[1]	2.702	0.897	2.37	10	121
nickel[1]	8.90	0.444	0.907	8	59
copper[1]	8.92	0.385	4.01	14	132
tungsten[1]	19.35	0.132	1.74	7	101
silicon[1]	2.32	0.705	1.48	†	117
polyimide[2]	1.42	1.09	0.12	46[3]	34
PMMA[4]	1.19	1.40	0.21	200 μm^3,[**]	42
PTFE[4]	2.18	1.045	0.25	200 μm^3	57
PET	1.41[5]	1.425[4]	0.15[4]	33[5]	47

[*]For irradiation at 248 nm
[**]Dominated by incubation effects
†Strongly temperature, wavelength, and dopant dependent
[1]Handbook of Chemistry and Physics
[2]Kapton^{TM} Summary of Properties
[3]Philip et al., 1986
[4]Encyclopedia of Polymer Science and Engineering, Second Edition
[5]Furzikov, 1990

Table 2.1. Thermal and absorption properties of several common laser ablation targets.

the larger absorption depths. If tightly focused beams are used for processing of metals lateral diffusion of heat will require the problem to be treated as a two dimensional one.

Detailed temperature modeling begins with the complete thermal diffusion equation (Bäuerle, 1986),

$$\frac{\kappa(T)}{D_t(T)}\frac{\partial T}{\partial t} - \nabla[\kappa(T)\nabla T] = Q \qquad (2.10)$$

where $D_t(T) = \kappa(T)/\rho c$ is the temperature dependent thermal diffusivity, $\kappa(T)$ is a temperature dependent themal conductivity, T the subsurface temperature distribution and Q the deposited heat which also depends on space and time. From equation (2.10) we can begin to make approximations and arrive at solutions for particular situations. In some cases it is still not possible to have an analytic or simple numeric integration of the equation and numerical techniques such as finite difference and finite element analysis can be used. Implicit in equation (2.10) is that convection and blackbody radiation from the surface do not play a significant role which is almost always a good approximation for pulsed laser irradiation. The first and most important approximation we make to equation (2.10) is to consider only one dimensional heat flow into the bulk substrate. Such as picture is valid so long as the thermal diffusion length l(t) for the time scale of interest is much smaller than the irradiated feature size. A one dimensional partial differential equation of even a high degree of complexity can be solved efficiently with an ordinary microcomputer. The form of Q and the boundary and initial conditions specify the solution to equation (2.10). A typical form for Q that assumes that the laser energy is deposited following an exponential decay according Beer's law and circular Gaussian beam is given by (Bäuerle, 1986):

$$Q = 2\alpha F(1-R)\exp\left\{\frac{-2r^2}{w_0^2} - \alpha \bullet z\right\}P(t) \qquad (2.11)$$

where F is the laser fluence (the energy divided by the square of the beam waist), R the reflectivity, r the beam radius coordinate, z the direction into the material, $P(t)$ the temporal pulse shape, α the absorption coefficient and w_0 the beam waist at the sample. With the 1d approximation the Gaussian beam portion ($\exp(-2r^2/w_0^2)$)is simply left out. Often times Q is put at a delta function in z for highly absorbing materials ($\alpha > 10^4$ cm^{-1}) which simplifies solutions though analytic solutions using the exponential decay are still possible in many cases.

As an example we take the thermal conductivity and diffusivity to be constants and integrate equation (2.10) directly via the Green's function for the case of a semi-infinite medium. In such a case we can solve the spatial part of the problem analytically leaving only a simple temporal integral to be solved numerically. The appropriate Green's functions is then,

$$G(z,t;\xi,\tau) = \frac{1}{2\sqrt{\pi l(t-\tau)}}\left[\exp\left\{\frac{(\xi-z)^2}{4l(t-\tau)}\right\} - \exp\left\{\frac{(\xi+z)^2}{4l(t-\tau)}\right\}\right] \qquad (2.12)$$

which comes from the boundary condition that $dT/dx = 0$ at the surface and that the temperature should go to zero at infinite depth. The validity of the semi-infinite medium approximation is established when the diffusion length $l(t)$ is much smaller than the thickness of the medium. Thus even thin films can sometimes be "semi-infinite" if the time scale under consideration is small. To find the subsurface temperature distribution one simply multiplies Green's function equation (2.12) by the source term equation (2.11) and integrates over ξ and τ.

$$T(z,t) = \iint d\xi d\tau G(z,t;\xi,\tau)Q(\xi,\tau) \qquad (2.13)$$

Which for the spatial integration yields,

$$T(z,t) = \frac{\alpha F}{4\rho c} \int_0^t d\tau P(\tau) \left[\begin{array}{l} \left(erfc(\alpha l(t-\tau) + \frac{z}{2l(t-\tau)}) \right) \left(exp(\alpha^2 l^2(t-\tau) + \alpha z) \right) + \\ \left(erfc(\alpha l(t-\tau) - \frac{z}{2l(t-\tau)}) \right) \left(exp(\alpha^2 l^2(t-\tau) - \alpha z) \right) \end{array} \right] \qquad (2.14)$$

Here *erfc(x)* denotes the complimentary error function, and *l(t-τ)* is as defined in equation

(2.9). Such a solution can be easily implemented on a computer. Fig. 2.4 shows a set of

solutions for different times where for each point in space the time integral in equation

(2.14) is performed numerically. The constants used are for polyimide at room temperature

and $P(t) = t/\tau^2 exp(-t/\tau)$ pulse shape was used to give a 30 ns FWHM pulse with a fluence

of 50 mJ/cm^2. These equations yield good results for polymers and metals where the

thermal diffusivity is only slightly dependent on the temperature. Larger errors are found

for semiconductors since the diffusivity is strongly temperature dependent. Silicon, in

particular, has been extensively studied and the literature provides the results of detailed

numerical analysis (Boyd, 1987).

There are three basic effects excluding chemical reactions related to the large

temperature increase produced by laser irradiation i) phase transitions, ii) the formation of a

powerful shock wave, and iii) material removal. All three of these are interrelated,

complicating a rigorous analysis.

2.4.4 Phase Transitions

Phase transitions provide some of the most interesting opportunities to use surface

modification by lasers to produce novel properties. The primary advantage of laser

techniques is the ability to create high temperatures in a surface layer in a short time without

depositing a large amount of heat into the target as a whole. To model a phase transition,

we utilize the thermal diffusion equation (2.10) for both phases seperately, though the

introduction of the change of state significantly complicates the solution. The desired phase

transition in metals and semiconductors is generally melting, either for introduction of a

dopant, a planarized surface, or crystallization. As the diffusion coefficients for mass
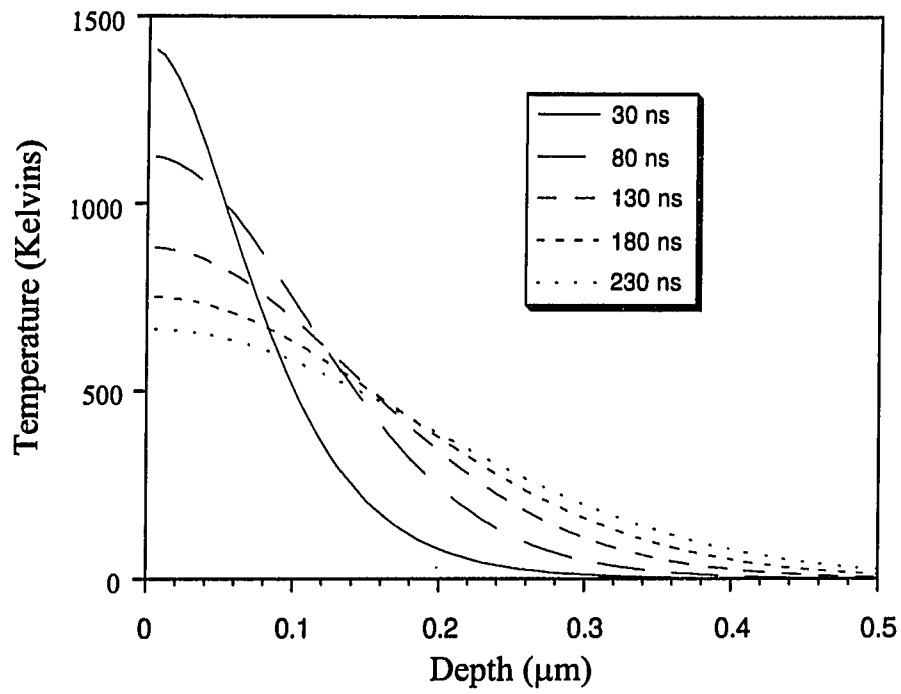
Fig. 2.3. Temperature profiles for a polyimide film irradiated with a 30 ns KrF pulse at different times after irradiation.

transport are several orders of magnitude higher for the liquid state, it is most necessary to know to what depth the melt is present and its duration. Numerous theories of pulsed laser melting have been put forward (Baeri et al., 1979; Meir et al., 1980; Wood, 1982; Kwong and Kim, 1983) both analytical and numerical. All are based on the same general framework of Neumann's solution (Carlslaw and Jaegar, 1959) where a moving reference frame corresponding to the melting front is chosen for the heat diffusion equation with appropriate boundary conditions. The desired 'solution' is not so much a temperature distribution as the trajectory of the melt front. Analytical solutions for pulsed laser absorption can be obtained, though speed and convenience of modern microcomputers and analysis software may make numerical analysis a more flexible and even more intuitive approach. Different approaches focus on special difficulties associated with a given target material. Silicon has been the most studied and presents the additional problem of a strongly temperature dependent absorption coefficient.

As an example we can consider the simplest case of a solid where the surface is held at a constant temperature T_s greater than the melting point T_m. A schematic of the problem is shown in Fig. 2.5. Following Carlslaw and Jaegar (1959) we identify the parameters D_1, c_1, κ_1, ρ, and $T_1(x,t)$ with the solid and D_2, c_2, κ_2, ρ, and $T_2(x,t)$ with the liquid where these quantities are the thermal diffusivity, specific heat, thermal conductivity, mass density and temperature respectively. An additional assumption here is a constant density for both phases. We define L as the latent heat of fusion (the amount of energy per unit mass consumed by melting). Confining ourselves to one dimension, we define $X(t)$ as the position in time of the solid liquid interface. At this interface both the solid and liquid temperature distributions must be at the melting temperature, yielding the boundary condition:

$$T_1 \, (X(t),t) = T_2 \, (X(t),t) = T_m \, . \tag{2.15}$$
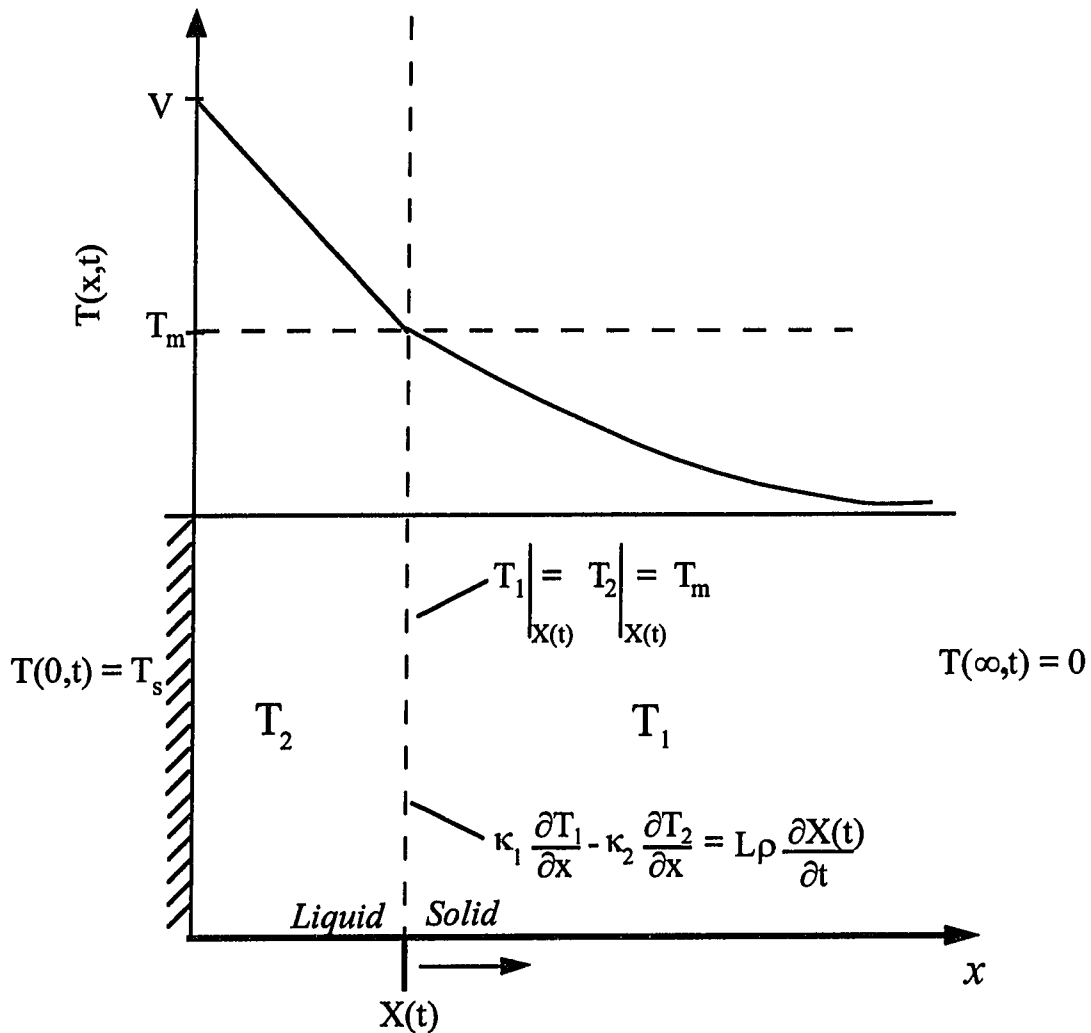
Fig. 2.5. Schematic of Melting problem and Neumann's approach. The surface is held at a

constant temperature above the meling point of the semi-infinite solid where the

Temperature is assumed zero deep into the material.

As the solid begins to melt a quantity of heat $L\rho\,dX$ per unit area is absorbed, yielding a second boundary condition at the interface,

$$\kappa_1 \frac{\partial T_1}{\partial x} - \kappa_2 \frac{\partial T_2}{\partial x} = L\rho \frac{dX}{dt}. \tag{2.16}$$

We then write the homogeneous temperature equation for both temperature distributions,

$$\frac{\partial^2 T_1}{\partial x^2} - \frac{1}{D_1} \frac{\partial T_1}{\partial t} = 0$$

$$\frac{\partial^2 T_2}{\partial x^2} - \frac{1}{D_2} \frac{\partial T_2}{\partial t} = 0 \tag{2.17}$$

Where the additional boundary conditions necessary to specify the problem are

$$T_1(x->\infty,t) = 0$$

$$T_2(0,t) = T_s \tag{2.18}$$

Which give the well known solutions,

$$T_2(x,t) = T_s - A erf\left(\frac{x}{2\sqrt{D_2 t}}\right)$$

$$T_1(x,t) = B erfc\left(\frac{x}{2\sqrt{D_1 t}}\right) \tag{2.19}$$

We then apply the boundary condition equation (2.15) to equation (2.19)

$$T_s - A erf\left(\frac{X(t)}{2\sqrt{D_2 t}}\right) = B erfc\left(\frac{X(t)}{2\sqrt{D_1 t}}\right) = T_m \tag{2.20}$$

which is clearly only true if $X(t)$ is proportional to $t^{1/2}$ so the trajectory of the melt front is then given by,

$$X(t) = 2\lambda\sqrt{D_2 t} \tag{2.21}$$

Where λ is a parameter given by application of the boundary condition equation (2.16). A and B are also then found from equation (2.20) in terms of λ to define the temperature profile as well. Upon application of equation (2.16) λ is then the root of the following equation:

$$\frac{\exp(-\lambda^2)}{erf(\lambda)} - \frac{\kappa_1\sqrt{D_2}\,T_m \exp\left(-\lambda^2\frac{D_2}{D_1}\right)}{\kappa_2\sqrt{D_1}(V - T_m)erfc\left(\lambda\sqrt{\frac{D_2}{D_1}}\right)} = \frac{\lambda L\sqrt{\pi}}{c_2(T_s - T_m)}. \qquad (2.22)$$

Naturally the addition of an exponential heat source, a temporal pulse shape and temperature dependent thermal constants severely complicates the solution. Utilizing this basic framework, however, intuitive numerical approaches can be devised to deal with most any situation. An important tie-in to experimental measurements is that the melted surface's decreased reflectivity can be detected with a temporally delayed probe beam and the results--fluence dependence and time dependence--compared to a model calculation.

2.4.5 Shock Waves and Acoustic Phenomena

An acoustic wave can be produced at low laser fluences through thermoelastic phenomena, though once fluences above the ablation threshold are reached the acoustic signal is dominated by the recoil of ablating material and at higher fluences by stress from plasma formation and expansion (Zweig et al., 1993). In the latter two cases the acoustic signal is in reality a supersonic shock wave.

Thermoelastic expansion of the surface is a significant phenomenon and is exploited in laser cleaning. Following Tam et al. (1992), we can estimate this effect by considering the normal expansion of the surface ξ which is given by $\xi = \mu l(\tau)\Delta T$ where μ is the coefficient of thermal expansion, $l(\tau)$ the thermal diffusion length for the pulse width τ of the laser pulse. Taking some typical numbers of $\Delta T = 1000$ K, $l(\tau) = 100$ nm, and $\mu = 2\times10^{-5}$ K^{-1}, we find $\xi = 2$ nm. This distance may seem insignificant, but since this expansion takes place in only 20 ns, it corresponds to a velocity of $\xi/\tau = 10$ cm/s and an acceleration of $\xi/\tau^2 = 5\times10^8$ cm/s^2, more than 500,000 times the acceleration due to gravity.

If ablation is ocurring the recoil from ejected material creates stress transients of much larger proportions. This of enormous concern in medical applications where

transients in these shock waves can be large enough to damage the target material away from the ablated spot. Studies in water indicate that the range of such shocks is about 100-200 μm at which point the shock wave has become an ordinary acoustic wave (Zysset et al., 1989). Damage from such phenomenon away from treatment area is a focus of attention in medical applications as damage to surrounding tissue is unacceptable, though in some cases such as kidney stone fragmentation the shock is actually exploited for treatment (Doukas et al., 1991). In strongly absorbing organic media, peak stresses in acoustic waves away from the interaction region are observed in the range 10^4 to 10^9 Pa (Zweig et al., 1993) where the larger end of this range can easily damage a fragile or otherwise brittle material. In medical applications of laser ablation, using low fluences and short pulses can minimize the effect of intense stress transients. Mode locked Nd:YAG systems are reliable sources of picosecond pulses at high repetition rate and may prove the most favorable system for medical application where collateral damage from shock waves is an issue.

2.4.6 Material Removal

Material removal in the case of metals and semiconductors is generally the result of further heating beyond the melting transition to vaporization. Such a phase transition, accompanied by a large change in density in short times, is generally explosive in nature. A purely thermal picture of material removal does not describe all results and excitation of localized lattice vibrations which can break bonds is also present (Haglund and Kelly, 1993). In the case of polymers, chemical processes dominate as in Fig. 2.2, whether photothermal degradation or direct photochemical bondbreaking (Srinivasan, 1989).

2.4.7 Chemical Effects in Laser Processing

Potentially, some of the most useful applications of laser surface modification may come from the ability of the laser to induce chemical reactions at the surface such as in top surface imaged photoresists in deep uv lithography. The laser can induce a chemical reaction in two ways, when the temperature rise of the substrate (and/or reactants) exceeds

the activation energy of a reaction, or when direct electronic excitation results in bond breaking. These are termed pyrolytic and photolytic processes respectively. There are four types of reactants: adsorbates, gases, liquids, and solids, each of which define a set of experimental techniques. Much work has been done with cw lasers (usually Ar^+ lasers) using a focused spot for direct writing. This work is well reviewed in the literature (Bäuerle, 1987), and we will look primarily at pulsed laser applications.

The most important feature of any chemical reaction is the rate at which the reaction occurs. In laser processing there are two possibilities that can limit the reaction rate: reaction kinetics or mass transport. The mass transport is strongly affected by the phase and density of the reactants and products while the kinetics are given by the chemistry of the reaction itself and the laser energy. At lower laser energies and temperatures, kinetics are usually more important while at higher energies and temperatures, mass transport tends to become more important.

In the kinetic limited case the reaction rate is often given by an Arrhenius type equation:

$$R(t) = kn(t)\exp\left\{-\frac{E_a}{k_B T(t)}\right\} \qquad (2.23)$$

Where k is a constant, $n(t)$ is the density of of reactants at the surface, E_a is the activation energy of the slowest step in the given reaction, and k_B is the Boltzman constant. The temperature $T(t)$ is the surface temperature. What has been omitted in equation (2.5) is that there is, of course, a spatial dependence to the surface temperature and the reactant density given by the irradiated pattern. This spatial dependence of great importance in determining the spatial resolution of a given process and determing what edge effects are present at the boundaries of the irradiation.

In the mass-transport limited case the diffusion of reactants into the reaction zone is considered and is particularly important for interactions with gas and liquid phases. In this

case we assume the reaction rate is directly proportional to the density of reactants in some region about the surface where laser irradiation is present and then solve for this density by computing the flux of reactants into the reaction region with the diffusion equation. In such a case there can be sharp differences between pulsed and cw processing. In cw processing the steady state solutions are all that is necessary, but in pulsed irradiation, the time dependence of the solutions must be investigated, though in some cases a steady state picture may also be appropriate for nanosecond pulses. If broad area irradiation is considered, only the 1-dimensional diffusion equation need be considered, but if small feature sizes or focused spots are used a fully three dimensional picture may be necessary. Three dimensional diffusion of reactants results in far greater rate of diffusion of reactants into the reaction zone such that the mass transport limited case occurs at much higher temperatures for gas and liquid phase reactions. Mass diffusion is of primary consideration in self terminating reactions like thermal oxidation where oxide growth on the surface, the desired effect, is itself the diffusion barrier that prevents the oxygen from reaching the bulk material.

Direct photochemical bondbreaking in an ambient, absorbate, or substrate occurs when a photon of sufficient energy or multiple photons whose sum has sufficient energy are absorbed by a molecule. Bond energies, typically several eV in magnitude, then require uv photons or multiphoton absorption of longer wavelengths. The mechanism of photodissociation is an electronic transition from an bound ground state to an excited dissociative state. As the time scale of the dissociation is in the tens of femtoseconds, relaxation processes and collisions can all be safely ignored (Levine, 1975).

Most photolytic processes that have been studied involve etching or deposition. Deposition occurs as a complex molecule is dissociated by the laser in the vicinity of the substrate. One of the dissociation products attaches to the surface and the other products leave the reaction area in the gaseous phase. Etching is similar except that the laser

photodissociation creates a highly reactive radical such as Cl or F which combines with and removes molecules on the surface.

Photolytic processes often termed "surface modifications" are laser enhanced oxidization and nitridation. Oxide and nitride growth on semicondutors for passivation and use as an electrical insulator are of crucial importance for semiconductor device manufacturing and traditional furnace based oxide growth techniques detract significantly from the thermal budget of a given process. It has been observed that under laser processing SiO_2 growth rates can be substantially increased. Though there is likely a strong thermal component to the enhancement, it is believed that electron-hole pair creation catalyzes the growth process. Laser processing is usually less economical than rapid thermal annealing (RTA) and CVD techniques and has thus not been significant in manufacturing.

More recent research has shown photolytic reactions with polymers, particular fluoropolymers, can alter reactive, mechanical, and adhesive properties (Niino and Yabe, 1993; Okoshi et al., 1992). Such results are of tremendous interest in the microelectronic industry since the low dielectric constant of such polymers together with their chemical and thermal stability would be ideal as interlayer dielectrics for packaging and metallization applications (Cho et al., 1995).

2.5 Laser processing of teflon

Two primary types of teflon are of technological interest and laser modification of both has been achieved. These are Teflon AF, which is an amorphous polymer, and the more common PTFE (poly(tetrafluoroethylene)). Teflon is widely known for its chemical intertness which has found innumerable applications in various industries and consumer products. Not surprisingly adhesion to teflon of anything is a considerable problem for which ultraviolet laser treatment is an important solution with the principal advantage of high spatial resolution.

First we consider the work of Okoshi et al. (1992), who irradiated a PTFE surface with an ArF excimer laser in various solutions and atmospheres where the 193nm photons could break the F-C bonds and promote a reaction with the ambient. The surfaces could then be studied with X-ray photoelectron spectroscopy to determine the nature and extent of surface modification. A solid piece of teflon irradiated in this way could then be epoxied directly onto metallic material (in this case steel) with a degree of adhesion completely uncharacteristic of teflon.

Gas phase reactants have also been reported including hydrazine and $B(CH_3)_3$. In the former case activation of the surface for selective electroless plating of Ni was achieved although intermediate steps were required. All such modifications resulted in hydrophillic behavior with a measured decrease in contact angle with increasing fluence and number of laser shots. Changes in contact angle (water or benzene) were on the order of 100° or more in these experiments. It should be emphasized that these modifications were performed, at least with the lower fluences studied, without change to the surface morphology of the material and without visible damage. Similar results were obtained by Matienzo et al. (1994) using VUV radiation from a helium microwave plasma.

2.6 Surface modification of metals and semiconductors

Surface modification of semiconductor materials has been the most active research area in laser processing of materials and has been reviewed previously in the literature (Bäuerle, 1986; Boyd, 1987). Laser processing offers many unique abilities to manipulate a surface without depositing a large amount of heat into the system. The most important of these is laser crystallization of amorphous silicon (a-Si) which can be used for thin film transistor (TFT) fabrication for active matrix videographic displays. Laser induced doping and alloying in metals have also been important for industrial applications.

2.6.1 Surface modification of metals

It is often desirable for an engineering material's surface to have contrasting properties with the bulk such that one can take advantage of an inexpensive material's mechanical properties and avoid what may be poor surface qualities such as lack of hardness or poor resistance to corrosion. Often simple coatings are employed through electroplating or other means, but in particularly high performance applications a surface layer may not be adequate due to poor adhesion at high temperatures or cracks that can form in the coating. In these cases a true intermixture of surface and bulk materials is required, and as high temperature processing can lead to deterioration of bulk properties, low temperature processes are very desirable. Two primary low temperature processes that have been explored for metal processing are ion implantation and laser induced diffusion.

A good example is surface modification of stainless steel which has been investigated recently by Jyumonji et al. (1995) In this work Si was simultaneously deposited from a silane ambient and diffused into the steel substrates with an excimer laser. The 248 nm excimer laser pulse melts a thin surface layer for about 100 ns and allows Si atoms to diffuse rapidly into the melted surface as the diffusion constant of the melted surface is several orders of magnitude higher than the solid. RBS spectra confirmed an intermixing layer of about 100 nm in thickness and where this thickness varied linearly with the number of laser pulses. The concentration profile of the Si could be predicted by a simple mass diffusion model and followed the resulting error function distribution to good accuracy. At a fluence of 400 mJ/cm^2, a dosage of 2×10^{17} atoms/cm^2 was achieved, and the profile could be controlled with gas pressure, fluence and number of pulses. One particular advantage is the agreement between relatively simple models of dopant profiles and experimental results allowing parameters to be adjusted in a straightforward way to produce a desired doping profile.

Generally speaking when thin sub-micron layers are desired, short wavelengths and short pulses are necessary, while for deeper intermixture layers longer pulses in the infrared region can be used. CO_2 lasers or the fundamental of an Nd:YAG laser are typically used in this case. One recent example investigated by Haferkamp et al. (1994) is alloying of pure copper with various metals to improve surface hardness. Pure copper is a desirable material for its electrical conductivity and is often used in electric motors and dynamos. Wear on copper components from brush contacts and thermal loading is a serious concern for soft copper surfaces. The alloying element was either deposited as a mixture with turpentine oil before laser processing or in a one step process where thermal spraying was used. Laser alloying of copper with various dopants was achieved at 1.06 μm with 5 ms pulses where interdiffusion depths as large as 1mm were possible, yielding significant increases in hardness for Sn, Al, Cr, and B elements, though only marginal increases in hardness were found for Ni.

One potentially very useful application of laser induced melting is reflowing and planarization of metal interconnection layers in the semiconductor industry (Tuckerman and Weisberg, 1986). A short laser pulse melts the deposited metal layer, typically aluminum, and in the short duration of the melt the metal completely fills vias and leaves a planarized surface. Good results are possible due to the high surface tension of the melted Al. The primary obstacle to implementing the technique in manufacturing lines is the careful control over the laser energy which is required in order to avoid ablation while supplying enough energy to melt the entire layer. Best results were obtained with the short wavelengths and nanosecond pulses of excimer lasers, though dye lasers have also been used.

2.6.2 Laser annealing of implanted semiconductors

One of the principle technologies of modern semiconductor manufacturing is ion implantation of dopants, though lattice damage and amorphization of the surface are serious problems which become worse with higher doping densities. Annealing is therefore

necessary to recrystallize the lattice and activate the dopants, but bulk annealing can cause redistribution of dopants. In laser annealing only the surface layer is melted and for only a short time, and subsequent epitaxial regrowth has been demonstrated with a number of laser sources.

Epitaxial regrowth after laser melting was conclusively demonstrated by Auston et al. (1978) where 50 ns Nd:YAG laser pulses were used to anneal amorphous ion implanted Si. Full annealing was accomplished for fluences greater than 3 J/cm^2. Transient reflectivity measurements were used to verify surface melting and determine the melt duration which was about 300 ns. The work of Venkatesan et al. (1978) has shown that absorption of the 1.06 μm pulses and annealing characteristics have a strong dependence on the implant dose, complicating the process.

As thermal growth of oxide is the highest temperature component of semiconductor processing, laser annealed ion implanted oxide layers are a possibility. A particular advantage of the laser annealed method over more common CVD techniques is the ability to create buried oxide layers hundreds of nanometers into the surface (Boyd, 1987).

2.6.3 Laser induced diffusion in semiconductors

Laser induced melting of semiconductors can result in epitaxial regrowth of the lattice and presents an opportunity for laser controlled introduction of dopants. Laser induced diffusion has some advantages over conventional ion implantation particularly with regard to the lack of lattice damage and the very sharp concentration gradients that are possible. Thin doped regions occur essentially because pulsed laser irradiation only allows a thin melted layer where diffusion rates are significant. While for most applications ion implantation is clearly the preferred technique, laser induced diffusions may find practical application in areas such as ohmic contact formation, passivation, and metallization of GaAs and other compound semiconductors for optical communcations applications.

Excimer laser doping of semiconductors was demonstrated more than a decade ago by Deutsch et al. (1980, 1981, 1982) where ohmic contacts were made in InP and GaAs while *p-n* junctions fabricated in Si and GaAs could made into efficient solar cells. Similar to results above for doping of metals, depths were thin (< 1μm) and sharp. Dopant material was simultaneously deposited from an ambient gas by photodissociation of organometallic molecules in the case of Si and by both photodissociation and thermal activation of H_2S for GaAs. In both materials quality photocells could be constructed. The technique was of particular interest for GaAs where traditional techniques of ion-implantation and laser annealing suffer significant problems due to material loss (owing to the high vapor pressure of arsenic), requiring a capping layer which can itself diffuse into the substrate.

More recently these techniques have been used for dope passivation of GaAs surfaces to reduce interface state density for field effect transistor fabrication. Zhang et al.[73] (1994) used a two step method where the surface was slowly etched with an $(NH_4)S_x$ solution. Samples prepared in this fashion retain a few monolayers of sulphur on the passivated surface and were then placed in vacuum chamber for irradiation. Secondary ion mass spectrometry (SIMS) measurements and RBS characterization of lattice damage were performed, and good quality surfaces were obtained.

Laser induced diffusion may take on much greater importance in the future as device sizes shrink to levels where the inability of ion-implantation to create shallow highly doped regions becomes significant.

2.6.4 Laser crystallization of a-Si

Investigations of laser annealing of implanted silicon wafers in the late 1970's revealed two fluence thresholds for laser processing, a lower one where polycrystalline material was formed and a higher one where true epitaxial growth was observed which, for annealing of ion implantation damage, is the desired affect. In the last few years processes for the production of high quality polycrystalline Si have taken on great importance for the

production of thin film transistors (TFTs) on glass substrates for flat panel display technology. It is in this area that laser processing of semiconductors is currently seen as a likely manufacturing process.

TFT technology generally consists of CVD deposited a-Si on quartz substrates which is then crystallized via furnace or laser techniques, and, by controlling the CVD gas mixture, doping is accomplished simultaneously with deposition. A key problem with furnace based techniques is to maintain low substrate temperatures to avoid deformation of the glass, and low temperature solid state annealing is prohibitively slow. The high defect densities associated with polycrystalline material are reduced greatly by hydrogenation accomplished either by diffusion or plasma techniques.

In excimer laser crystallization of a-Si the excimer pulse melts the amorphous layer and a polycrystalline phase appears during solidification. The process is also reversible if higher laser energies (dependent on thin film thickness) are used, termed excimer laser amorphization. Comparisons of excimer laser and furnace based recrystallization techniques have demonstrated lower in-grain defect densities in laser crystallized films and higher carrier mobilities (Sameshima, 1994). Further improvements have been found in combinations of laser and furnace based techniques (Carluccio et al., 1995). Furnace annealing is not particularly economical requiring ~8 hours (Duhamel and Loisel, 1994), and laser crystallization and rapid thermal annealing (RTA) are seen as the most likely technologies where excimer laser methods yield better device properties but with poorer reproducibility than RTA methods.

In the work of Carluccio et al. (1995), comparisons for different irradiating conditions were made where initial furnace annealing was followed by laser annealing. Grain sizes of up to 1.5 μm could be produced with low densities of in grain defects and low surface roughness (5 nm), though such slow processes do little to increase throughput, one of the key advantages of excimer laser recrystallization.

Laser annealing of a-Si is not only limited to TFT technology. El-Kader et al. (1994), have recently demonstrated formation of luminescent "porous" silicon from hydrogenated amorphous thin films. In this work a XeCl excimer laser was used to irradiate a-Si thin films under vacuum at fluences from 0.3 J/cm^2 to 0.8 J/cm^2 where only a few laser pulses were required to produce a stable layer with voids and craters of about 2 μm diameter. Photoluminescence spectra peak around 700 nm and are comparable to those prepared through HF processing. Such work illustrates the interesting behavior that can be observed due to the nonequilibrium nature of the rapid heating and cooling induced by nanosecond laser pulses, and as these experiments correspond to the boundary between crystallization and amorphization, the final (optically active) phase is likely a combination of both phases.

2.7 DUV Photolithography

Excimer laser lithography is the most advanced optical lithography method, the first to utilize a coherent source, and the designated successor to mercury lamp based methods. As KrF (248 nm) lithography is currently being brought into production for 0.25 μm processes such as for 256 Mbit DRAMs, it is clear that most difficulties have been overcome. However, many problems remain research considerations, particularly with regard to the laser-polymer interaction. Further reduction in design rule to 0.18 μm is still a research issue with the possiblity of improved KrF technology or a move to ArF excimers at 193 nm. The only alternative to excimer laser based methods would be a major paradigm shift to proximity X-ray lithography, a technology that becomes more attractive as lithography stepper costs soar.

2.7.1 Laser System requirements

Initially the principal obstacle to excimer-based lithography was poor reliability, low beam quality, high cost, and a lack of adequate achromatic optics. Each of these problems can now be considered solved and no longer an issue for applications. First new laser

systems have been developed with high reliability and low maintainance costs. These lasers can operate for up to 10^8 pulses on a single gas fill, and components are robust for orders of magnitude more pulses.

Beam quality has been addressed through beam homogenization techniques, primarily the 'fly's eye' type beam homogenizer which uses an array of small lenses to produce a 'top hat' beam profile. In this technique, the laser pulse is divided into segments which are recombined at the mask plane, producing a flat intensity distribution. This has the highly desirable side effect of destroying the spatial coherence of the beam across the mask, eliminating speckle.

As fluorite based optical materials are both expensive and have difficulty meeting standards of reliability necessary for mass production, achromatic optical systems have largely been rejected in favor of line narrowing of the laser. Thus, conventional high quality fused silica optics are used in most systems. In order for chromatic aberration to be eliminated, the laser linewidth must be reduced to 3 pm or less, far less than the natural linewidth of the excimer. This is accomplished by making one mirror of the resonator highly frequency selective. Initial designs used etalons to provide frequency selection, but poor reliability of the etalons has motivated designs to use hybrid grating-prism-etalon configurations to provide high frequency selection and long component lifetime.

Thus all primary problems associated with the integration of excimer sources into a manufacturing line have been overcome with considerable success. However, the development of resists has become the primary limitation on excimer laser lithography.

2.7.2 Resists for excimer laser lithography

The essential problem for excimer resists is the high absorption of organic molecules at excimer wavelengths. Process requirements dictate that 1 μm resist layers be patterned. The absorption length in most polymers at 248 nm is more than 10 times smaller

than this. The laser must be able to expose homogeneously a full 1 μm layer of resist. The key to full penetration of the laser light is bleachable absorption characteristics. Recalling the laser absorption discussion in section 2.3, the material must have saturable absorption properties at low fluences. Non saturable absorption must be minimal and excited state absorption crossections should be insignificant

The class of resists now used in excimer laser lithography are called *chemical amplification resists*, where deprotection of the resist comes from a uv absorbing photoacid. These resists have been successful but feature a number of problems, such as the tendency for a soluble layer to form at the substrate resist boundary resulting in under cutting or insoluble layer formation resulting in sloped walls.

Perhaps the most serious problem with resist technology results from the temporal coherence of the laser which is an unavoidable consequence of linewidth narrowing. Full exposure of the resist implies that significant amounts of laser light reach the resist-substrate inteface. A portion of this light is then reflected, resulting in multiple reflection interference. These beams are reflected at considerable angles and thus expose resist and limit resolution. Depending on the substrate materiall, multiple reflection interference can erode resolution by as much as 0.05 μm. One solution has been to spin on a soluble antireflection coating before resist application. Variations in resist thickness cause similar problems.

2.7.3 193 nm Lithography

193 nm lithography is considered a prime cadidate for the move to 0.18 μm design rules. Most of the problems associated with KrF lithography exist for ArF lithgraphy as well but with greater severity. Absorption properties at 193 nm are significantly different and will require fundamentally different resist materials. ArF laser systems are fundamentally less powerful and less reliable than KrF lasers but the same technology used

in KrF steppers to extend gas and component lifetimes are probably adequate for ArF systems as well.

The traditional resist for ArF and other extremely short wavelengths is PMMA (Poly(methylmethacrylate)). Processing of PMMA with excimer lasers has been studied for a long time, primarily in terms of laser ablation. In lithography however, photochemical modification does not have to lead to material removal, just significant degradation for chemically based development. For an effective resist, a methacrylate type resin is used with a photoacid generator to produce a relatively transparent amplification resist for 193 nm. Such resists have the added advantage that they should work equally well at 248 nm. The limitations of methacrylate based resists are twofold, poor resistance to plasma-based etching and the lack of a suitable antireflectance coating.

Top-surface imaged (TSI) resists have also been developed for ArF lasers. These processes do not require light penetration through the whole volume of resist. In a TSI resist, a silyl amine is selectively in-diffused into a phenolic polymer. This diffusion process creates a silyl ether, and development takes place in the form of an oxygen plasma etch. Depth of focus limitations are thus avoided as exposure is necessary only at the surface of the resist layer, and the resolution of the etching process determines the final resist profile.

2.8 Excimer Laser Induced Electrical Conductivity in Polyimide

In 1990 it was first reported (Schumann et al., 1990) that excimer laser irradiation at moderate fluences could permanently increase the electrical conductivity of the surface polyimide films by 15 orders of magnitude. The transition from insulator to conductor had the peculiar feature that until a critical number of laser shots was incident on the surface (about 300) the surface was completely insulating despite visual damage and blackening.

A further more comprehensive study of the phenomenon was pursued by Feurer et al. (1993) where not only the dependence on fluence and number of laser shots was investigated but also the conduction mechanism was studied. A spectroscopic study of the irradiated surface, the temperature dependence of the conductivity, and I-V characteristics were examined.

The result of a basic experiment is shown in figure 2.4 where the conductivity is shown as a function of the number of laser pulses for irradiation at the 248 nm wavelength of the KrF excimer laser. The threshold nature of the process is clear from the figure as well as the dramatic nature of the change in electrical conduction. The maximum conductivity and the threshold are fluence dependent with an earlier threshold and higher overal conductivity values being found for higher fluences. All of these fluences are above the so-called "ablation threshold" of 20 mJ/cm^2 reported by Küper et al. (1993) for KrF ablation of polyimide. The same threshold was observed for the conductivity modification process as well and it was speculated the the measurements of Stuke et al. might simply be detecting the mass loss from a thermal decomposition process into carbon induced by the laser. However, as will be examined carefully in chapter 4, even thousands of pulses at fluences well above this threshold would not puncture the 75 μm films used.

Several spectroscopic analyses of excimer treated polyimide have been carried out including micro-Raman (Gu, 1993), attenuated total reflectance Fourier transform infrared spectroscopy (ATR-FTIR) (Feurer et al., 1993), parallel electron energy loss spectroscopy (PEELS) (Bentley et al., 1993), X-ray photoelectron spectroscopy (Kokai et al;., 1989). All of these analyses have more or less said the same thing: that the process decomposes the surface into a layer that is principally carbon and that this carbon exhibits only short range order. Transmission electron microscopy studies (Phillips et al., 1992) revealed a microstructure consisting of 50 to 100 nm approximately spherical clusters, presumably carbon with at least a conducting core.
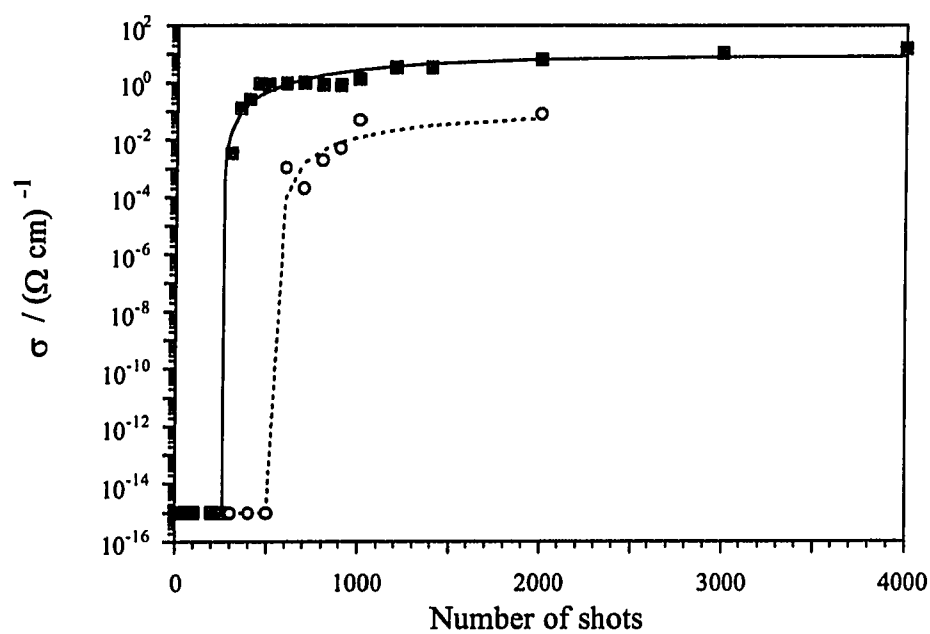
Fig. 2.4. Electrical conductivity as a function the number of excimer pulses in laser processed polyimide films.

The threshold nature of the process was explained by Feurer et al. (1993) simply in terms of percolation theory. Stated simply, each laser shot increases the density of small electrically conducting carbon concentrations which are distributed randomly throughout the surface layer affected. Since with each laser shot the density of these sites increases eventually a critical point is reached where a conducting pathway exists through the sample. Since the change from no conducting path to the existence of a conducting path is a geometric one that may depend on a single site, one would expect the threshold to be extremely sharp. Such a situation is exactly that depicted in percolation theory.

In order to further consider the possibity of a percolative description, visible transmission spectra were taken of samples irradiated with differing numbers of laser shots. When regions of the spectrum transparent to the unirradiated polyimide film are considered the decreasing transmission with irradiation can be considered a direct measure of the density of carbon clusters. With this data a determination of the percolation threshold can be made which was found to be 0.3, in good agreement with percolation theory (Feurer et al., 1993; Phillips, 1992).

In order to understand the conduction mechanism the temperature dependence of the material was investigated for samples near threshold and far from threshold. The results are shown in figure 2.5. The result of the analysis is that the conduction follows the following relation:

$$\sigma \propto \exp\left\{\left[\left(\frac{T}{T_0}\right)^{\frac{1}{4}}\right]\right\} \tag{2.24}$$

which is known as Mott's law and is indicative of a conduction mechanism known as phonon assisted variable range hopping (VRH). VRH conduction occurs in materials where carriers are confined to localized sites beneath the conduction band. Conduction occurs when a site is thermally activate and 'hops' to a vacant site. Equation (2.24) comes from considering the formation of an optimal path from differences in energy and distance
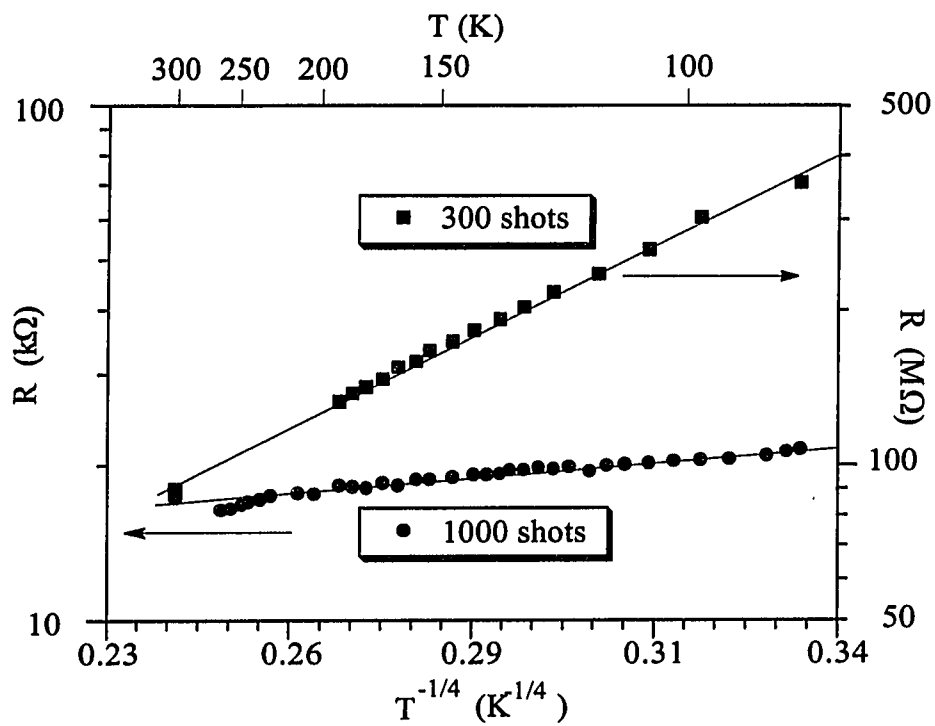
Fig. 2.5. Temperature dependence of the electrical conductivity for laser irradiated samples near threshols and far from threshold.

between sites. The observation of VRH according equation (2.24) confirms the existence of localised states and implies that conduction is occurring three dimensionally since the two dimensional solution to the VRH problem yields a different temperature dependence. Similar conduction has been observed in ion and proton beam irradiated polyimide as well as pyrolyzed polyimide samples providing further support to this interpretation of the data in figure 2.5.

The spatial resolution of the conductivity modification process was investigated by Phillips et al. (1992) where an interference pattern was used to create an array of sub-micron wires. Similar levels of conductivity were observed but the temperature dependence indicated that a two dimensional VRH mechanism might be responsible. Also far greater numbers of laser pulses (> 5000) were necessary to observe conduction which is also consistent with percolation theory in a constricted geometry.

A comprehensive discussion of percolation theory and its relation to excimer laser induced conductivity is presented in chapters 6 and 7.

2.9 Conclusion

Laser processing of materials is a large field with much potential for applications in the future. There are several common features to many of these processes such as thermal diffusion and phase transitions, chemical transformation of a surface through decomposition or reaction with an ambient. The key advantages of laser processing are low temperature processing, the ability to manipulate chemistry through photolytic and photothermal effects, and microstructural transformation through laser induced phase changes that can exploit the extremely rapid heating induced by laser processing.

CHAPTER THREE

MULTIPLE PULSE EFFECTS

3.1 Introduction

Though excimer laser processing of polyimide has been the subject of many experimental studies, most have focused on the results of a single excimer pulse incident on a virgin polyimide surface or averaging over the effects of ten to 100 pulses (Küper et al., 1993; Srinivasan et al., 1993). In particular, the study by Küper et al., provides very precise results for the single excimer pulse even for removal rates of only a few angstroms per pulse. In an industrial setting and for processing other than ablation, such as laser induced electrical conductivity, several hundreds or even thousands of laser pulses are used, and the effects are not a simple extrapolation of the one pulse results in all fluence regimes. In addition, it is often convenient to use higher repetition rates than those usually used to study single shot ablation if several hundred or thousand pulses are involved in a

given process. The effects of thermal coupling between pulses become more and more important both with increasing repetition rate and with increasing numbers of pulses. It is therefore of considerable interest to understand what happens when laser processing is no longer well approximated by extrapolation of the single shot results.

One of the first observations in the study of excimer laser ablation of polyimide was that for relatively low fluences, less than 200 mJ/cm^2 for KrF irradiation, that the surface was considerably roughened. For fluences above 200 mJ/cm^2 the surface was more or less smooth (Koren and Yeh, 1984). Clearly, continued irradiation at fluences where the surface has been visibly changed will not yield precisely the results of the first pulse, particularly if the changes to the sample increase with increasing irradiation. Recall also that in this same fluence regime, electrical conductivity is observed when a critical number of laser pulses is exceeded. In this chapter the relation between these two phenomena, the rough to smooth transition and laser induced electrical conductivity, is pursued.

Initially the ablation threshold of polyimide was believed to be around 55 mJ/cm^2 for KrF lasers (Gorodetsky et al., 1985), above that needed for laser induced electrical conductivity. Later, however, once more careful measurement techniques were used to determine etch depths, the threshold for ablation of polyimide at 248 nm was found to be just at 20 mJ/cm^2 (Küper et al., 1993), the same fluence necessary for conductivity modification. This seems to represent a contradiction: does the material actually ablate or merely decompose into the carbon layer at these fluences? In this chapter it is shown that for fluences below 260 mJ/cm^2 ablation only occurs for a limited number of pulses as the carbon layer forms, after which ablation effectively ceases. For higher fluences an essentially clean surface is left after each ablating pulse, not allowing the carbon layer build up with each pulse. In this case ablation is not limited by the number of pulses, at least not in such a drastic way. Also presented is that the properties of this carbon layer are strongly dependent on thermal coupling between pulses, and thus also on the laser repetition rate

and substrate thermal conductivity. This result is explained with through thermal coupling betweeen successive pulses

3.2 Experimental methods and results

3.2.1 Analysis of multiple shot ablation

In this study 75 μm polyimide foils of type Kapton HN^{TM} from DuPont corporationwere irradiated. Samples were irradiated with the output of a Lambda Physik LPX 105i excimer laser using a KrF gas mix for 248 nm operation in air or with nitrogen gas blown over the surface. A homogeneous section of the beam was selected with an aperture and imaged onto the polyimide surface. The homogeneity of the beam was examined and found to be satisfactory, though no beam homogenizer was used. Spot sizes were kept relatively large, 2 to 4 mm in diameter, such that a one dimensional picture of all effects would be appropriate. The excimer pulse energy was measured with a Gentec ED500 energy meter and the fluence calculated from this value and the spot size. Typically 90 pulses were averaged for each energy measurement. Etch depths and profiles were measured with a DekTak profilometer. Resistance measurements were performed with a Keithley 6517 electrometer/high resistance system in a simple two terminal arrangement. Electrical contacts were made using colloidal silver paint which makes an ohmic contact with the laser induced conducting surfaces (Feurer, 1993).

A series of samples were irradiated at a number of fluences from 50 mJ/cm^2 to 600 mJ/cm^2, all well below the point were plasma formation dominates absorption. For those samples irradiated at fluences below 260 mJ/cm^2 it was impossible to cut through the film with any number of excimer pulses. As many as 40,000 pulses were used at a 15 Hz repetition rate with no difference in etch depth after the first several hundred pulses. For fluences above 260 mJ/cm^2 a cleanly cut hole was made in the free standing film. We identify this value with the idea of a *multiple shot* ablation threshold defined as the

minimum fluence necessary to cut through the 75 μm film with an arbitrarily large number of pulses.

A simple observation during the ablation process was that for all fluences used above 70 mJ/cm^2 a long orange plume of approximately 6 mm in length formed above the sample. After a specific number of pulses which was dependent on the fluence, the plume would become smaller and eventually disappear entirely if the fluence was below multiple shot threshold of 260 mJ/cm^2. At this point ablation had effectively ceased. In Fig. 3.1 the number of pulses required for the plume to disappear is shown as a function of fluence. For fluences higher than 260 mJ/cm^2, the plume would show no reduction in length until punchthrough of the film had been achieved. Samples where processing was halted after the disappearance of the plume were measured for etch depth and compared with samples that had been irradiated with 40,000 pulses using the DekTak profilometer. No change in etch depth was found. This shows that the disappearance of the plume coincides with the cessation of ablation. Also plotted in Fig. 3.1 is the ultimate etch depth achieved after 3000 pulses at the given fluence. Fig. 3.1 shows that the saturated depth is proportional to the number of shots required for the plume to disappear. At higher fluences, the correlation is not as strong since the surface roughness is becoming comparable to the thickness of the film. On the samples where the fluence is above 200 mJ/cm^2 tiny pinholes of white light (in contrast to the orange color of the virgin film) can be observed through the sample if it is held up to a bright light. Some UV transmission can also be observed under continued excimer irradiation, though the transmitted signal does not continue to increase after ablation has ceased (i.e. the disappearance of the plume) and is in total magnitude at most 3% of the input energy. The reverse side of the sample is still fully intact, however, indicating that the deepest points are only near to puncturing the rear surface. Such deep points are not seen in the profilometer data indicating that the aspect ratio limitations of the probe have been exceeded for some areas of the surface. The determination of the etch
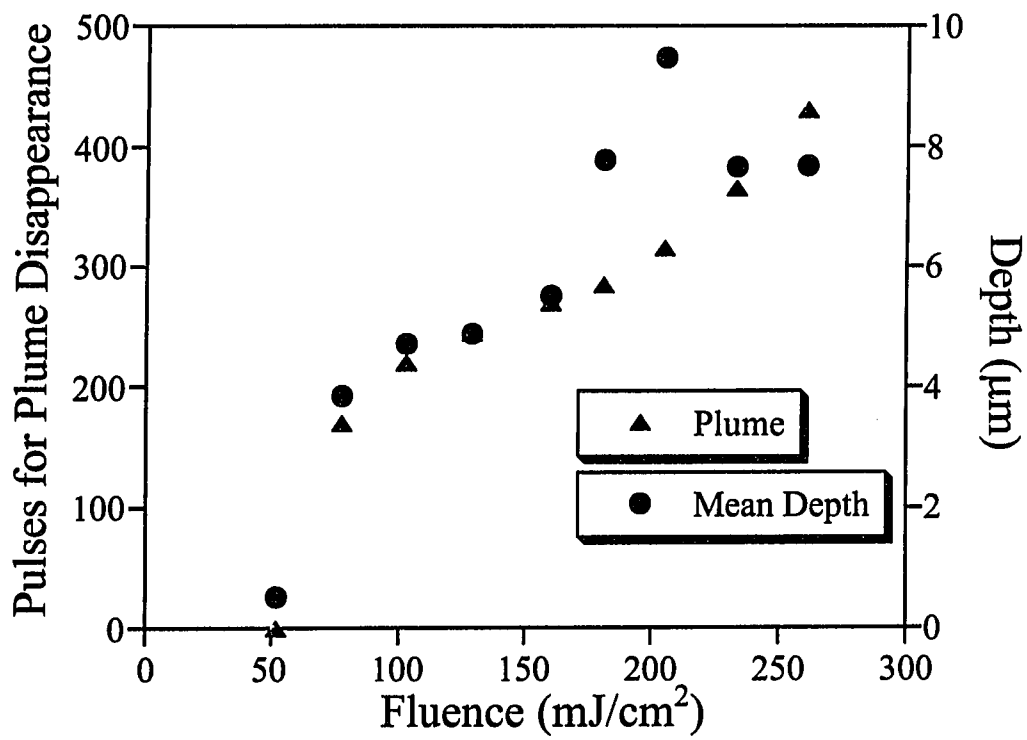
Fig. 3.1. The number of pulses for plume disappearance is shown as a function of fluence together with mean depth calculated from profilometry data taken from the same samples.

depths from profiles was therefore complicated by the large degree of surface roughness. The amount of surface roughness is strongly dependent on the laser fluence, and the etch depth was then taken simply as the average of the digitized profilometer data, the accuracy of which is therefore questionable for the measurements at the higher fluences.

In Fig. 3.2, three of the DekTak profiles from Fig. 3.1 are shown for fluences of 52 mJ/cm^2, 78 mJ/cm^2, and 129 mJ/cm^2. Each of these samples was irradiated 3000 times, well past that necessary for ablation to cease. The degree of roughness clearly has a strong relation to the laser fluence and thus to the ultimate limitation on etch depth. Such surface roughness is likely connected to the halt in ablation as the effective surface area over which the laser energy is deposited has greatly increased. Thus the effective fluence on the local level is much lower than the measured value. It is possible that the surface area has increased to the point that this effective fluence is below the ablation threshold of the modified polyimide.

To examine the cessation of ablation and the formation of surface roughness more quantitatively, a series of ablated spots were made for a few values of the fluence and several different numbers of laser shots. In Fig. 3.3 the etch depth is shown as a function of the number of shots for these samples where the etch depth was again measured with the profilometer. Clearly, at the beginning of laser processing the etch depth per pulse is constant and the etch depth increases linearly with the number of shots. As laser processing continues, however, the rate decreases and the etch depth approaches a limiting value. At the same time the surface roughness increases dramatically. This is indicated in Fig. 3.3 by the error bars which represent the standard deviation of the profilometer data.

The result of the irradiation process at fluences below 260 mJ/cm^2, then, is a rough black layer of carbon which conducts electricity. The formation of such a layer at low fluences (below 80 mJ/cm^2) has been studied extensively (Ball et al., 1994; Phillips et al.,
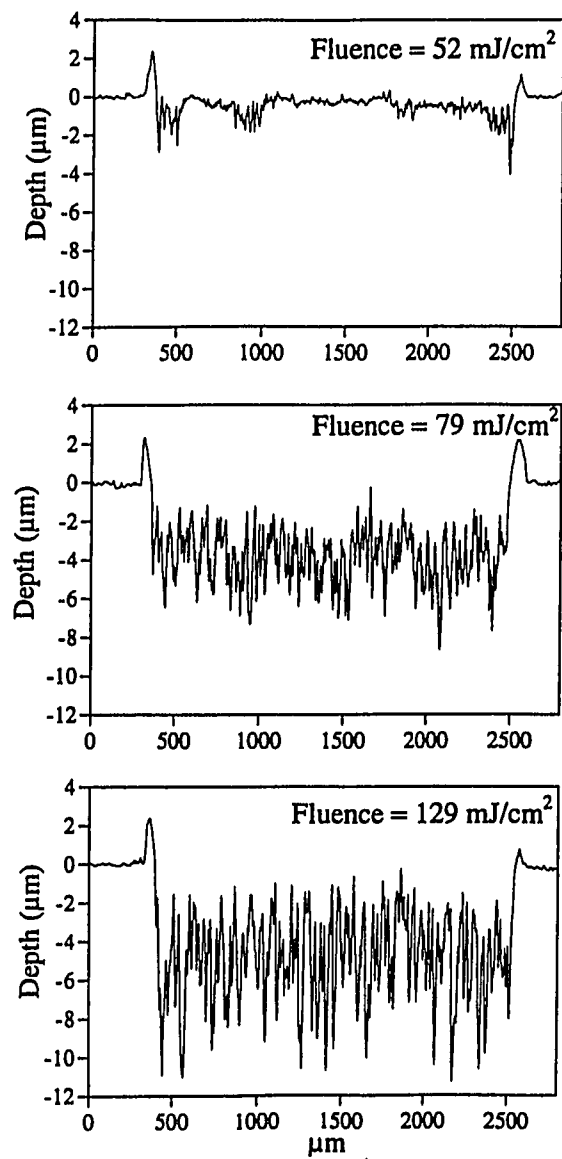
Fig. 3.2. Dektak profiles for samples irradiated 3000 times at a) 50 mJ/cm^2; b) 79 mJ/cm^2; and c) 129 mJ/cm^2.
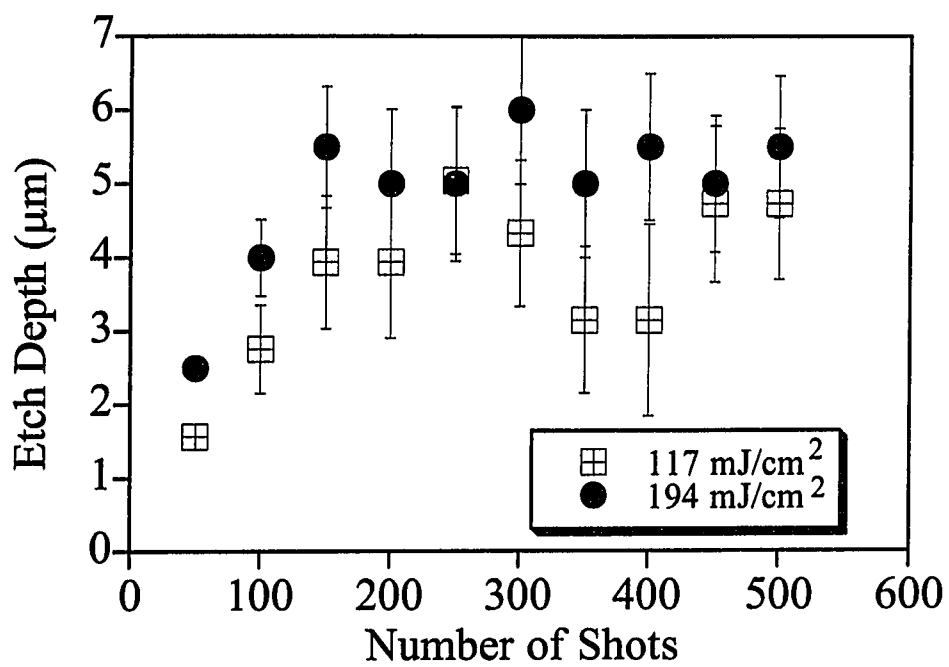
Fig. 3.3. Etch depth as a function of the number of laser shots. The error bars correspond to the surface roughness of the ablated spot ($\pm\sigma/2$).

1992; Feurer et al., 1993). There are two possible effects that could contribute to the ability of such a layer to resist further ablation: i) the carbon layer itself, as a different material altogether, may have different ablation properties, i.e., a higher threshold; ii) the increased surface area due to the surface roughness strongly reduces the effective fluence. A simple experiment demonstrates the two effects. A film was first irradiated at a low fluence (50 mJ/cm^2) with 5000 pulses just as in the well known laser induced electrical conductivity experiments. This spot was only about 1.5 mm in diameter. Then, with a much higher fluence (150 mJ/cm^2) the same spot was irradiated 5000 times but with twice the diameter. The DekTak profile of this sample is shown in Fig. 3.4. The interior section which was treated with the low fluence shows little etching while the surrounding area that did not receive the low fluence treatment was sharply etched. Thus the low fluence treatment provides an effective mask against ablation even at higher fluences than was required to create such a layer. However, the interior section has developed the same degree of roughness as the edges. A straightforward interpretation is that the carbon layer is highly resistant to ablation, though not uniform. Ablation can occur through gaps in this carbon layer. Such gaps do not allow cutting through the film however as the sloped sides reduce the effective fluence.

It is also possible, through formation of a carbon layer at lower fluences, to make a surface resistant to further ablation at fluences even higher than the 260 mJ/cm^2 threshold where cessation of ablation is not observed. It is of interest therefore to know what the ablation 'threshold' of the carbon layer is and if this threshold depends on the fluence used to create the layer. A simple experiment demonstrates the fluence dependence: a foil is first treated with a given fluence for 5000 pulses such that a carbon layer is formed. Then the sample is irradiated with a higher fluence for 5000 pulses as well. The experiment is then repeated for a series of higher fluences for each lower pre-treatment fluence. If the multiple shot ablation threshold of the preprocessed film is exceeded then a hole will quickly be
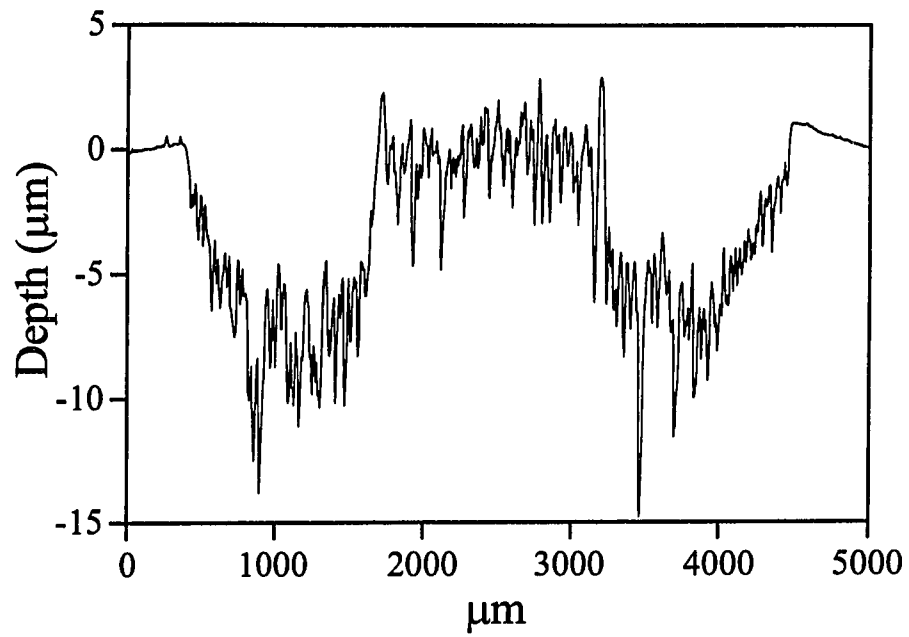
Fig. 3.4. DekTak profile of a sample that was first treated with a low fluence (small spot

size) and then treated with a high fluence (larger spot size). The low fluence treatment

effectively shields the surface from continued ablation.

drilled in the remaining polyimide film as the fluence in all cases is above the normal multiple shot polyimide ablation threshold. Such a method does not reveal the etch rate of the carbon layer but this would be difficult to determine in any case as the surface roughness becomes increasingly large with fluence. Fig. 3.5 shows the multiple shot threshold fluence determined in this way as a function of the pretreatment fluence. For low pretreatment fluences the multiple shot threshold of the sample is the same as that necessary to cut through a virgin film, 260 mJ/cm^2. For higher fluences, however the value increases rapidly to about 360 mJ/cm^2. The $\pm$ 5% error bars represent the error present in measuring the spot size which was different for each measurement as variation of the fluence was accomplished through changing the imaged spot size.

During such measurements it was observed that if a pretreated, blackened foil was irradiated with a high fluence (between 260 mJ/cm^2 and 380 mJ/cm^2), but only 50 pulses, that the black carbon layer had been removed. Continued irradiation produced a new carbon layer and the end result was the familiar blackened surface. This seems to indicate that it is the surface roughness, not the intrinsic properties of the carbon layer, that plays the greater role in cessation of ablation and that the carbon layer can be ablated whenever the effective fluence exceeds 260 mJ/cm^2. The results of Figs. 3.4 and 3.5 can also be understood in this way. An initially roughened (pretreated) film will reach the critical degree of roughness much faster than an untreated film leading to the enhanced resistance to ablation.

Therefore, what has been observed is that after a number of pulses, which is dependent on the fluence, ablation halts and that this cessation of ablation is accompanied by a dramatic increase in surface roughness which is also strongly dependent on fluence. If the fluence is greater than 260 mJ/cm^2, no halt in etching is observed and a clean hole can be etched in the film, and this value is termed the multiple shot ablation threshold. It has also been demonstrated that it is possible to make a surface resistant to ablation for fluences
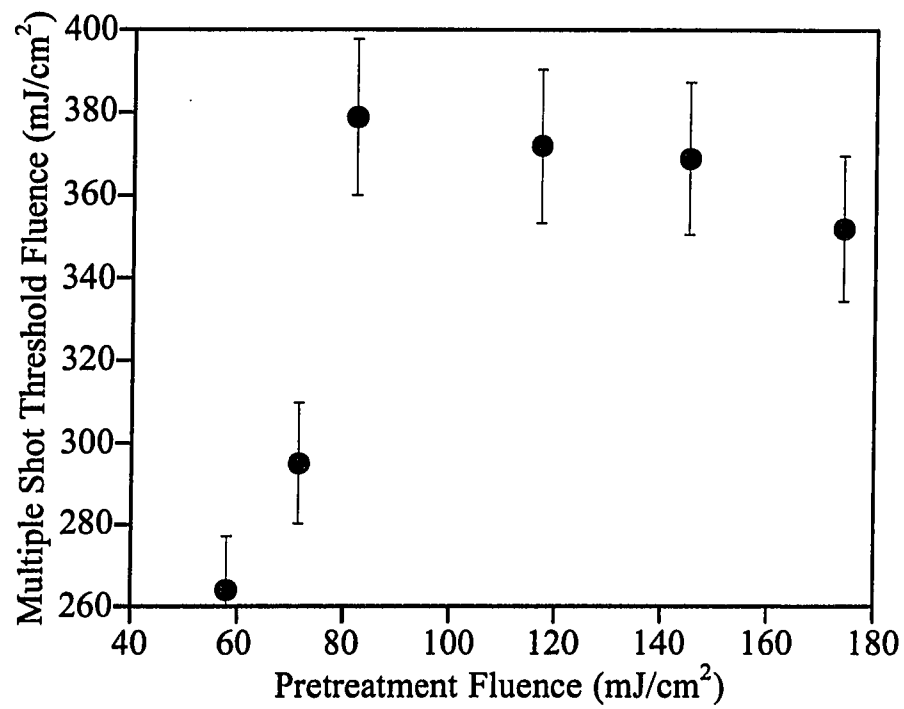
Fig. 3.5. The multiple shot ablation threshold (fluence necessary to penetrate the film) is shown as a function of pretreatment fluence. Error bars are from uncertainty in fluence measurements.

as high as 380 mJ/cm^2 through pretreatment at lower fluences and that this is most likely the result of the surface roughness created by the low fluence treatment.

3.2.2 Microstructure and electrical properties of the carbon layer: thermal coupling

If a polyimide sample, mounted on a metal or other thermally conducting sample holder, is irradiated at 1 Hz for 2000 pulses at a fluence of 50 mJ/cm^2, then the surface does not become electrically conducting. If a higher repetition rate of 5 Hz or a thermally insulating sample holder is used, then the sample does conduct. It would seem likely, therefore, that it is the accumulated residual heat of each laser pulse that is altering the properties of the carbon layer responsible for laser induced electrical conductivity.

To examine the effects of such thermal coupling several samples were prepared using different laser repetition rates and both thermally insulating and conducting sample holders. The thermally insulating holder was a quartz disc and the thermally conducting holder was a copper disk of roughly the same size. The 75 μm thick Kapton samples were taped to the holders in such a way that the film was in good contact with the holder surface and irradiated under identical conditions. Samples were irradiated at a fluence of 42 mJ/cm^2, and a square plastic mask was used such that a 5 mm by 5mm area of the surface was irradiated. The samples were irradiated with dry nitrogen gas blowing over the sample surface as the nitrogen improves the mechanical stability of the conducting layer (Feurer et al., 1993), and the sample was rotated within the irradiating beam for enhanced homogeneity. Fig. 3.6 shows the conductance of these samples. Clearly lower repetition rates (< 3 Hz) result in a sharply reduced electrical
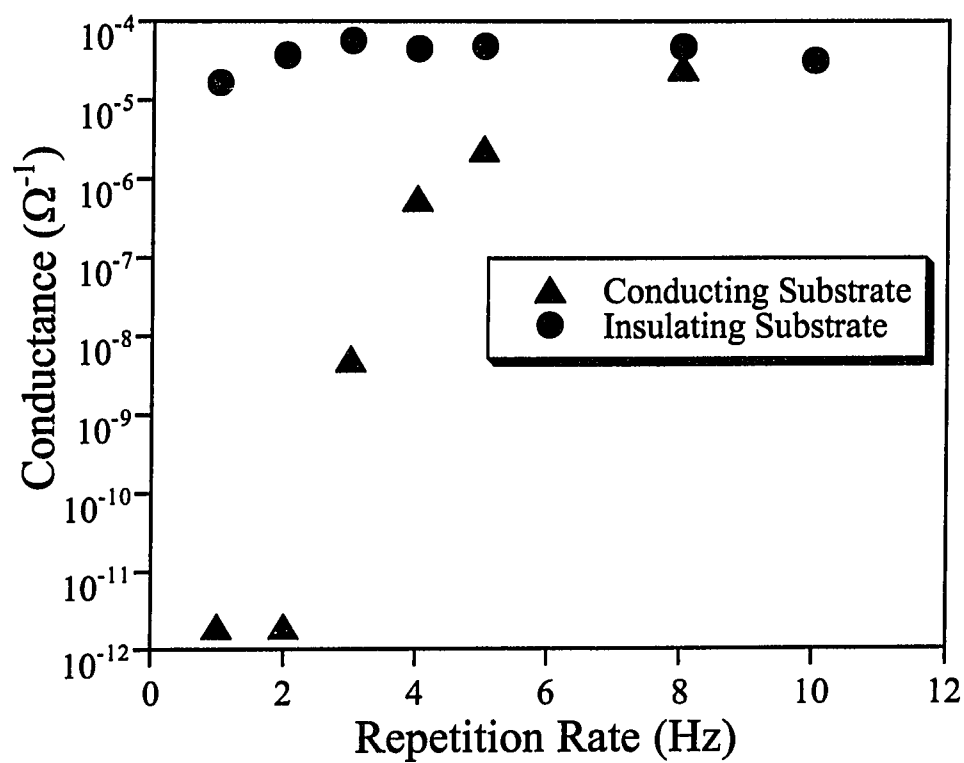
Fig. 3.6. Electrical conductivity as a function of repetition rate for a thermally conducting

and thermally insulating holder or substrate. The strong dependence of conductivity on

repetition rate and substrates suggest thermal coupling between pulses is a significant

effect.

conductivity for the conducting holder, while the conductivity of the samples prepared on the quartz substrates were uniform for all repetition rates tested. Further increases in repetition rate did not yield higher values of electrical conductivity for samples of either type up to the 25 Hz repetition rates tested. The lowest values in Fig. 3.6 represent the limitations of the measurement configuration and the real conductance may be even lower, approaching that of an unirradiated polymer film. Fig. 3.6 is certainly strong evidence that thermal coupling is important and highly sensitive to the boundary condition at the rear of the sample. While a reduction in conductivity is always observed for low repetition rates, the exact repetition rate dependence for the conducting holder is very sensitive to the experimental conditions. For example if the sample is rotated faster or a different mask is placed on the surface the effect can change significantly. The nitrogen gas also affects the results, particularly if the outlet is at a steep angle to the surface, however, the same basic behavior is observed in all cases.

As the outward appearance of the samples was the same, it is not obvious why the repetition rate was responsible for such an enormous change in properties. Therefore, further study of the microstructure of the conducting layer was necessary to understand the exact role the thermal coupling plays in the modification of the electrical conductivity.

In Fig. 3.7 transmission electron micrographs (TEM) of crossections of 75μm thick samples irradiated 2000 times at a fluence of 50 mJ/cm^2 are shown. The crossections were obtained by using epoxy to mount the sample between two silicon wafers which were then cleaved and etched back . The white areas above the samples are the epoxy.

In the first micrograph a sample irradiated at 1 Hz is shown. Here the surface exhibits some surface damage but there is no significant porous carbonaceous layer like that previously observed (Ball et al., 1994; Phillips et al., 1992). In the second micrograph, a sample irradiated at 5Hz is shown. The conducting layer appears as a diffuse region with a

a) 1 Hz

500 nm

b) 5 Hz

500 nm
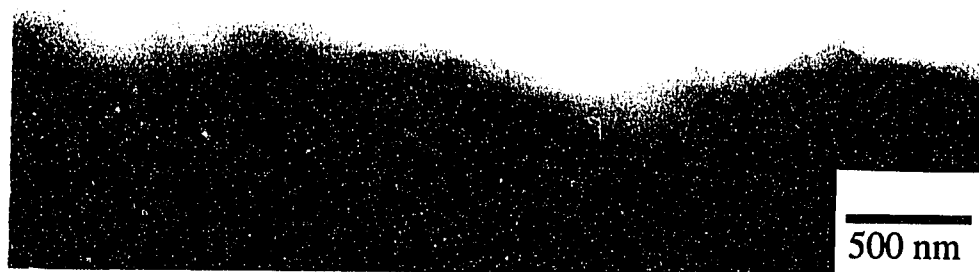
Fig. 3.7. TEM micrographs of crossections of irradiated polyimide samples. a) A sample irradiated at 1 Hz has a significantly different microstructure than b) a sample irradiated at 5 Hz.

density clearly much lower than the bulk polymer and is about 0.5 μm in thickness and is generally similar to that previously reported though perhaps more uniform (It should be noted that the layer is less dense than the bulk only in the sense that carbon matrix is highly porous and that the intrinsic density of the carbonaceous clusters that make up the conducting phase are actually much denser than the bulk polyimide.). In some samples layers thicker than 1 μm have been observed but with increased roughness (Ball et al., 1994). As the absorption depth of 248 nm radiation in polyimide is only about 50 nm, this indicates that decomposition of the polymer is present to a depth 10 to 20 times the radiation penetration depth. The absorptive properties of the differently treated samples are apparently the same though their microstructure, i.e., the density profile observed with TEM, is markedly different. Thus the microstructure shown in the TEM micrograph for the 5 Hz sample is likely the source of electrical conductivity, and it is clear that the formation of this structure is dependent on the thermal coupling between laser pulses.

3.3. Discussion and Analysis

3.3.1 Multiple shot ablation

The results of section 3.2.1 reveal three basic facts. First for KrF ablation of polyimide for fluences less than 260 mJ/cm^2, ablation only occurs for a given number of pulses and then stops. Second, the roughness of the surface increases during irradiation to a final degree that is strongly dependent on the fluence. Third, a layer of connected conducting carbon clusters is formed during irradiation. The exact contribution of the intrinsic properties of carbon and the geometrical properties of the surface to the observed halt in etching is difficult to determine experimentally, though some simple considerations will be presented here.

That the carbon layer exhibits a higher ablation threshold than the polyimide is easy to understand. Many carbonaceous materials, notably graphite, exhibit ablation thresholds much larger than that of polyimide for 248 nm radiation. Previous studies (Feurer et al.,

1993; Phillips et al., 1992) indicate that the carbon layer has properties somewhere between amorphous carbon and graphite and that it is best described as a phase that exhibits only short range order. Its ablation properties would therefore likely fall in the range between those of amorphous carbon and graphite.

The nonhomogeneous nature of the carbon layer is well established. Simple observation through a microscope reveals the broad and random distribution of islands in the first few tens of pulses. The electrical properties of the layer have been accurately modeled with percolation theory (Ball et al., 1994) which implies a truly disordered and inhomogeneous distribution of conducting carbon sites. Such sites (and gaps) have been directly observed by TEM in plan-view on a submircron length scale (Phillips et al., 1992). To what degree some parts of the carbon matrix may ablate, in addition to ablation through gaps, is difficult to determine.

Once the assumption of gaps in an ablation resistant layer has been made it is easy to see that ablation through narrow openings will not allow holes of indefinite depth to be drilled, even well above the fluence threshold. That geometry can so strongly affect ablation with strong positive feedback can be explained when one considers a simple Beer's law approach to the radiation transport which is justified close to threshold (Pettit et al., 1993). In the lower fluence ranges the etch depth per pulse, d, depends on the fluence, F,

$$d = \frac{1}{\alpha} \ln\left(\frac{F}{F_{th}}\right), \tag{3.1}$$

where F_{th} is the threshold fluence. If the surface is not flat then the incident fluence at a local level, assuming a constant energy, will not be constant and thus the etch depth per pulse will not be constant across the profile. Successive pulses will then produce further

modified etch rates according to the new profile. It is a straightforward matter to modify (3.1) to account for such considerations:

$$d(x,y) = \frac{1}{\alpha_n} \ln\left(\frac{F\dfrac{A}{A_n(x,y)}}{F_{th,n}} \right).$$ (3.2)

By introducing a local area function A(x,y) we allow the fluence to vary according to the morphology of the irradiated surface. Then the effective local fluence is then the measured fluence multiplied by the spot size, A, divided by the local area function. The etch depth resulting from a single pulse will thus vary across the rough surface. Because of the role of the carbon layer, the threshold fluence and absorption depth will also change with the number of shots and in a spatially inhomogeneous way. Equation (3.2) does not represent an ablation depth since the profile and thus A(x,y) will change with each incident pulse and (3.2) must then be applied iteratively to produce successive profiles. As the surface continues to roughen the value of A(x,y) will increase both locally and over the whole profile. After a number of pulses the numerator will be smaller than F_{th} and further etching will not occur. If such is the case then the surface area of the final surface (after ablation has ceased) should depend linearly on the fluence used to create that surface. An estimate of the surface area of each profile taken for Fig. 3.1 was calclulated and is shown as a function of fluence in Fig. 3.8. That the surface area increases linearly is evident, particularly when one considers how far from linear the etch depth is in fluence in Fig. 3.1. The degree of increase in surface area calculated is not sufficient to reduce the fluence below the ablation threshold. This is not particularly surprising since the roughness on smaller lengths scales than measureable by this technique could easily dominate the overall value of the surface area. Surface roughness on the scale of 1 μm has been observed previously through TEM (Ball et al., 1994).
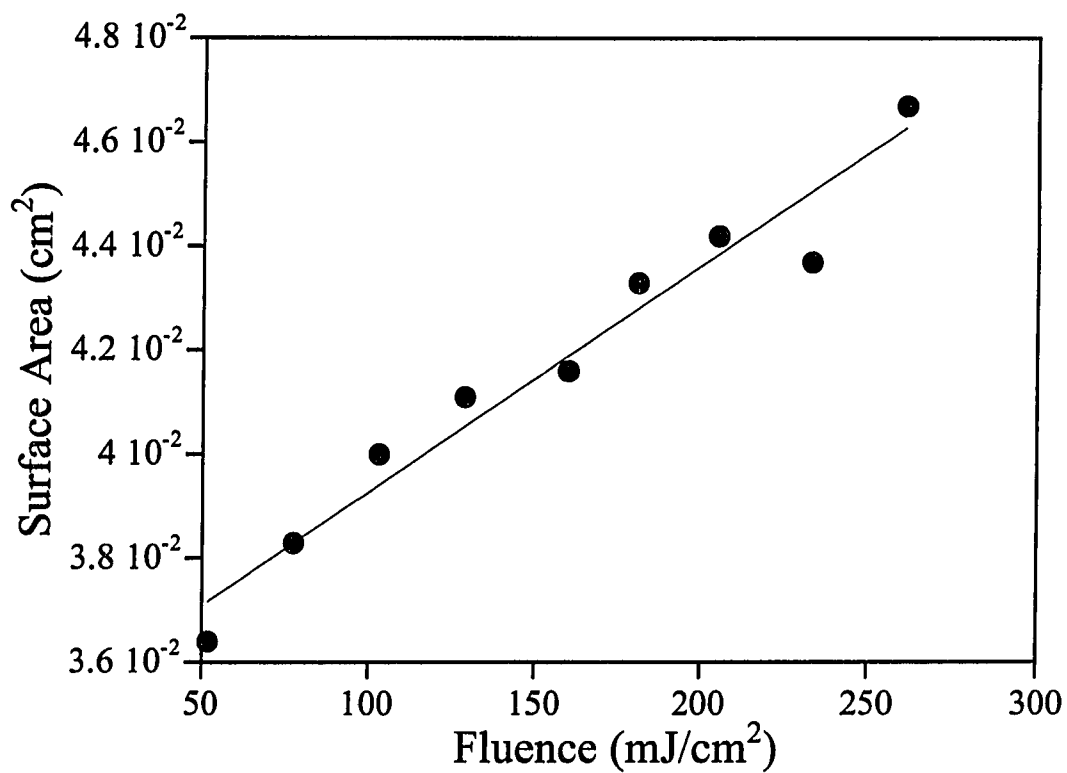
Fig. 3.8. Surface area calculated from DekTak profiles in figure 2 are shown as a function

of fluence. The linearity of the graph supports the idea that increasing surface area plays a

large role in the cessation of ablation.

One objection to such a model is that peaks in the roughness should ablate faster than slopes and iteration should lead to a flat surface. This is the case only if the peaks are relatively blunt, but in the case of laser ablation exceedingly sharp peaks can be produced. Experimentally, the peaks are certainly sharper than the 3 μm resolution of the profilometer used in these measurements. In the present experiments this is also where the role of the different properties of the carbon layer becomes important.

It should also be considered why at higher fluences (above 260 mJ/cm^2) the effect goes away and smooth surfaces and clean etching penetrating the film is observed. Three effects may contribute: i) the shock wave produced from the ablation reaches a magnitude that ejects all decompositon products leaving no initial roughening or shielding material, ii) the ablation threshold of the carbon material itself is in this range and iii) For higher fluences, as the slope of the etch depth per pulse versus fluence curve becomes increasingly flat with increasing fluence, the difference in etch rate for fluences separated by a constant value decreases with increasing fluence. Without a large difference in etch rates for different fluences, enhancement of roughness through equation (2) is clearly undermined. The second point is strongly supported by the observation from section 2.1 that pulses with fluences above 260 mJ/cm^2 ablated the carbon layer produced at lower fluences and formed a new carbon layer with subsequent pulses.

That higher fluences (> 200 mJ/cm^2) yield smooth surfaces was one of the first observations in excimer laser ablation of polyimide (Koren and Yeh, 1984) . The discrepancy in the exact fluence (200 versus 260 mJ/cm^2) is likely due to the fact that in these experiments we are looking at the combined effects of hundreds of pulses and the initial studies looked at the surface after only a few or even 1 pulse.

Rough surfaces produced by fractures, metal deposition, or even sand blasting and erosion are often described by the theory of self-affine surfaces (Gouyet et al., 1991). Self affine surfaces are closely related to scale invariant objects or fractals but are invariant only

with respect to dialation in one dimension. The scaling properties of such surfaces are usually described by the height correlation function C(r),

$$C(r) = < (\ h(r + r_0) - h(r_0) \ )^2 >$$ (3.3)

where h is the height of a point, r some point on the surface. C(r) is then obtained by averaging over all points on the surface r_0. For large r, the correlation function converges to $2\sigma^2$, where σ is the standard deviation of the distribution of points. The point in r where C(r) converges to this value is the correlation length, ξ, and marks the upper limit where scaling relations are valid. Using the values of the one dimensional profile given in Fig. 3.2 (c), C(r) is plotted in Fig. 3.9. The expected behavior is found with a simple scaling law for small values of r converging to $2\sigma^2$ which is shown as a horizontal line in the figure. The correlation length, ξ, is about 20 μm and the scaling exponent of C(r) for small r can be readily deduced to be about 1.1. We conclude, therefore, that polyimide surfaces produced by laser ablation may be described as self-affine surfaces. A more detailed analysis of the scaling properties of these surfaces may be fruitful since equation (3.2), if correct, is a simple analytical expression that could yield exact theoretical results for a variety of input profiles which could be compared to experiments. Future work may establish the universality class of such a surface and compare the detailed results to other models of deposition and erosion.

3.3.2 Thermal Coupling

To determine why a change in repetition rates of only a few Hertz so dramatically alters the electrical properties of the carbon, a simple thermal analysis can be performed to estimate the temperatures present.
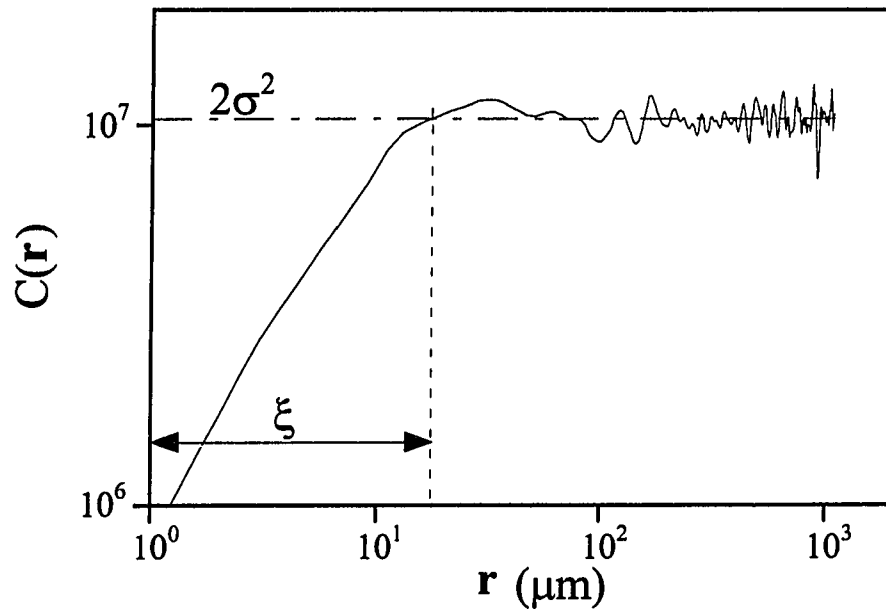
Fig. 3.9. The height correlation function (equation 3.3) is shown as a function of **r** on a

log-log scale. The scaling region is identified by the correlation length ξ, at which point the

the uncorrelated surface gives a steady value related to the standard deviation.

We begin with the one dimensional homogeneous thermal diffusion equation on the interval 0 to sample thickness D of the x-axis,

$$\frac{\partial^2 T}{\partial x^2} + \frac{\rho c}{\kappa}\frac{\partial T}{\partial t} = 0 \qquad (3.4)$$

taken with the boundary conditions $T(D,t) = 0$ and $\dfrac{\partial T(0,t)}{\partial x} = 0$ and initial condition $T(x,0)$ $= \dfrac{\alpha F_0}{\rho c}e^{-\alpha x}$. These conditions correspond to an instantaneous, spatially distributed heat source at the surface of the sample and an efficient heat sink at the back side of the sample. As we are interested in the thermal effects at times long compared to the pulse width of the laser pulses (200 ms compared to 15 ns), the time dependence of the pulse is neglected and replaced with the instantaneous temperature derived from the deposited energy density. Equation (3.4) may be solved readily by separation of variables with a Fourier series solution.

Utilizing the linearity of the thermal diffusion equation, the temperature present to a depth x after n laser shots for a repetition rate R at a time just before the next (or $n+1^{th}$) excimer pulse can be expressed as

$$T_n(x,n/R) = nT(x,1/R). \qquad (3.5)$$

The maximum temperature experienced by the polymer at a given depth is therefore given by adding the temperature due to thermal coupling given by (3.5) to the contribution from the last pulse at its maximum which occurs at a time of approximately $t = x^2\dfrac{\rho c}{\kappa}$,

$$T_{max}(x,n/R) = T_n(x,n/R) + T(x, x^2\frac{\rho c}{\kappa}). \qquad (3.6)$$

In Fig. 3.10 the situation is depicted schematically .The temperature is shown as a function of time for a fixed point in depth for four excimer pulses. The single pulse solution to (4), T(x,t) is shown for comparison on the first shot. Each laser pulse on this timescale appears as an impulse function and the slow decay of each increases the background temperature according to (3.5), yielding the sum (3.6) for the correct maximum temperature.

Though there are many simplifications in such a simple model such as the use of room temperature physical constants, neglecting the role of diffusion and convection at the surface, and the assumption of a perfect heat sink on the back side of the sample, the correct time dependence and an order of magnitude estimate of the importance of thermal coupling should be attainable with such a model even within even these limitations. In Fig. 3.11, the maximum temperature given by (6) is plotted as a function of depth for n = 500 (corresponding to roughly the number of pulses needed to observe electrical conductivity) laser pulses for various repetition rates. The sample thickness D was put at 75 μm to correspond to the experiments while the standard room temperature values were used for the physical parameters of thermal conductivity, κ = 0.12 W/(mK), specific heat, c = 1.09 J/(gK), and density, ρ = 1.42 g/cm^3.

Fig. 3.11 indicates that thermal coupling can play a role in the maximum temperature and has the effect of causing enhanced temperatures to be present at depths comparable to the decomposition depths seen in Fig. 3.7, but only for repetition rates greater than 5 Hz. Though not quantitatively accurate, it is clear that thermal coupling begins to play a role at repetition rates close to those in the experiments. If we consider that the thermal contact in the experiment is not perfect and the experimental observation of the sensitivity to thermal properties of the rear boundary and other experimental conditions, it seems plausible that such significant coupling could occur in the range of 3 to 5 Hz.

What is also evident from the analysis is that the thermal coupling is probably not responsible for the decomposition itself. The coupling broadens the temperature profile to
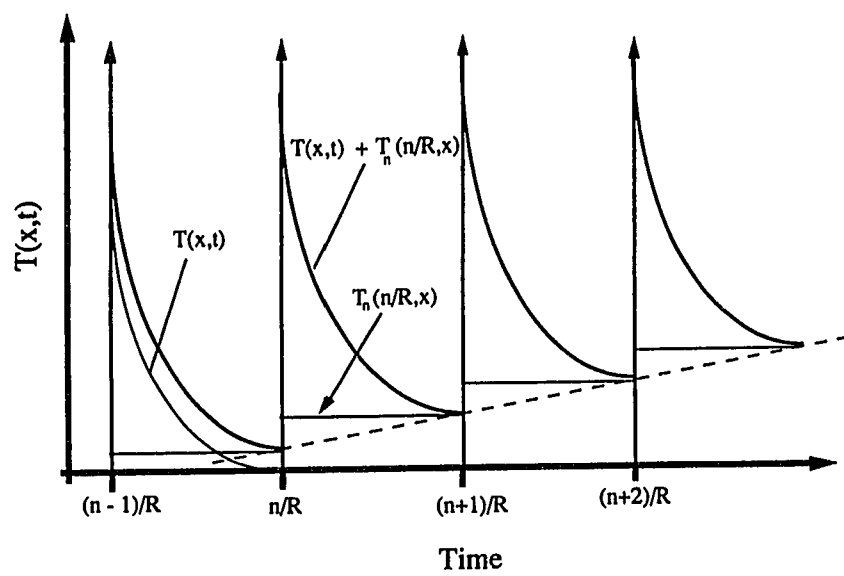
Fig. 3.10. Schematic of temperature calculation for four impulses. The background
temperature increases with each pulse
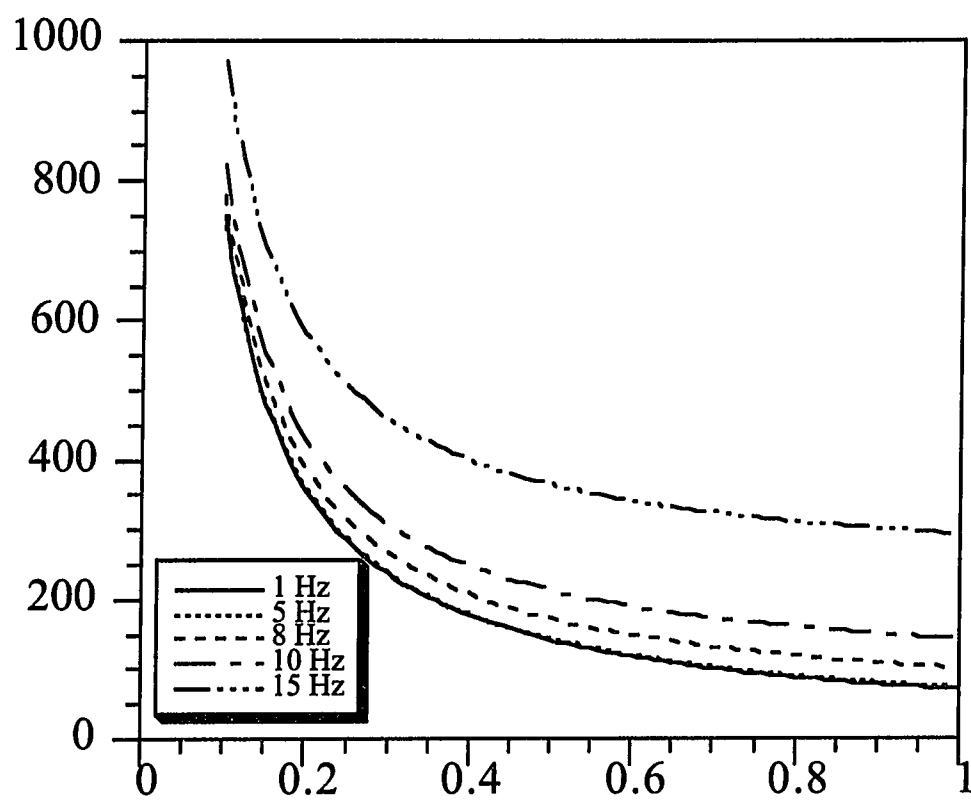
Fig. 3.11. Maximum temperature as a function of depth is shown for a series of repetition rates.

depths exceeding that observed in the crossections and the absolute value of the temperature is not particularly higher than the decomposition temperature of the polyimide (600°C) even for repetition rates of 10 Hz. One can also consider the observation in Fig. 3.6 that further increases in repetition rate even far beyond 5 Hz do not result in higher conductivities even though such increases would create high temperatures much deeper into the polymer. The effect of the thermal coupling is most likely in promoting the formation of clusters of six member carbon rings (which are electrically conducting) from the disordered carbonaceous remains of the decomposed polymer. Evidence in the next chapter will show that the carbon clusters responsible for conductivity form only some tens of nanoseconds after the excimer laser pulse where enhanced background temperatures of a few hundred Kelvins due to coupling could play a large role in determining their structure and properties.

3.4 Conclusion

The effects of multiple shots in excimer laser processing of polyimide have been examined. Mechanical coupling in the form of enhancement of surface roughness and a robust carbon matrix results in cessation of ablation after several hundred pulses for fluences below 260 mJ/cm^2. The increased surface roughness increases the effective area over which the laser energy is absorbed eventually to the point that the effective fluence is lower than the ablation threshold. The role of thermal coupling was also examined and found to impact the electrical properties of the conducting carbon layer that forms on polyimide during laser processing. TEM analysis demonstrated that the microstructure of the surface layer was strongly dependent on the repetition rate and thus the thermal coupling. Simple thermal modeling indicates that the role of thermal coupling is to raise the background temperature by a few hundred degrees at the surface which, though not sufficient to induce further decomposition, may facilitate the formation of conducting clusters.

The issue of competition between ablation and conductivity modification is made clear by these results as well. Ablation in the regime from 20 to 260 mJ/cm^2 is complicated by the carbonaceous material that is the result of decomposition but not ejected from the surface, and the threshold measurement in by Küper et al. (1993) of 20 mJ/cm^2 is indeed accurate but the measured etch 'rate' is valid only in the case of a single or a few pulses. Therefore for processes involving many shots, such as laser induced electrical conductivity or ablation through thick films, a simple extrapolation of single shot measurements does not always apply to multiple shot processes.

The results of this study also suggest new applications for laser induced electrical conductivity and ablation of polyimide. The ability to create a conducting surface with such a high degree of roughness may be useful as an electrochemical electrode. Work along these lines using argon ion laser irradiation appears promising (Srinivasan et al., 1994), and those results might be improved upon with the techniques discussed here, particularly since the fluence can be used to directly control the degree of roughening. One of the primary motivations for the study of polyimide is its attractiveness for use as a low dielectric constant material in packaging and metallization applications, and a primary difficulty with such applications is adhesion between polyimide and copper layers. If excimer laser processing were employed such a rough conducting surface would be ideal for the plating of high resolution interconnections with good adhesive properties. Such a process was developed and is presented in chapter 5 The scaling properties of such surfaces may offer a promising experimental technique for the study of self-affine surfaces as the physics of the generation of such surfaces is well defined and since the individual parameters of the roughness generation can be specified experimentally.

CHAPTER FOUR

TRANSIENT OPTICAL PROPERTIES OF LASER IRRADIATED POLYIMIDE

4.1 Introduction

To better understand the formation of the conducting layer in laser irradiated

polyimide, time delayed pump probe experiments were used to observe changes in optical

properties with time. In this chapter measurements of reflectivity, transmissivity, and

scattering are presented and related to the dynamics of laser processing. The interaction of a

high power laser pulse with a highly absorbing organic substance is complicated by

chemical reactions that occur in the extreme thermodynamic conditions created by the high

energy density present in the absorption depth of the polymer. It has been observed that

the optical properties, i.e., the reflectivity, of the surface are dramatically altered during

excimer laser irradiation (Klopotek et al., 1987; Singleton et al., 1990; Parakevopoulos,

1991; Ediger et al., 1993; Hahn et al., 1994; Ediger and Pettit, 1992) In this chapter we discuss experiments using electronically delayed dye laser pulses to probe the time dependence of changes in optical properties of the polyimide during and immediately after excimer laser irradiation. There were two basic results of this study. First, a transient refractive index change during the first 150 ns after the incident excimer laser pulse was found and related to the dynamics of the ablation process. Second, the time dependence of the increase in scattering resulting from the formation of the carbon crystallites responsible for laser induced electrical conductivity was found.

4.2 Transient refractive index during excimer irradiation

The aforementioned studies have examined the reflected excimer pulse in an attempt to characterize the dynamics of the ablation mechanism since changes in optical properties may be sensitive to the details of the ablation process. The various organic materials irradiated in these studies exhibited a dramatic decrease in reflectivity early in the excimer pulse. In particular it has been observed that the reflected portion of the excimer pulse in ArF irradiated polyimide is truncated after a fluence threshold of 24 mJ/cm^2 is reached (Singleton et al, 1990). The time dependence of the reflectivity has been studied (Ediger and Pettit, 1992) but the lack of knowledge of the behavior of transmission and scattering seriously limits the conclusions that can be drawn from these observations. In addition these previous measurements were performed at fluences significantly higher than the present work where the influence of the plume cannot be entirely separated from the change in optical properties. Because of the strong absorption at excimer wavelengths, transmitted light could not be used to determine if the effect was due to an index of refraction change, scattering, or absorption. A recent study has eliminated scattering as a possible explanation (Ediger et al., 1993). The time dependence of the phenomenon is perhaps the most revealing quantity that can help determine the origins of the effect. Also, by studying transmission as well as reflectivity we can establish whether the effect has its origins in a

time dependent refractive index, as has been proposed (Singleton et al., 1990), or some type of transient absorption process. In this section, measurement of the detailed time dependence of this phenomenon through time resolved transmissivity, reflectivity, and scattering measurements with visible dye laser probe pulses is reported.

4.2.1. Experimental Method

The experimental method employed is illustrated in Fig. 4.1 for the case of a transmission measurement. The most homogeneous part of the output of a Lambda Physik EMG 102 MSC ArF excimer laser (193 nm, 15 ns FWHM) was selected by a 3 mm aperture. This aperture was then imaged (1:1 image) onto a 0.8 μm thick polyimide sample on a quartz substrate. The probe beam, a nitrogen laser pumped dye laser (pulsewidth of 1 ns), was passed through the sample at an angle of 45° before entering a PIN photodiode detector. The time delay between the dye and excimer lasers was controlled electronically with an accuracy of ± 5 ns. The majority of experiments were performed with a coumarin 47 (461 nm) dye laser although nile blue (695 nm) and an ArF pumped fluorescein dye laser (520 nm, pulsewidth of 2.5 ns) were used in certain cases. A 461 nm interference filter was placed in front of the detector to reject light at wavelengths different from the probe, and sufficient attenuation was used to assure operation in the linear range. The absorption of the 461 nm probe pulse through a 0.8 μm polyimide film was measured to be only 17% while absorption is negligible at 695 nm. In the case of reflectivity measurements a similar arrangement was used at an incident angle of 45°. A thicker 75 micron foil was used to avoid reflections from the back surface of the foil since absorption of 461 nm light through the 75 μm polyimide foil is essentially 100%.

The time dependence of changes in transmission, reflectivity, and scattering was investigated for fluences between 30 and 35 mJ/cm^2. The value of the transmitted, reflected, or scattered signal was recorded on ten successive shots at the given delay. An
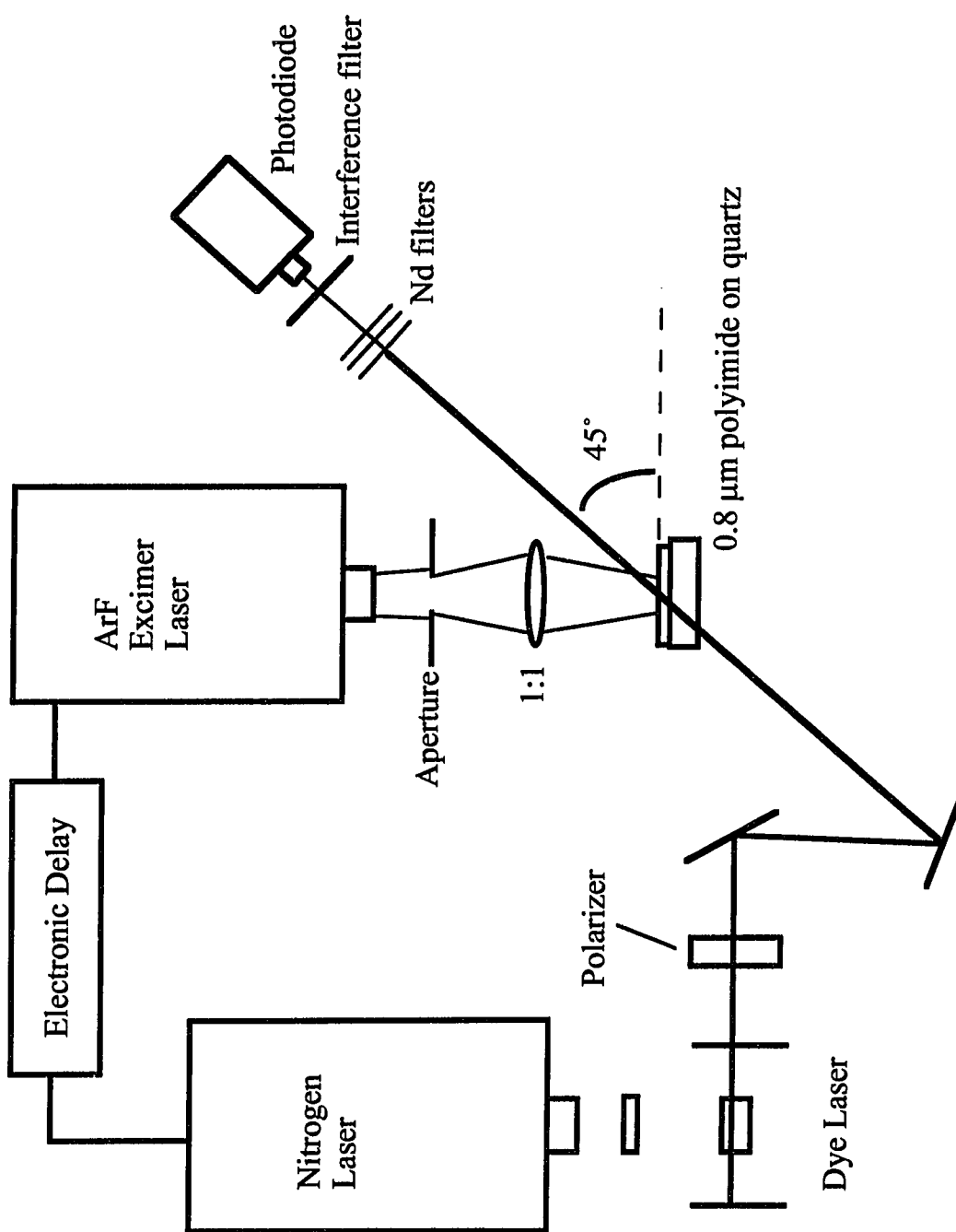
Fig.4.1. Experimental setup for time-resolved transmission measurements.

average of several dye pulses after the excimer pump pulse was recorded as well, corresponding to the value of the signal at long times.

4.1.2 Results

The results of the transmission measurement are shown in figure 4.2 where the transmitted signal, T_{delay}, normalized to the average transmitted signal before the excimer probe pulse, T_0, is shown as a function of delay. First we notice that at short time scales the transmissivity of the sample increases significantly, clearly indicating that there is no significant increase in absorption in the first 150 ns. This effect was observed with three separate dye laser wavelengths at 695 nm, 520 nm and 461 nm as well as in vacuum. An ArF pumped fluorescein dye laser (520 nm) was used with a spatial delay for the shortest time delays and the effect was determined to begin even before the peak of the excimer pulse. The onset of a dark area at 8 ns in ultrafast photography of XeCl ablation of polyimide (Simon et al., 1989) corresponds closely to these observations as does a similar dark region observed in KrF ablation of PMMA (Srinivasan et al, 1989). By 150 ns the transmission begins to decrease below the pre-irradiation value corresponding to increased absorption or scattering from the presence of carbon from the decomposed polymer (Ball et al., 1994; Feurer et al., 1993).

In Fig. 4.3 the reflectivity is shown as a function of delay. Here the reflected signal, R_{delay}, normalized to the value at long delays, R_{avg}, is shown as a function of delay where each point represents an average of ten successive excimer pulses just as in the transmission measurements. At the earliest delay of 20 ns the signal has decreased by more than two thirds its initial value of 14% and subsequently the effect decays on a time scale consistent with that observed in the less accurate transmission measurement. The basic time dependence observed is likewise consistent with that obtained by Ediger and Pettit (1992) using a broadband Xe flashlamp as a light source, however, their observation that the reflectivity does not recover to its pre-ablation value until 1 ms after irradiation is not found
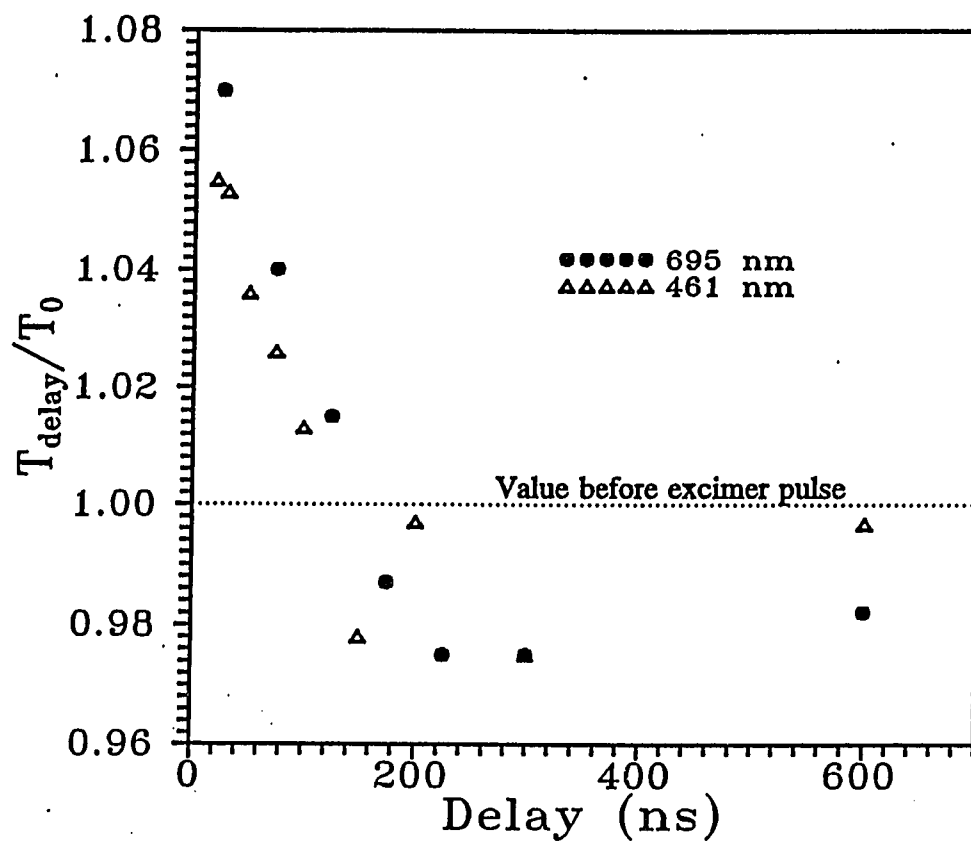
Fig. 4.2. Normalized transmission of the dye laser pulse as a function of delay from excimer laser pump pulse. The dashed line is the value before the excimer pulse.
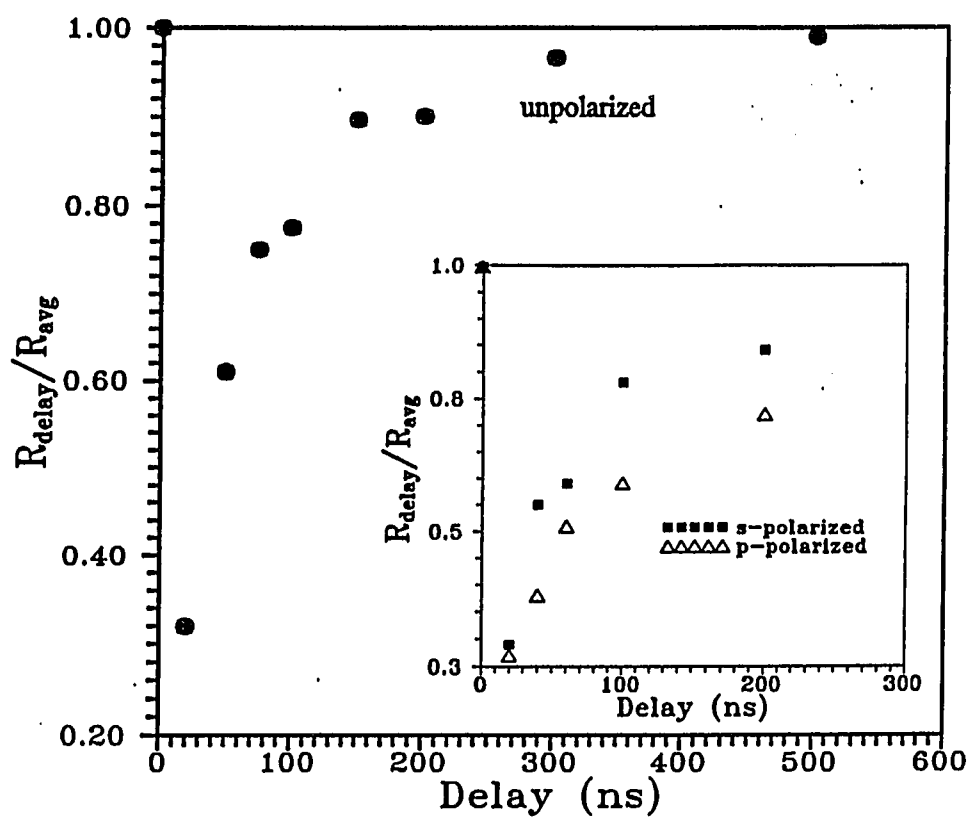
Fig. 4.3. Reflectivity normalized to the value at long times as a function of delay. The inset shows the dependence for polarized probe pulses.

here. The most likely explanation for the discrepancy is that the higher fluences (110 mJ/cm^2) used in the study led to plume formation and considerable material removal which in turn attenuated the probe pulse in the interim time.

Since the Fresnel equations predict that the reflectivity change for p-polarized light may be enhanced due to the movement of the Brewster's angle if an index of refraction change is present (particularly since the angle of incidence used in these experiments is relatively close to the Brewster's angle), the polarization dependence of the time resolved reflectivity was investigated as well. The results are shown in the inset to figure 4.3. For all but the first data point at 20 ns, the p-polarized light signal decreased more strongly. The observation of a stronger effect for the p-polarization is therefore consistent with the Fresnel equations if a change in refractive index at the surface is assumed. (Note that each point in figure 3 is normalized independently such that the differences between s and p reflectivity present in the figure are only due to the presence of the excimer laser pump beam.)

Because of the greater precision of the reflectivity measurement, the time dependence can be examined in more detail. It is clear that a single exponential decay does not agree with the data as the initial relaxation is more rapid than at later times. The fast decay is estimated to be about 60 ns and the slow decay to be about 115 ns. This may indicate that two competing processes are the cause of the change. A similar time dependence has been observed in detailed studies of acoustic waves in excimer laser irradiated polyimide (Dyer and Srinivasan, 1986; Zweig et al., 1993). In the work by Zweig et. al. (1993), this time dependence was explained by considering rapid expansion of gases during irradiation and mass diffusion as the fast relaxation. The slower process of thermal diffusion is attributed to the longer decay. Such a picture is consistent with the observed refractive index change as well. One would expect that the initial expansion responsible for a powerful acoustic event would result in a drastic change in density which

could effect optical properties just as dramatically. It is also reasonable to expect that slower relaxation through thermal diffusion would have a measurable but less dramatic effect on the refractive index.

The fluence dependence of the reflectivity change was also investigated. The delay was fixed at 14 ns after the peak of the excimer pulse, a time at which the change in reflectivity is large. In order to avoid jitter between the probe and the excimer pulse, a fluorescein dye laser (520 nm, puslewidth of 2.5 ns) pumped by the excimer laser was used with a spatial delay line. The result is shown in figure 4.4. Here a sharp threshold is observed around 30 mJ/cm^2 before which the reduction in reflected light is rather modest and above which it is quite drastic. In ArF ablation of polyimide, large scale material removal only occurs at a threshold fluence of 25 to 30 mJ/cm^2 (Dyer and Sidhu, 1985; Lazare and Granier, 1989; Gorodetsky, 1985) although mass losses have been detected at fluences as low as 14 mJ/cm^2 (Küper et al., 1993). Above this type of ablation threshold, the type of explosive gas pressure from the rapid decomposition of the polymer that could be responsible for a dramatic index change would likely be present. Beneath this threshold, however, one would expect only the less dramatic thermal effects to remain which is consistent with the data of figure 4.

Although scattering has been discounted as a cause of the decreased intensity of the reflected excimer pulse by Ediger et al. (1993), the scattering signal was analyzed as well. The experimental setup was similar to that of Fig. 4.1 where a beam stop was added after the sample. The scattered light was then imaged onto the detector with an additional lens. In Fig. 4.5 scattering data is shown for the shortest time scales. Here the change in the scattering signal, normalized to the total change in scattering signal measured at long times (an average of many dye laser pulses), is shown as a function of delay. What is striking about figure 4.5 is that the scattering signal *decreases* on a time scale similar to that of the

reflectivity. Though less precise than the reflectivity measurements it is obvious that the

signal decreases over this same time frame. Therefore, an increase in scattering of the
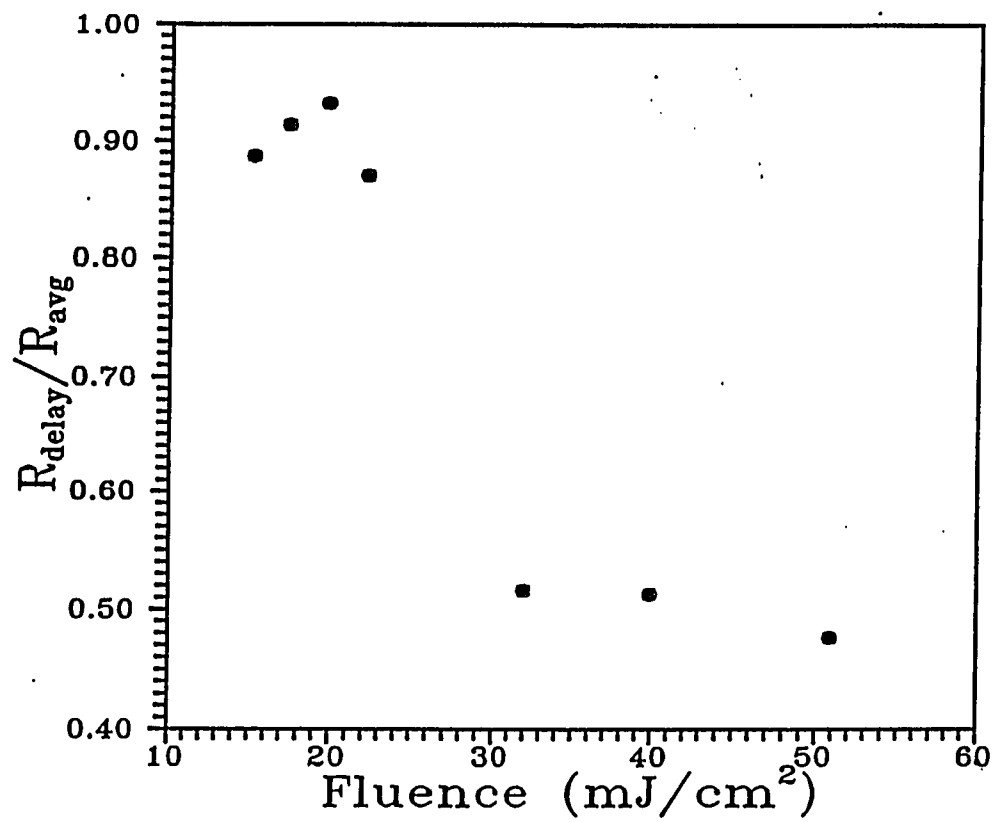
Fig. 4.4. Reflectivity as a function of excimer laser fluence. A sharp threshold is seen as fluence passes the ablation threshold.
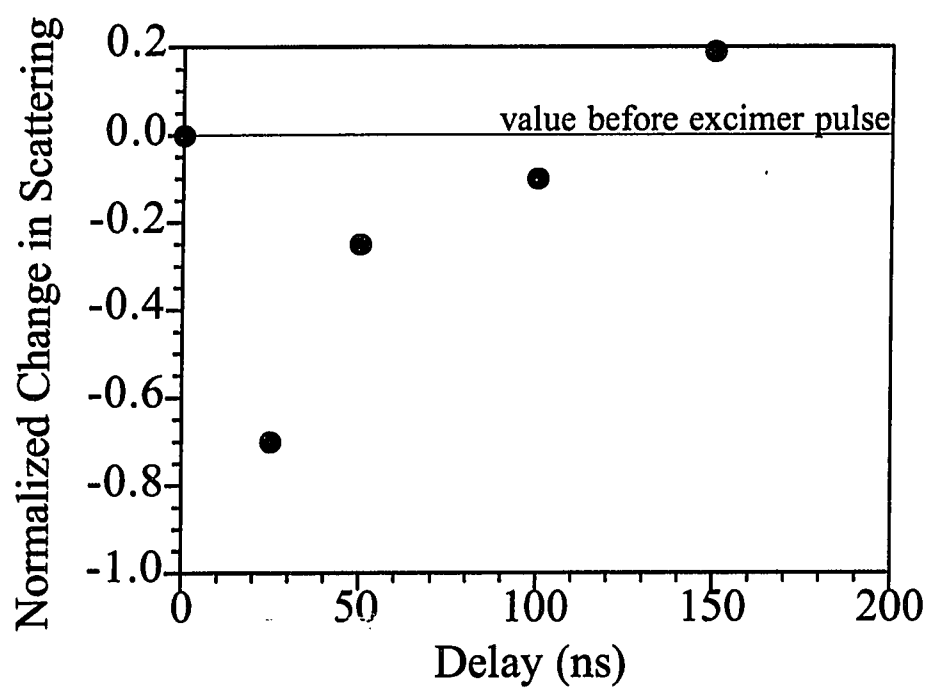
Fig. 4.5. Normalized change in scattering as a function of delay.

surface layer could not account for the decrease in reflectivity. These results corroborate the observation by Ediger and Pettit (1992) that the truncated reflected pulse signal and the scattering signal have the same pulse shape and duration. It should also be noted that the total magnitude of the scattered light is substantially less than the transmitted signal, indicating that the observed increase in transmission cannot be explained by the decrease in scattering.

4.2.4 Transient Refractive Index Profiles

There are only four things that can happen to the probe pulse light: reflection, transmission, scattering, and absorption. We have observed that the reflectivity of the surface during excimer laser irradiation decreases substantially and that the transmision simultaneously increases. These changes are such that from our measurements we see quantitatively that all the light which disappears from the reflected pulse appears in the transmitted pulse to within the error of the measurement. The inevitable conclusion is that absorption and scattering are not cause of this remarkable decrease in reflectivity but a change in the refractive properties of the polymer surface. Specifically, the measured reflectivity of the unirradiated surface with the same apparatus and same angle of incidence was 14% of the total probe pulse. The change in reflectivity at the shortest delay of 20 ns indicates that about 2/3 of the reflected signal (9% of the total incoming probe pulse) disappears. The transmission was observed to increase typically by 7%, just enough to account for the decrease in the reflected signal within the error of the measurements. Furthermore, few differences were observed in the effects for the wavelengths used (460-695 nm). It is also clear that the magnitude of this change is quite large given that the reflectivity decreases by as much as two thirds its original value.

The reflectivities of various index profiles were modeled using the effective matrix method outlined in Born and Wolf (1980). First, a Gaussian interface was assumed, that is, where the refractive index is given by

$$n(z) = n1 + (nf - n1)(1 - \exp[-(\alpha z)^2]),$$ (4.1)

where n1=1 is the index of the ambient medium, nf = 1.7 is the index of the bulk

polyimide, z is the depth into the surface, and α is a parameter. In Fig. 4.6 this profile is

plotted as a function of z for a value of $\alpha = 1/70$ nm^{-1}. The wavelength of probe pulses

used in the model was 461 nm. The interface defined by (4.1) or any other function is first

divided into d layers of thickness h each with a constant refractive index given by (4.1) and

labeled n_j. For each layer a characteristic matrix is defined,

$$\mathbf{M}_j(h) = \begin{bmatrix} \cos(k_0 n_j h \cos(\theta)) & -\frac{i}{p}\sin(k_0 n_j h \cos(\theta)) \\ -ip\sin(k_0 n_j h \cos(\theta)) & \cos(k_0 n_j h \cos(\theta)) \end{bmatrix},$$ (4.2)

where h is the thickness of the layer, θ, the angle of incidence, and k_0, the magnitude of

the incident wave vector. For a Transverse Electric wave, or TE wave, p is given by

$$p = \sqrt{\frac{\varepsilon}{\mu}}\cos(\theta)$$ (4.3)

where μ and ε are the electrical permitivity and magnetic permeability respectively. For the

case of a Transverse Magnetic wave, or TM wave, p is defined by,

$$p = \sqrt{\frac{\mu}{\varepsilon}}\cos(\theta).$$ (4.4)

Equations (4.2) to (4.4) are a direct and exact result from Maxwell's equations for a

nonabsorbing dielectric and will transform a column vector of field amplitudes accordingly.

The effective matrix for a series of dielectric layers is then found by simply multiplying the

effective matrices of the constituents together following the rules of matrix multiplication,

$$\mathbf{M}_f = \mathbf{M}(1)\mathbf{M}(2)...\mathbf{M}(d).$$ (4.5)

The amplitude reflection and transmission coefficients can then be derived from the

elements of the effective matrix:
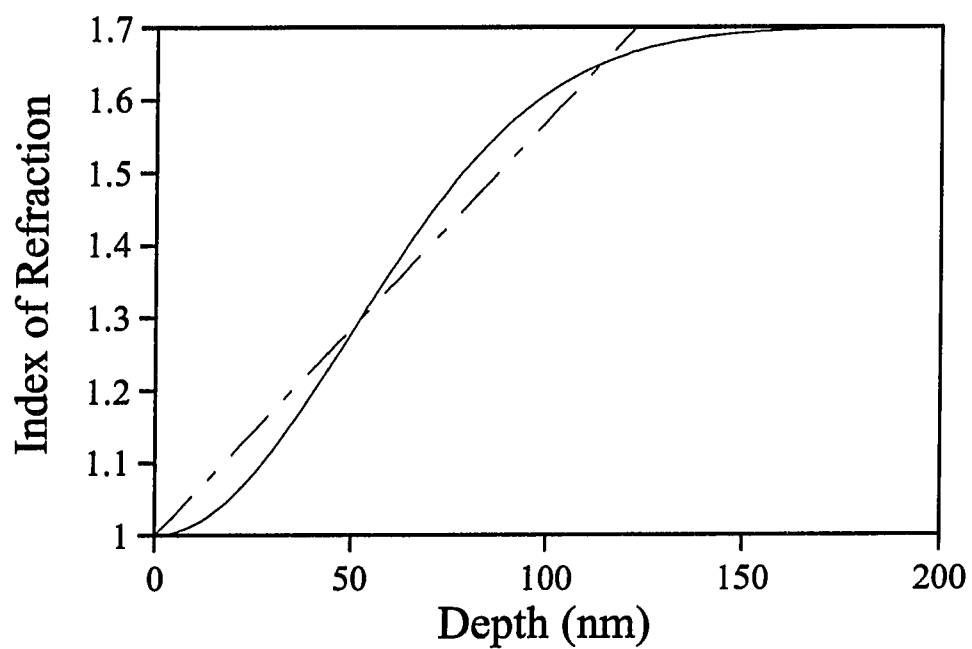
Fig. 4.6. Index of refraction as a function of depth calculated from equation (4.1). A parameter of α = 1/70 nm^{-1} was used corresponding to values obtained from experiments. A linear profile is shown for comparison with slope 1/175 nm^{-1} also corresponding to experiments.

$$r = \frac{(m_{11} + m_{12}p_f)p_i - (m_{21} + m_{22}p_f)}{(m_{11} + m_{12}p_f)p_i + (m_{21} + m_{22}p_f)}$$

$$t = \frac{2p_i}{(m_{11} + m_{12}p_f)p_i + (m_{21} + m_{22}p_f)}$$

(4.6)

Where p_i and p_f are the values of p for the first and last layers respectively. With the treatment shown here an arbitrary index profile can be modelled including the Gaussian profile of (4.1). The magnitude reflectivity $|r|^2$ is plotted in Fig. 4.7 as a function of angle for various values of the parameter α. Fig. 4.7 (a) is for TE polarization and Fig 4.7 (b) is for the TM polarization.

Corresponding to the experiments, a reduction in reflectivity of approximately 60% is found for an angle of incidence of 45° when α is set to 1/70 nm^{-1}. This value is interesting since it is close to the absorption depth of 193 nm radiation (1/64 nm^{-1} when measured from ablation rates (Jellinek and Srinivasan, 1984)). Greater reductions are found when α is decreased. If a linear index profile is used (n = n1 + αz), a value of α = 1/175 nm^{-1} must be used to achieve the same reduction in reflectivity. When the relative change in reflectivity for the two polarizations are compared the results of figure 3 are also recovered with the relative change of p-polarized light being substantially larger for an angle of incidence of 45°.

While the conclusion that the observed changes are due to a transient change in refractive index is strongly supported by the experimental results, it is not clear what mechanism is responsible for the change. It was suggested by Hahn et al. (1994) that a change in refractive index could be due to saturation effects similar to that presented in chapter 2. Simple calculations with the model presented predict significant saturation at the surface, even at the low fluences used in the present experiments. This model is not entirely satisfactory, however, as it does not explain the sharp fluence dependence at 25 mJ/cm^2 observed in the present work and by Singleton et al. (1990). The theory predicts significant
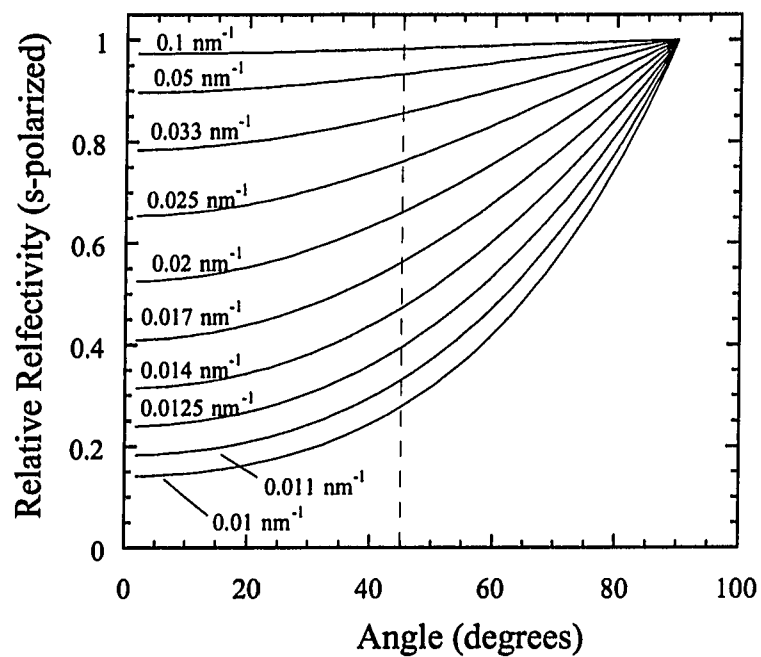
Fig. 4.7(a). Reflectivity of a Gaussian interface relative to an abrupt interface as a function of angle for s-polarized light. The vertical dashed line is a an angle of 45° corresponding to the experiments.
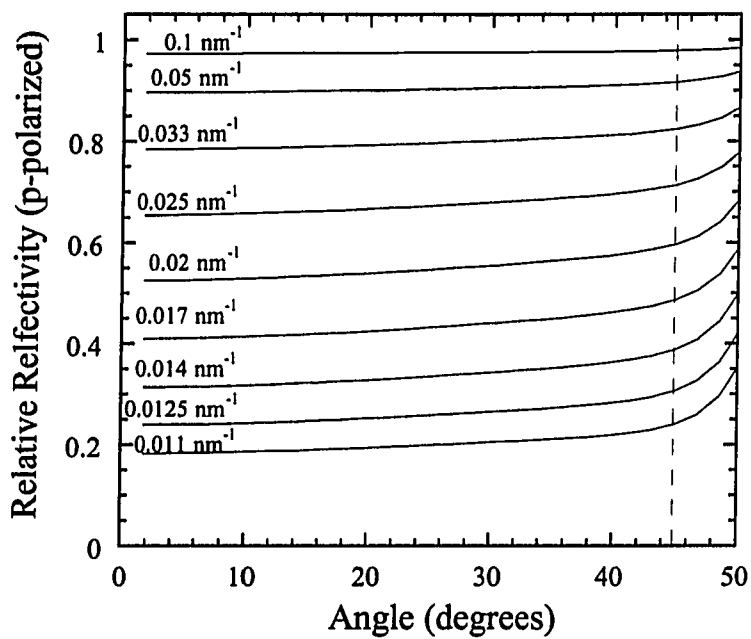
Fig. 4.7(b). Reflectivity of a Gaussian interface relative to an abrupt interface as a function of angle for p-polarized light. The vertical dashed line is a an angle of 45° corresponding to the experiments.

depletion of the ground state at this and lower fluences as well where the change in optical properties is not observed (at a fluence of 10 mJ/cm^2, the ground state at the surface is depleted by more than 20%). It should be noted that ground state depletion affects more than just the absorption coefficient. Both the real and imaginary parts of the refractive index are dependent on the ground state density and saturation effects therefore necessarily affect both. In the present experiments where polyimide is transparent to the visible probe pulses, it is clear that the dominant role would have to come from the real part while those experiments dealing with the reflectivity of the excimer pulse itself at highly absorbing UV wavelengths would be influenced by the change in both the real and imaginary part. As the influence of the properties of the upper state on the refractive index are not known quantitatively, it is impossible to compare the saturation model with the experimental results. It is likely in light of previous experiments (Pettit et al, 1994), that ground state depletion does occur, however, whether this effect is responsible for the observed refractive index change must be the subject of further study.

Given the correspondence in the fluence threshold of the reflectivity reduction with known ablation thresholds, it is likely that the index of refraction change is related to decomposition of the polymer during the laser pulse . The decomposition of the polymer takes place at a minimum in the absorption depth of the 193 nm radiation. If this were to create a density gradient over approximately the same distance, then a reflectivity decrease of the type observed in the experiments would be found. The correspondence of the time dependence with the thermal relaxation of the polymer as discussed above would also be explained well by this model.

Another possible explanation may lie in the extreme temperatures present in the laser irradiated samples. If the polyimide were to undergo some type of phase transition and if this new phase were to have significantly different optical properties, many of the observed phenomena could be explained. The time dependence of the reflectivity change is

similar to the thermal relaxation time as one can see in calculations such as in Fig. 4.10. The thermal diffusion length during the 30 ns pulsewidth is approximately 50 nm and would be sufficient to account for the observed changes on the reverse side of the thin 90 nm samples used in Hahn *et al.* (1994). Clearly such an effect, having a critical temperature, would have a sharp fluence dependence as well. Perhaps most interesting is that a phase change could explain why the scattered light intensity decreases on the same time scale as the reflectivity. It is not clear how either of the first two explanations, ground state depletion or decomposition at the interface, could account for this observation. As polyimide does not melt, the results here cannot correspond to phase transition induced changes such as with metals and semiconductors discussed in chapter two. However, as the effect is only present at fluences where decomposition of the polymer is occurring, a phase transition in the carbonaceous remnants of the polymer is possible. As these remnants are mostly carbon, an investigation of the optical properties of amorphous and partially ordered carbon would show if this is a real possibility.

It is clear that several extreme conditions are present in laser irradiated polyimide and that any or all of them may contribute towards the observed refractive index change. These are an intense flux of photons which can deplete the ground state, high temperatures (> 1000 °C), and rapid thermal decomposition.

4.2.5 Summary

Time resolved transmission, reflectivity, and scattering measurements of ArF excimer laser irradiated polyimide were performed to investigate the orgin of the previously observed transient decrease in reflectivity under irradiation. A sharp increase in transmission and a decrease in scattering were observed for time delays less than 150 ns while an even more dramatic decrease in reflectivity is observed with a similar time dependence. These three observations demonstrate that the refractive index of the polyimide interface is significantly altered by the laser-polymer interaction. The fluence

dependence of the reflectivity change exhibits a threshold like behavior near the ablation threshold, and the specific time dependence was found to be consistent with results from acoustic measurements. Three possible mechanisms are discussed: rapid thermal decomposition at the air-polymer interface, ground state depletion, and a thermal phase transition.

4.2 Carbon cluster formation

In order to understand the processes that give rise to the conducting carbon clusters their time of formation should be known. When this is compared to temperature calculations it is possible that a greater understanding of the properties of the layer can be gained. In particular the peculiar repetition rate dependence of the conductivity discussed in chapter 3 may be a consequence of the time dependence of the cluster formation.

The carbon layer formed by excimer irradiation of polyimide has been studied with transmission electron microscopy (TEM) and the conducting crystallites were observed directly. These crystallites were found to be approximately 50 nm in diameter. Electron diffraction patterns from the same study revealed an increasing degree of short range order in samples with a limiting case of polycrystalline graphite (Phillips et al., 1992). The term "crystallite" is therefore used loosely here denoting only localized concentrations of carbon with short range order, not the presence of an actual crystalline lattice. Crossections of 75 μm Kapton films that have been irradiated at 248 nm indicate that the layer of carbon clusters can be as thick as 1 μm, significantly larger than the absortion depth of excimer radiation.

The experimental arrangement for the measurement of scattering is shown in figure 4.8. The sample, a 0.8 micron thick polyimide film on a quartz substrate, is irradiated by an ArF laser pulse of fluence 30 to 35 mJ/cm^2 and pulse width of approximately 15 ns. The most homogeneous portion of the beam is selected by a 3mm aperture and imaged
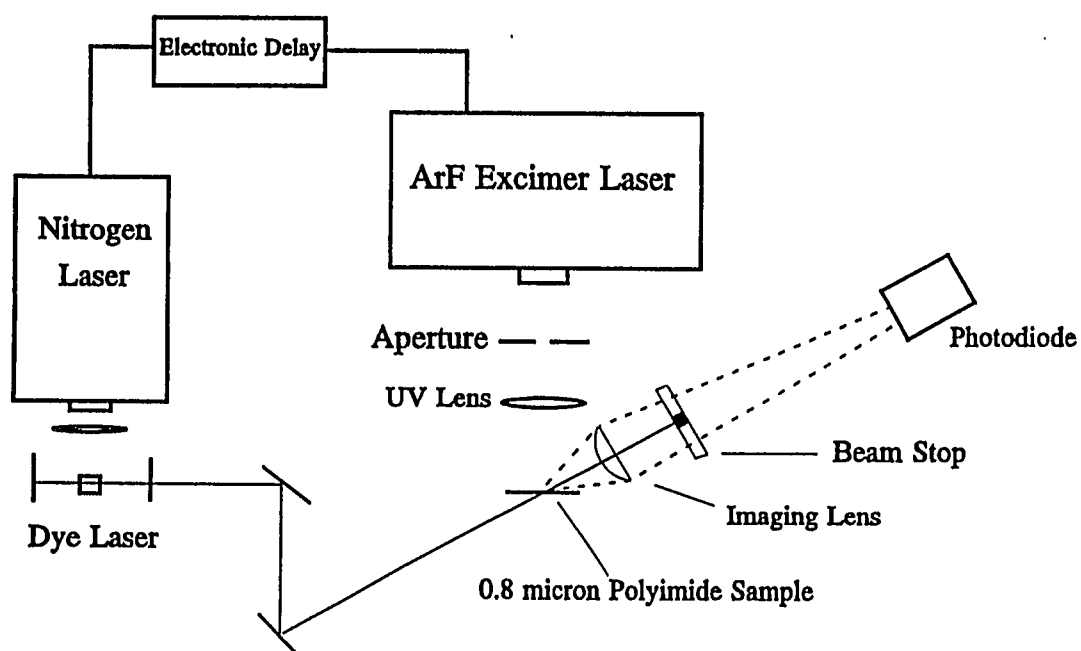
Fig. 4.8. Experimental arrangement for the measurement of time-resolved scattering

(1:1) onto the sample. The output of a nitrogen laser pumped coumarin 47 dye laser at 461 nm (pulse width 1 ns FWHM) is passed through the sample from the reverse side at an angle of approximately 45°. The beam is then blocked at the focus of a lens positioned to image the irradiated sample onto a PIN photodiode detector. The time delay between the dye and excimer lasers is controlled electronically to an accuracy of ±5 ns. In front of the detector a 461 nm interference filter was placed to insure that the only light collected was that from the scattering of the dye laser beam. In the case of transmission measurements additional attenuation was used to insure operation of the detector in the linear range. In this manner the scattered intensity could be measured at delays from 10 ns to 100 microseconds. Transmission measurements were performed in the same manner by simply removing the beam stop and imaging lens. In transmission measurements, a longer wavelength of 695 nm (nitrogen laser pumped nile blue) was used in addition to the 461 nm, corresponding to a region of much higher transparency of the polyimide film. Results indicated little difference for the two values of the wavelength. The absorption coefficient for 461 nm radiation in polyimide was measured with a spectrometer to be approximately 0.4 μm^{-1}. Absorption in polyimide is negligible for 695 nm. Therefore essentially 100% of the 695 nm beam is transmitted through an unirradiated 0.8 μm sample and 72% of the 461 nm beam is transmitted through such as sample. Although ArF irradiation is used to produce this effect for the first time in the present work, there is little evidence that there are significant differences between the carbon layer formed by this wavelength and that previously reported at 248 nm (Schumann et al, 1991; Feurer et al., 1993; Phillips et al, 1993).

The total change in scattering after each laser shot was investigated in order to determine the best conditions for the time resolved measurement. The scattering signal, averaged over many dye laser shots, was measured after excimer pulses on a shot to shot basis for several values of the laser fluence. The result of these measurements is shown in
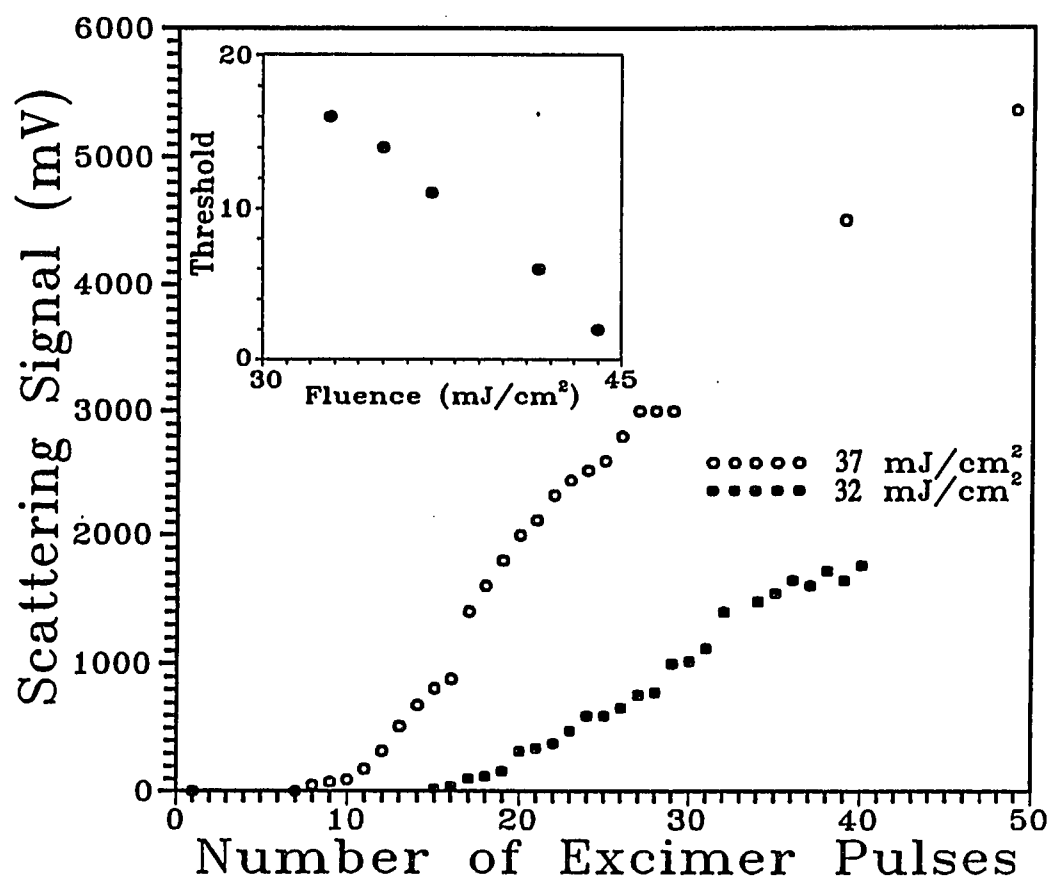
Fig. 4.9. Scattering signal as a function of the number of excimer laser pump pulses.

Fig. 4.9 where the scattering signal is plotted versus the number of laser shots. Each point represents an average of 64 dye laser pulses. The threshold behavior is likely related to the percolation nature of laser induced electrical conductivity. The scattering signal of the unirradiated film has been subtracted from the data. Initially no change in scattering is observed. After several excimer pulses, a threshold is reached and the scattering signal increases. Eventually a saturation behavior is observed as a significant portion of sample has been transformed. The slope of the curve and the threshold are both strongly dependent on the laser fluence which is the reason fluences between 30 mJ/cm^2 and 35 mJ/cm^2 were chosen for the time dependent measurements. At fluences higher than 35 mJ/cm^2, significant ablation of the film could take place during the first 50 excimer pulses and distort observation of the formation of the carbon layer. The inset shows the fluence dependence of the threshold in scattering. It was observed on samples which were carefully examined under an optical microscope after each excimer pulse that the increases in scattering were correlated to discoloration of the sample which is the result of carbon cluster formation. The discoloration of the samples is expected to be a bulk effect under these conditions because the thickness of the carbon layer has been measured on other samples to be about 1 μm in thickness (Ball et al., 1994) which is more than the thickness of these films. It is possible that some of the scattered light could be the result of some roughening of the surface due to the presence of the disordered carbon layer in lieu of a smooth polymer surface. However, in section 4.2, we found that after an initial, sharp decrease, the reflectivity recovered to almost the same value as before irradiation within 150 ns, indicating that surface roughening could play at best a minimal role.

The appearance of a threshold in the scattering intensity may be explained by considering the percolation nature of the process. It has been shown previously through TEM studies that the conducting layer consists of carbon crystallites of < 50 nm diameter, the density of such crystallites increasing with each excimer laser pulse (Ball et al., 1994).

In isolation the crystallites would not be efficient scatterers in that they are significantly smaller than the wavelength of the dye laser probe pulse. From percolation theory however we realize that the size of *clusters* of these randomly placed scattering centers increases with each excimer pulse. When this cluster size approaches the wavelength of the probe pulse, the efficiency of the scattering will increase dramatically. For example, the scattering efficiency of a sphere, as a function of radius, increases very sharply as the probe wavelength is approached. For radii greater than the wavelength the scattering crossection goes only as the square of the radius (Deirmendjian, 1969). Therefore, when the density of clusters whose linear size is larger than the wavelength becomes significant, a threshold would be observed in the scattering signal. As the value of the probe wavelength is small compared to the size of the sample, the scattering threshold appears well before the conductivity threshold of 400 laser shots. As it has been shown that the number of sites produced by each excimer pulse depends on the laser fluence it is clear that this threshold should be fluence dependent as well (Feurer et al., 1993). It should be noted that a thorough analysis of the scattering of a disordered system with scaling properties extending from sizes smaller than the wavelength to sizes much larger than the wavelength would be quite complex, particularly when one considers that the complex dielectric constant of the constituent particles is unknown and might vary with cluster size as well.

The time dependences of changes in transmission and scattering were then investigated for fluences between 30 and 35 mJ/cm^2. For each value of the temporal delay, a separate area of the same 0.8 micron thick polyimide film was irradiated by the excimer laser until the scattering threshold was reached. The value of the scattering was then recorded on ten successive shots at the given delay. An average of the scattering signal was also recorded after each pulse. The results are shown in Fig. 4.10 for a probe wavelength of 461 nm where the change in scattering signal is shown as a function of delay. Here the change in scattering is normalized to the value of the change in scattering at effectively

infinite delay, the average of several dye pulses after each excimer pulse. Therefore a value of 1 in Fig. 4.10 corresponds to a change in scattering at the given delay equal to the change in scattering observed at infinite delay while a value of zero corresponds to no change in scattering at the given delay. First we notice that at short time scales the change in scattering is negative. This effect may be due to processes that produce the transient refractive index change in the irradiated layer that is described in the previous section. The change in scattering becomes positive after 150 ns and increases to its final value at about 400 ns. We conclude, therefore, that carbon crystallites form during this period.

Shown in Fig. 4.10 along with the scattering data is a normalized temperature curve calculated from the Green's function solution of the heat diffusion equation with room temperature physical constants as discussed in chapter 2. Although heating on nanosecond time scales to 1000° C or higher temperatures is surely a nonequilibrium thermodynamic event, this simple temperature model serves only to illustrate the basic time dependence of the thermal diffusion. The limitations of such a simple model are obvious given the vast temperature and chemical changes occurring in the material, not to mention the time scales involved. A further limitation of the model is the thin (0.8 μm) nature of the samples, this is not a pressing concern since the thermal diffusion length in polyimide over 400ns is about 180 nm (calculated with room temperature physical constants) which is significantly less than the sample thickness. Even given these concerns, it is clear that the formation of scatterers occurs in a region after thermal diffusion has caused significant cooling in the irradiated layer.

The transmission measurements were performed in a similar manner to the scattering measurements except that no initial excimer pulses were used. The results of the time resolved transmission experiment have already been shown in Fig 4.2 where the transmitted signal, normalized to the value before the excimer pulse, is shown as a function of the delay. For short time scales there is a sharp increase in transparency which is due to
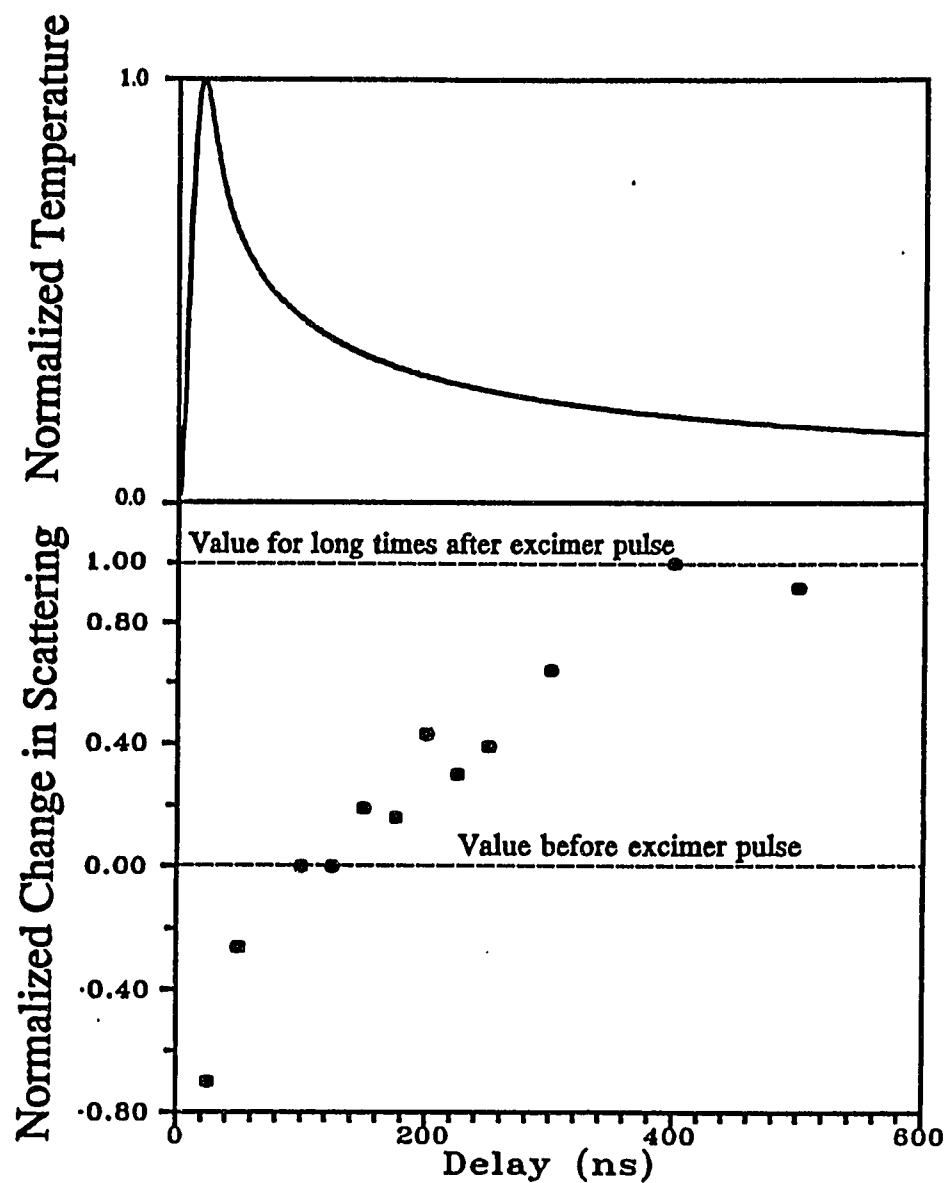
Fig. 4.10. Change in scattering normalized to the value at infinite time is shown as function of delay. The scatterers are shown to form in 400 ns. A simple temperature model is shown for comparison.

the time dependent refractive index. At about 150 ns, the value of the transmission has decreased to below its initial value indicating increased absorption from the presence of carbon from the decomposing polymer.

The time dependence of the formation of the crystallites is now clear. Decomposition of the polymer begins some time before 150 ns after excimer irradiation. The refractive index changes occurring before 150 ns reported in the previous section obscure measurement of the scattering or absorption from carbon such that some ambiguity exists for these shorter delays. At 150 ns there is a concentration of disordered carbon which becomes increasingly ordered into the crystallites from 150 ns to 400 ns. Such a picture is consistent with the fact that these crystallites can be produced in different carbon rich materials since the crystallites form only after the polymer has been degraded into carbon.

Etch rates of 280 Å per pulse have been observed at these fluences (Küper et al., 1993) and the issue of material removal versus material modification must be addressed. Two interpretations are possible to explain both formation of carbon clusters and the observed etch rate. First we can consider that at low fluences, such as the ones in these measurements, that the energy density in the polymer is just above that necessary to decompose the polyimide. This decomposition results in some decomposition products (particularly gaseous products such as nitrogen and oxygen) being ejected from the surface and others remaining. The majority of the remaining material is carbon and this organizes into the clusters observed in these measurements. As one moves to higher fluences even this carbon is ejected from the surface and few carbon clusters are formed and laser induced electrical conductivity is not observed as discussed in chapter 3. Thus the process of decomposition (eventually followed by cluster formation) and ablation at low fluences are then the same phenomenon, one is measured by the nature of the material that remains and the other by the amount of material that is ejected. As a second possibility, we can consider

that each pulse etches a given depth of surface and that the remaining energy serves to pyrolyze the surface. In this scenario an equilibrium situation can exist where each pulse both removes and creates clusters. In chapter 3, we saw that the relation between ablation and carbon layer formation was a strong one which supports the first interpretation.

<u>4.3 Conclusion</u>

These time resolved pump-probe measurements are a powerful tool for investigation of the laser materials interaction. These measurements probed the optical properties of the material during irradiation but a different wavelength than the probe pulse. This is significant in that it represents the first time that the real part of the refractive properties of the surface have been examined. Further, the use of a visible probe for which the target is transparent results in the ability to measure transmission, reflection and scattering in the same configuration with nanosecond time resolution. The ability to change probe wavelengths has conclusively shown the effects of the excimer irradiation to be one of a transient change in at least the real part of the refractive index profile.

The other focus of these measurements, the time development of carbon cluster formation is also of value and may lead in future work to a more comprehensive understanding of the carbon chemistry at work in the formation of conducting clusters. The results of chapter 3, namely that a background temperature is necessary for electrical conduction, should also be considered in this future work.

CHAPTER FIVE

EXCIMER LASER CONTROLLED COPPER METALLIZATION OF POLYIMIDE

5.1 Introduction

One of the primary limitations of semiconductor product speed is RC propagation delay as interconnection lengths get longer. In multi-chip modules (MCMs) where propagation lengths can be measured in centimeters, this delay is of paramount concern. In order to minimize delay, it is natural to use conductors with high conductivity and insulators with a low dielectric constant, so called "low k dielectrics". Copper is generally the material of choice for the metal while the search for a suitable low k dielectric has become its own research subfield (Cho, 1995). The primary candidates for such a material are polyimides, already in use in MCMs, Teflon and silica aerogels. New custom materials such as FLARE have also been developed specifically for this application (Singer, 1994).

Each have there own advantages and disadvantages but all suffer from reliability problems due to a combination of poor adhesion to copper and other metals, and a large mismatch in thermal expansion properties. Another important problem is diffusion of metal atoms into the dielectric over time. For Cu / low k dielectric technology to succeed, specialized processing methods must employed to alleviate these problems. There are also process advantages to using a copper based system such as good step coverage and reduced electromigration compared to aluminum (Singer, 1994).

The most work has been with the Cu/polyimide system and the first production lines with low k dielectric technology will likely use this combination, though many properties of the other candidates are in many ways superior to polyimide including better resistance to moisture absorption and a substantially lower dielectric constant. The primary advantage with using polyimide is its familiar use in MCM production which is very similar to interconnection applications on-chip but on a much larger scale (~10 μm). As MCM technology continues to become more important in high performance applications such as in communications and mainframe computers, research into this system is strongly motivated for this reason alone.

Typically in MCM production several dielectric/conductor layers are used and interconnection between those layers is accomplished by using an excimer laser to ablate vias in the polyimide and then using electroless plating to fill the holes. The excimer system is used in a projection patterning arrangement, and the technique has been increasingly successful as laser systems have improved (Lankard and Wobold, 1993). Because excimers are already used in the manufacturing process it is likely that excimer laser induced electrical conductivity in polyimide might be used to broaden the role of the laser processing and remove other lithographic steps in the process. In this chapter we will look at such a process.

The basic concept of using excimer processing as a total solution is illustrated in figure 5.1. The excimer laser is first used with a high (>200 mJ/cm^2) fluence to cut a wiring pattern into the polyimide layer. A second step of excimer processing is used at a lower fluence (~50 mJ/cm^2) to induce a conductivity change inside the cut pattern. Since this step would utilize the same patterning mask, it is in fact not really a separate step requiring only a reduction in laser energy. The device is then cleaned and placed in an electroless plating bath where the conducting surface induced by the laser seeds the plating process in the ablated trenches. Once the trenches have been filled with copper a polishing step may be required before the next layer can be applied.

Such a process has numerous advantages, first is the strong adhesion that can be obtained between the copper and the laser modified layer. Second is the process's inherent simplicity, requiring only an excimer laser projection patterning system. Finally, the process is entirely planar, increasing in cost only linearly with the number of interconnection layers. This final point is of serious concern since faster circuits can be produced when propagation lengths are minimized. The only way to significantly reduce signal propagation length is through the addition of more interconnection layers, normally an undesirable option due to dramatic cost increases. Another key advantage to planar techniques is a uniform dielectric thickness between metal layers which provides better signal propagation characteristics since the capacitance of the line is not varying along the conduction path. Planar manufacturing methods for MCM interconnection have received considerable attention (Schiltz, 1992), but the vast majority of these techniques require additional photolithographic steps which require substantial cost increases.

The goal of the study here is to focus on proof of principle type experiments in order to demonstrate the possibility of excimer laser seeding and to characterize the resulting interface properties.

High Fluence Excimer Micromachining

Polyimide

Low Fluence Excimer Surface Modification

Carbon Seed Layer

Electroless Copper
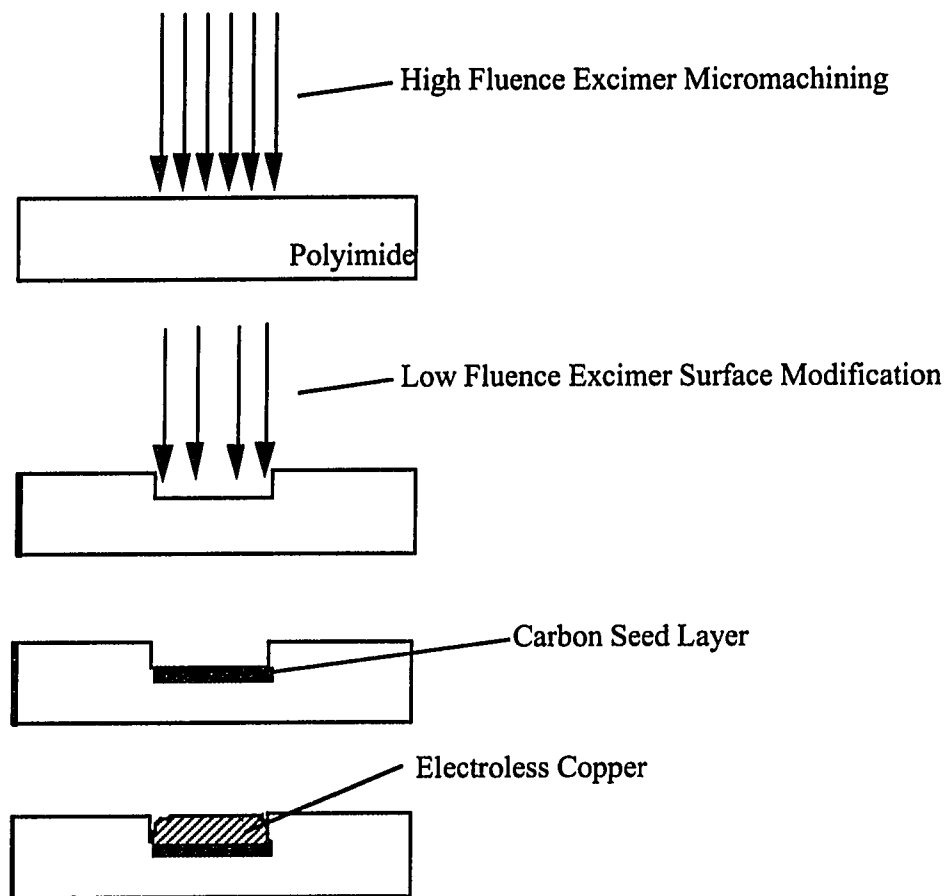
Fig. 5.1. Schematic of excimer laser patterning and seeding for Cu/PI interconnection.

5.2 Experimental Methods

Two types of experiments were performed: broad area irradiation for studying interface properties and small feature irradiation for spatial resolution investigation. Samples were plated electrolytically with a commercial plating solution from Atotech Corporation and electrolessly plated with a homemade solution.

Broad area irradiation was carried out using a 0.5 cm square contact mask. Samples were rotated within the excimer laser beam with a continuous flow nitrogen gas over the surface of the samples. Samples were irradiated 2000 times at repetition rate of 4 Hz at varying fluences. The best results were for samples irradiated between 40 mJ/cm^2 and 60 mJ/cm^2. Recalling the results of chapter 3, this corresponds to conducting samples where some roughness is observable on the sample surface.

An array of 10 to 20 µm wide lines was also irradiated on samples using a 15 cm lens to reduce an array of 200 µm wide slits that had been cut into a piece of polyimide foil with the excimer laser using the focus of a cylindrical lens.

The electroplating solution obtained from Atotech is a simple acidic Copper Sulfate solution with various organic additives to promote planarity and leveling. The electroless solution was based on solutions described by Deckert (1995). The content of the electroless solution is described in table 5.1. To keep the solution from decomposing spontaneously, air was bubbled through the solution at all times, the temperature was maintained between 40 and 50° C. Electroless plating rates were difficult to reproduce with times in the bath ranging from 1 to 3 hours for a visible continuous copper layer to appear over the irradiated areas. Different samples in the same bath might not plate at the same rate, and the amount of air bubbled through the sample could affect plating rates drastically. Better planarity and leveling properties can likely be obtained if a commercial additive is acquired for the electroless plating solution similar to that used in the electrolytic plating.

Table 5.1

Electroless Copper Solution
taken from Deckert (1995)

Ingredient	Quantity
Copper Sulfate	2.2 g/l
Chelate: Quadrol	13 g/l
Formaldehyde: HCHO	3 g/l
NaOH	8 g/l

In order to achieve greater control over the electroless solution in the future, it will be necessary to construct a plating cell where air flow rates can be controlled and measured and where the proximity of plating samples to the air flow are always the same. A regular agitation method for samples would also be desirable as well as a temperature control mechanism. For the present experiments a simple 1 liter beaker was used where samples were mounted on a teflon plate at the bottom of the beaker. The setup was adequate for the limited goals of investigating adhesion over broad areas but would be inadequate for construction of an interconnection pattern.

5.2 Results

A cross-section of a broad area sample plated electrolytically is shown in Fig. 5.2. These cross-sections were obtained by mounting the sample between two silicon wafers, cutting and polishing cross-sectional slices of the whole assembly. In the figure a 10 μm layer of copper with a planar top surface is on top of the laser processed polyimide sample. The surface of the polyimide is considerably roughened and was characteristic for the 50 mJ/cm^2 fluence used to laser process the sample. The copper is deposited completely into the roughness created by the laser processing, and this property is assumed responsible for the good adhesive properties observed in these samples.

A 15 μm wide copper plated wire is shown in Fig. 5.3, demonstrating that technologically significant length scales can be achieved easily. The fluence here was measured to be the same as in Fig. 5.2, but was likely somewhat higher do to uncertainty in accounting for the exact demagnification of the imaging system. A cross section of the same sample showed an ablated notch in the center of the copper plated strip, indicating a higher fluence was present.

Adhesion was investigated with the electroless plating method. Adhesion is not an easy property to measure in quantitative fashion and no attempt beyond the simplest
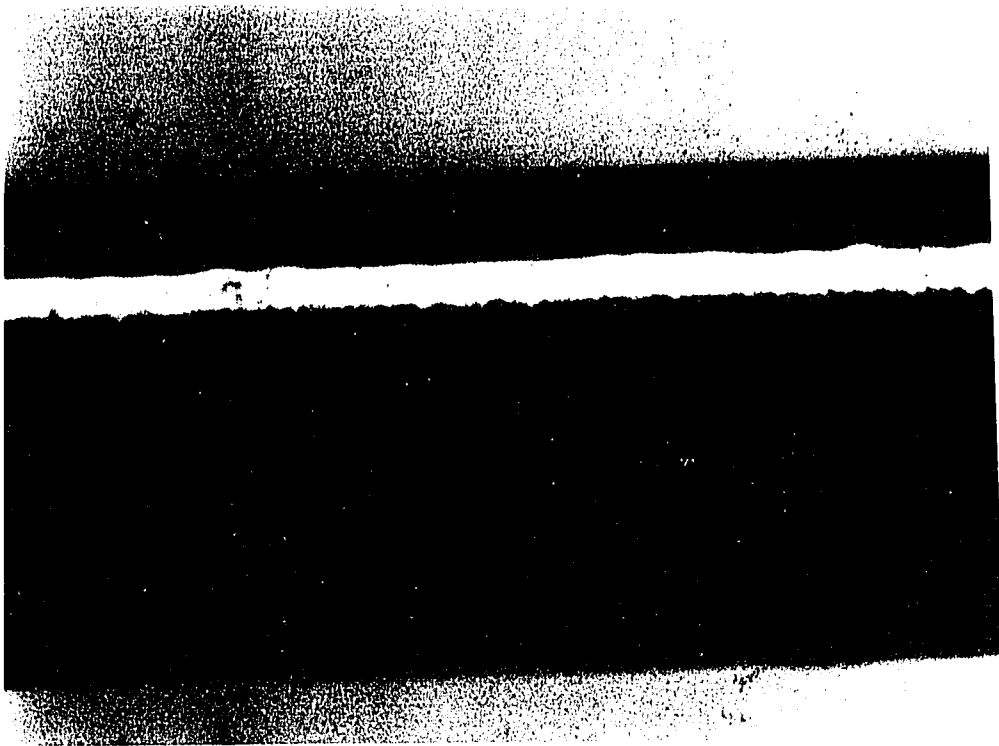
Fig. 5.2. Cross-section of an electroplated sample where the polyimide was irradiated with a fluence of 50 mJ/cm^2.
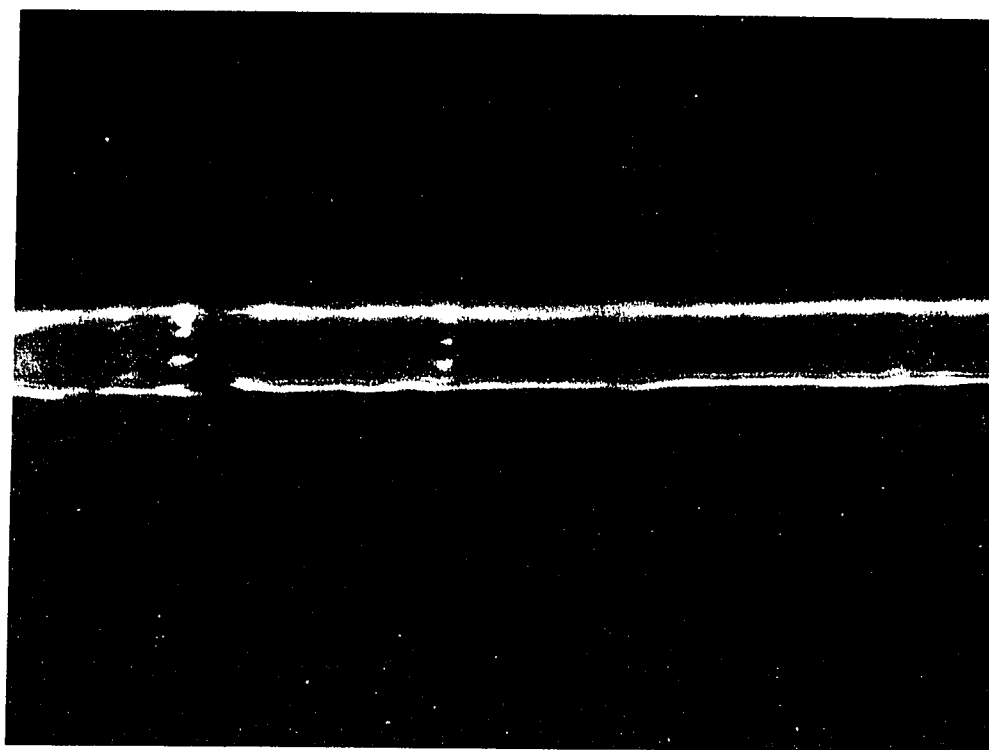
Fig. 5.3. Plan view optical micrograph of a 15 μm wide electroplated copper wire on polyimide.

qualitative methods were made here though future plans for quantitative testing have been made. Here we used the "scotch tape test" method where plated samples were covered with a piece of scotch tape and firmly pressed together. The tape was then peeled off and samples where the copper layer remained on the sample were said to have passed and those that did not to have failed. One of the principal drawbacks of this method is that the force brought to bear on the Cu/PI interface is strongly dependent on the properties of the Cu/tape interface. Cross-sections of the samples indicated that the electroless samples had a much rougher surface than that found in the electroplated samples such as in Fig. 5.2. This roughness likely made the test considerably harsher than one would normally expect. Since the electroless solution used was not commercial, it did not contain the organic additives necessary to produce a planar surface.

With those limitations stated it seems clear that any samples which passed the test must have excellent adhesive properties. Several of the samples did indeed pass the adhesion test and efforts were made to see the dependence of adhesion on laser fluence since it was felt that this was the primary experimental parameter that affects the surface geometry and thus potentially the adhesive properties. Samples prepared with fluences below 40 mJ/cm^2 did not adhere well, and samples prepared with fluences greater than 60 mJ/cm^2 also did not adhere well. However, samples with fluences between these two values did pass the scotch tape test. Therefore, the results of this study indicate that the use of moderate fluences where the conductivity of the surface is modified along with some surface roughening produces the best interface.

It is perhaps surprising that the more roughened surfaces with higher fluences did not adhere well since these are also conducting. Cross-sections indicated that these samples produced the least planar copper surface which could alter the test results. If a better plating solution were used that produced an equal surface on all samples, a better understanding of the actual Cu/PI interface would be available.

5.3 Conclusion

The simplicity of these experiments should not detract from the significance of the results. The adhesive properties of this interface, at least in the fluence range indicated, are truly excellent. The ability to achieve high resolution is clearly not a significant challenge with excimer laser processing. What remains to be demonstrated is only that selective seeding within micromachined structures can be obtained. This is of course necessary in order to demonstrate a planar process. In order to fully demonstrate the potential of this process more work needs to be done on improving the plating process such as through the acquisition of a commercial electroless solution and the design of a more specialized plating cell.

CHAPTER SIX

INTRODUCTION TO PERCOLATION THEORY

Percolation theory is the simplest description of a phase transition that has non-trivial critical behavior. Percolation theory has had many direct applications, but is most important as a model system for the study of critical phenomena in general. The percolation problem has, therefore, become one of the most studied systems in physics and has been at the center of theoretical developments in critical phenomena including renormalization groups, epsilon expansions, fractal geometry, monte carlo simulations, and other techniques (Creswick et al., 1992; Zallen, 1983). The theory is also a principal model for disordered systems, and has provided the basis for understanding of electrical conduction in amorphous solids and lightly doped semiconductors (Zallen, 1983; Shklovskii and Efros, 1984; Bunde and Havlin, 1991).

Here we will discuss the percolation problem in terms of random electrical networks which has been the primary means of posing the percolation problem. The

essence of the problem is simple: we consider a square lattice in two dimensions of $n \times n$ points where n is a very large number. We then wish to describe the electrical resistance of the system as the points on this lattice are connected to one another by resistors on a nearest neighbor basis and in a totally random fashion. The situation is depicted in Fig. 6.1. We describe the system in terms of the fraction of occupied connections or "bonds", p, which is then the probability that a given bond in the system is occupied. As p is increased from zero the system first consists mostly of single resistors (Fig. 6.1a) and the conductance of the whole system is clearly zero. As we increase p groups of resistors will be connected to each other (Fig. 6.1b), and we refer to these groups as *clusters*. As p continues to increase the average size of these clusters grows until a single cluster connects the two boundaries of the system. Here, the electrical conductance will immediately jump from zero to a finite value (Fig. 6.1c). This critical point separates the conducting and insulating phases by the difference of a single connection, and we refer to this cluster that first connects the lattice boundaries as the *percolating cluster* or the *infinite cluster*. As p is further increased beyond the critical point the electrical conductance will increase until all of the sites are occupied, and the system is fully conducting (Fig 6.1d).

The picture of a random resistor network of Fig 6.1 is very useful for illustrating the basic problem, but it can also be misleading. It tends to emphasize the discussion of the critical region in terms of being a conductor or not a conductor. In reality it is describing an *insulator* becoming a conductor. The incipient percolation cluster is *neither* a conductor or an insulator but retains properties of both while exhibiting totally new properties which exist only at the critical point, and it is these peculiar properties of the critical point that will be of the greatest interest.

The properties of the system far from criticality are simpler mixing problems as one is a dielectric mixture ($p \ll p_c$) and the other essentially a conductor ($p \gg p_c$). Averaging techniques collectively known as effective medium theory describe properties well in these
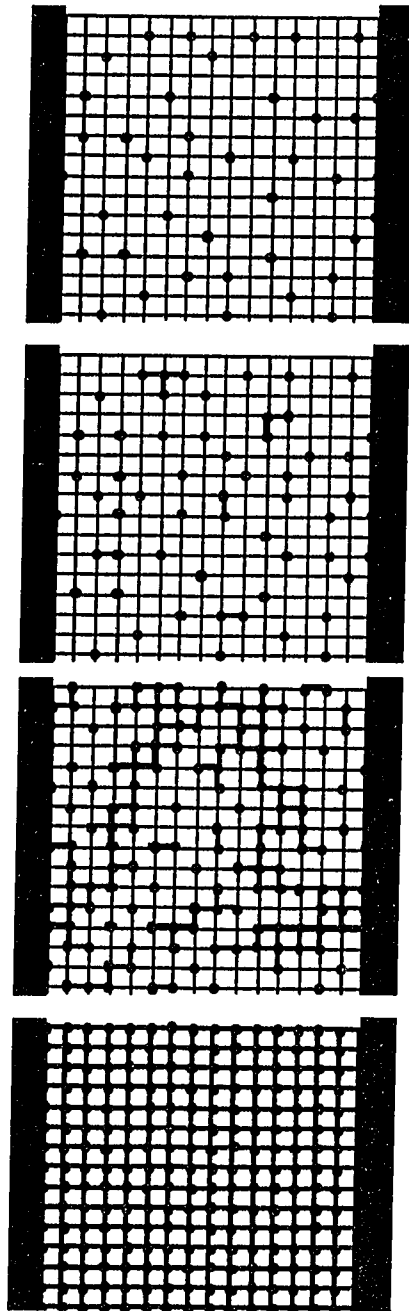
Fig.6.1. Example of a percolation network on a two dimensional lattice: a) well below threshold, b) small clusters of two or three sites form, c) at the percolation threshold, d) saturation.

regions. Near p_c, however, the properties of the system are largely determined by the geometry of the infinite cluster which has complex structure on all length scales from the bond length to the lattice size. The percolating cluster is then taken to be a fractal object, and its geometric properties can be described naturally in terms of fractal geometry. How normally well understood physical phenomena behave on a fractal geometry is a difficult problem in general, since the usual descriptions of such phenomena utilize differential equations. The primary assumption of a differential approach to a physical problem is that at infinitesimally small scales, all quantities involved are smooth. By their very definition fractals fluctuate at all length scales. The difficulty this poses can rarely be understated, since traditionally, physical phenomena are hardly separable from their differential-equation-based descriptions.

There are many variations on the percolation problem such as allowing the lattice to exist in three dimensions, altering the lattice type, or even removing the lattice altogether and letting the sites occupy a continuum of spatial points. All of these problems are still percolation systems, and many aspects of their behavior are independent of these exact differences. It is only a change in the real spatial dimension which fundamentally alters the properties of a percolation system. It should be pointed out that percolation is a geometrical problem, and the definitions of the quantities involved can be radically changed and the results applied to problems in vastly different fields. Some examples are hopping conductivity (where some dimensions are energy), gelation, and magnetism. In what follows we will describe the essential features of the percolation problem but substantially targeted towards the experiments that will be discussed in the next chapter. The phenomenon of laser induced electrical conductivity is described well by the percolation model where we consider a continuum of conducting sites in three dimensions in an insulating matrix. We will therefore focus on a three dimensional approach in our discussion of the theory even though the two dimensional results are simpler and more

intuitive. We will also concentrate on percolation theory as a model for electrical conduction in a conductor insulator mixture which ignores other interesting and varied applications but will more quickly lead us to results which can be applied to experiment.

6.1 The Geometry of the Critical Point

We first look at the geometrical properties of the percolation system near the critical point. We can completely specify this geometry with only two quantities: the correlation length exponent ν and the order parameter exponent β. These exponents describe many aspects of the system through scaling relations. This description has been augmented considerably with the powerful language of fractal geometry which will be very useful for discussing transport properties.

6.1.1 Critical Exponents in Percolation

Keeping in mind a system like that depicted in Fig 6.1, we would first like to describe the size of the largest cluster of the system as it is this cluster that will span the system and be responsible for transport properties. We call this quantity the correlation length ξ. One convenient definition of ξ is the mean square distance between sites on a cluster. It is clear from even the simplest numerical simulation of the percolation problem that the correlation length is negligibly small below the percolation threshold representing clusters of only two or three sites. It is only as p becomes quite close to p_c does it begin to increase appreciably where it then diverges rapidly. The correlation length is given by the following expression:

$$\xi = \frac{1}{|p - p_c|^\nu} \qquad (p < p_c) \qquad (6.1)$$

It is relatively straightforward to calculate the exponent from computer simulation and the result in three dimensions is $v = 0.880 \pm 0.008$ (Bunde and Havlin, 1991) and in two dimensions analytic analysis yields $v = 4/3$. The correlation length also forms the upper limit over which the system can be considered fractal with the lower limit being the unit lattice length. Equation (6.1) already provides a great deal of information about the system, but only before the critical point. For $p > p_c$ we consider the fraction of occupied sites that are connected to the percolating cluster, $P(p)$.

$$P(p) = (p - p_c)^{\beta} \qquad (p > p_c) \qquad (6.2)$$

The values of β are 0.417 ± 0.003 and $5/36$ in three and two dimensions respectively. $P(p)$ is often described as the order parameter for the system. By this we mean that this quantity determines the long range correlations of the system. In the case of percolation, long range correlation is taken to mean geometrical connection over macroscopic distances which is exactly what (6.2) describes. A plot of these two quantities is shown in Fig. 6.2. for the case of three dimensions.

Other quantities derived from the geometric properties of percolation clusters may be important at times as well such as the average number of sites of finite clusters which is also known as the mean cluster size or cluster mass. It can be shown, however, that all of these exponents can be calculated from any two of them, and as v and β are the best known, all geometric properties are given in terms of these two. Though we will not concern ourselves with the details, we should note the origin of this fact. If we wish to describe the entire percolation system in one quantity we consider the number of clusters of a given size s at a given conductor concentration p, $n_s(p)$. The exact form of $n_s(p)$ is not known except through simulation but it can be assumed to have the following very general form, known as a scaling *ansatz* (Bunde and Havlin, 1991):
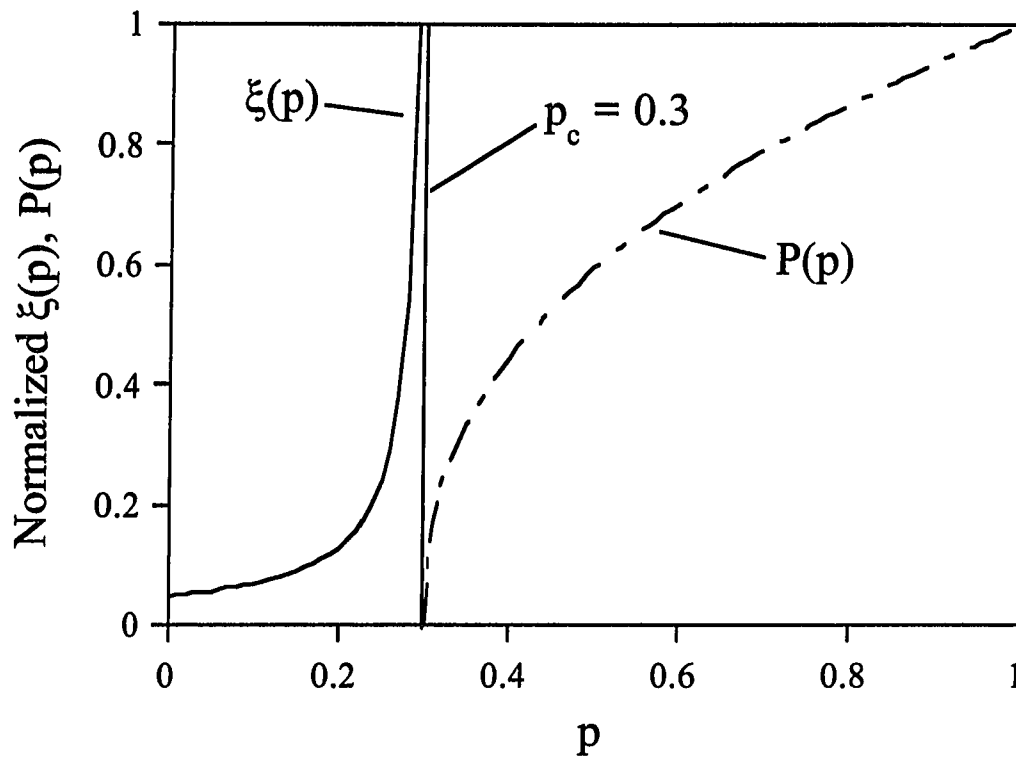
Fig. 6.2. Plot of P(p) and ξ(p) normalized to one. The critical point is set at 0.3

corresponding to three dimensional interpenetrating spheres in a continuum lattice.

$$n_s(p) = s^{-\tau} f_\pm (|p - p_c|^{1/\sigma} s) \qquad (6.3)$$

Such an assumption implies only that to first order this quantity has a power law relation. Supporting (6.3) are analyses for deterministic fractals and special lattices like the Cayley tree where exact results give power law forms for $n_s(p)$. The assumption here is only that of an arbitrary function which can have different forms above and below the critical point for which only minor assumptions about its analyticity are necessary. One can then find the exponents ν and β from (6.3) in terms of the exponents τ and σ. Other quantities such as the cluster mass can be determined similarly and then related back to ν and β.

6.1.2 Percolation and Fractal Geometry

Mandelbrot's fractal geometry has had a profound impact on physics (Mandelbrot, 1982; Bunde and Havlin, 1991), but nowhere more than in the study of phase transitions and percolation theory. We first look at the definition of a fractal and then apply this definition to the percolating cluster.

A fractal is an object with fluctuations at all length scales such that the geometry of the object at one scale is the same as at another. Put simply, if one views a fractal through a microscope it should look the same no matter which magnification you choose. One can divide fractals into to two types, exact and random, and we will focus more on the latter as this is the description of the percolation cluster. An exact fractal is an object such that a change in scale results in an exact duplicate of the figure. A typical example is the Sierpinski gasket which is depicted in Fig. 6.3. In the figure the process for generating the fractal is shown, and we see that the shape will ultimately meet the requirements of scale invariance. Such exact figures are often used as simple models for potential analysis
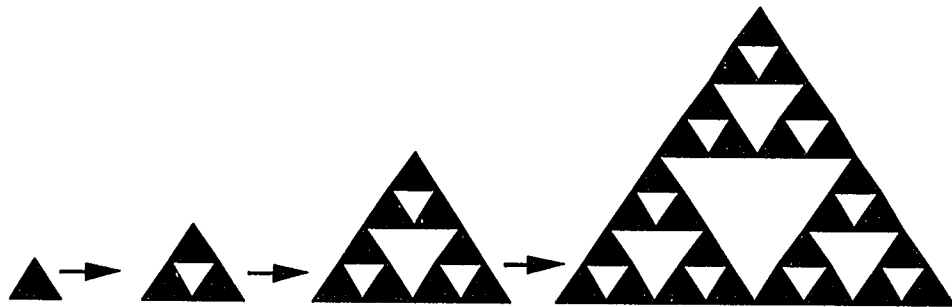
Fig. 6.3. The construction of the Sierpinski gasket, an exact fractal.

techniques since exact solutions can be found before applying a calculation to a more complex system like a percolation cluster. The second type of fractal is the random fractal where a change of scale results not in an exact duplicate of the geometrical shape but in a duplicate of the statistical distribution of points.

To describe a fractal object's properties we introduce a quantity known as the fractal dimension. We introduce this concept by refering to the 'mass' of the object and wish to describe how the mass of the object changes with length. For a homogeneous, non-fractal object the change in mass with length is just given by L^d where d is the number of spatial dimensions of the system. For a fractal this exponent is no longer the number of spatial dimensions and is generally not even an integer. We therefore write the mass of the fractal object in the slightly more general form:

$$M(L) \propto L^{d_f} \tag{6.4}$$

Where $M(L)$ is the mass, L the length, and d_f the mass fractal dimension. If we consider the object to be a real one, then the mass would represent exactly the mass of the object within a d dimensional sphere of radius L. To emphasize the inhomogeneous nature of the fractal object let us then consider its density, ρ, as a function of length defined as the mass of the object divided by the volume in d dimensional space:

$$\rho(L) \propto \frac{L^{d_f}}{L^d} = L^{d_f - d} \tag{6.5}$$

Equation (6.5) is quite interesting in that the density is not a constant but a function of the length scale over which we concern ourselves which means physical processes that take place at one length scale will see one density and those at a different scale see a different density. A good example (and common measurement technique) is to consider light

scattering where variations in refractive index, related to the density, alter the angular distribution of the scattered light. Essentially each length scale of the system scatters the light over a different angular distribution. This provides a very direct measurement of the fractal dimension and is used in studies of gelation and polymerization. By changing the probe wavelength to the x-ray region or even to neutron scattering one can explore a system's geometry over many orders of magnitude in length (Kjems, 1991).

We can then describe the shape of the percolation cluster as a fractal object. We assume that the correlation length, ξ, describes the characteristic length of the system and then associate this length with L in the fractal picture:

$$M(L) \propto L^{d_f} \propto \xi^{d_f} \propto (p - p_c)^{-v \cdot d_f} \tag{6.6}$$

We then consider the system just at the point where the infinite cluster forms and the quantity $P(p)$ has meaning. Now recall that the definition of $P(p)$ is the fraction of occupied sites belonging to the percolation cluster. We can write this as follows:

$$P(p) \propto \frac{M(L)}{L^d} \tag{6.7}$$

which we can justify by recalling that the system is homogeneous, not fractal, on scales larger than the correlation length. The denominator, then, scales only with the ordinary spatial dimension. Combining (6.2), (6.6) and (6.7) we see that we can relate the fractal dimension to the two principle exponents v and β:

$$P(p) \propto (p - p_c)^{-v(d_f - d)} \propto (p - p_c)^{\beta} \tag{6.8}$$

$$d_f = d - \frac{\beta}{v}$$

So we can look at the mass fractal dimension of the percolation cluster as an alternative description to the one given by (6.1) and (6.2) where we talk about the geometrical properties of the cluster in more intuitive language than the more statistical description.

6.2 dc Transport Properties of Percolation Clusters

From the description of the geometry supplied by critical exponents fractal dimensions, we can begin to analyze how different physical properties behave in this unique geometry. We begin by assuming that such quantites as electrical resistance and other measureable properties follow power law relations similar to (6.2), and therefore, we associate each transport property with a critical exponent. Such assumptions have proved correct when compared to the results of numerical simulations and analytic solutions obtained from exact fractals. Alternatively, we can speak of a transport fractal dimension where we refer to the property as a function of length. Such transport dimensions can be related to transport exponents through a similar analysis as that from which we derived the mass fractal dimension. For the case of electrical conductivity we then write,

$$\sigma \propto (p - p_c)^t \qquad (p > p_c) \qquad (6.9)$$

where σ is the electrical conductivity and t is known as the conductivity critical exponent.The exponent t is one of the most studied quantities in percolation theory and its values are known from simulations with good accuracy: $t = 1.9 \pm 0.1$ (3D) $t = 1.299 \pm 0.002$ (2D) (Clerc et al., 1990). Using fractal geometry we write a similar expression,

$$\sigma \propto L^{-d_c} \propto (p - p_c)^{v \cdot d_c} \qquad (p > p_c) \qquad (6.10)$$

where d_c is the conductivity fractal dimension. Thus the fractal dimensions and critical exponents can be transformed into one another without difficulty allowing us to use whichever interpretation is most convenient.

Transport exponents differ from static exponents in an important way as they correspond to real physical quantities. In a real system such as a conductor-insulator mixture there is no way to study such exponents as v and β as one cannot simply examine all the sites and their positions as one can in a computer simulation. Similarly, calculation of a transport exponent such as t is quite difficult by computer simulation but for a real system is a relatively simple laboratory measurement. Therefore transport exponents are of great importance since this is where real physical experiments can be compared to theory. The exponent t has been measured in several experimental systems with quite good agreement to the theoretical calculations quoted above. In particular excimer laser irradiated polyimide can be used to measure t in three dimensions with very high precision. The experimental value for this system was found to be 2.00 ± 0.05 (Ball et al., 1994)

There have been two basic approaches to understanding the dc electrical properties percolation clusters. One is to solve the problem of a random walker on the infinite cluster in order to derive a diffusion constant which can then be related to electrical conductivity via the Einstein relation (Bunde and Havlin, 1991). The second and more common approach has been to consider the percolation cluster as a random resistor network and try to solve the problem through considering Khirkoff's laws. This second approach has been pursued in many different ways including direct simulation where a computer generates successive random networks of some size and then solves the network equations as a function of p.

The use of the random walker for determination of the transport exponent t deserves special mention. This method, though numerically somewhat in disagreement with simulations, is attractive since a direct relation between t and the static exponents β and v

can be derived. Following Bunde and Havlin (1991), we write the mean square displacement of a random walker as function of time. The time, τ, it takes a random walker to diffuse is assumed to scale with a fractal dimension d_w:

$$r \propto \tau^{2/d_w} \tag{6.11}$$

This is then related to a diffusion coefficient D defined as:

$$D = \frac{\langle r^2(\tau) \rangle}{2d\tau} \tag{6.12}$$

Where d is again the number of real spatial dimensions. Now we assume that the Einstein relation holds and then relate the electrical conductivity to this diffusion constant:

$$\sigma = \frac{e^2 n}{k_B T} D \tag{6.13}$$

Where n is the charge density, e, the elementary charge, k_B, the Boltzman constant and T, the temperature. If we assume a constant microscopic charge density which contributes to conduction $n \sim L^{d_f - d}$, we can write an expression for the electrical conductivity:

$$\sigma \sim L^{-d_c} \sim L^{d_f - d + 2 - d_w}$$

$$d_c = d_w - d_f + d - 2 \tag{6.14}$$

We can also convert this expression from the fractal geometry picture to the critical exponent picture:

$$t = v \cdot d_w - 2v + \beta \tag{6.15}$$

Where have expressed the transport exponent only in terms of known geometric exponents and the random walk fractal dimension. The advantage of this approach is clear, studying the behavior of the random walk is far simpler than solving large random circuits. In three

dimensions (6.15) yields values somewhat higher than direct simulations for the exponent

t.

6.3 Lattice Types in Percolation Theory

We can consider percolation as defined by the random placement of sites and the definition of connectivity, but the lattice on which the sites are placed can effect the results. In particular in experiments with conductor insulator mixtures (and excimer-laser-induced conductivity in polyimide) conducting sites are not restricted to a lattice as in the simple example of Fig 6.1. How the lattice then affects percolation properties must be understood if quantitative comparison to experiments is desired.

The principal result of a switch in lattice is a change in p_c, but all critical exponents remain the same. Thus we speak of the universality of percolation exponents. The universality of static exponents such as β or v is well established and a number of lattice types have been examined. Transport properties are more difficult to test but increasingly the values of at least the exponent t are believed to be universal with respect to lattice type. This latter universality has been verified through experiments with real systems where changes in the shape of sites could effect the threshold concentration but not the scaling exponent of the electrical conductivity (Lyons, 1991).

The continuum case has been the subject of considerable investigation and one notable exception to the universality of t has been confirmed. In the work of Halperin et al. (1985), a three dimensional continuum was considered where the medium is conducting and insulating, interpenetrating spheres are distributed through the medium. Such a picture has generally been referred to as the 'Swiss cheese model' in comparison to the voids found in cheese. In this case the value of t loses its universality. This deviation is due to the fact that two spheres placed arbitrarily close to one another create a narrow conducting channel whose resistance diverges as the distance between spheres is reduced. Such deviations have been confirmed in experiments. All the more interesting is the fact that if

one reverses the roles of the medium and spheres--conducting spheres distributed in an insulating medium-- such narrow channels do not appear and t retains its universal value. That t retains its universality in this 'inverse Swiss cheese model' is of great importance for real experiments since virtually all experimental systems including excimer-laser-irradiated polyimide have the conducting elements distributed in an insulating continuum.

6.4 RC Models of Percolation Networks: AC and Dielectric Properties

So far our discussion of transport properties of percolation systems has been time independent. The fractal nature of the percolation cluster affects the time dependent behavior remarkably and is a further way that experiments can probe the geometry of the structure. The usual description of time dependent phenomena is to modify our original percolation model to include capacitive effects and then look at frequency response. This change is accomplished by simply letting all unoccupied sites in our previous model be considered perfect capacitors while still associating the occupied sites with perfect resistors. Such models are known as RC models and are discussed at length in an excellent review by Clerc et al. (1990), and here we will use the notation developed in this reference which is common throughout the literature.

First we need to reformulate the basic percolation problem into somewhat more general terms. We consider the system where there exist with occupational probability p, elements of conductance σ_1 , which can in general be a complex quantity, and in the remaining sites, i.e. with occuaptional probability 1-p, elements with complex conductance σ_2. We will further assume that $|\sigma_1| >> |\sigma_2|$ and define a new parameter $h=\sigma_2/\sigma_1$. Together these assumptions imply $|h| << 1$.

In this general framework, we can discuss limiting cases. The results of the section 6.2 are then just the limiting case where $\sigma_2=0$. The second limiting case that has been the subject of considerable theoretical (Clerc et al, 1990) and experimental work (Kiss et al, 1993) is that where superconducting sites are distributed in an ordinary conducting

medium, ie, where $\sigma_1=\infty$ and σ_2 is real but finite. In this case, the resistance of the system above the percolation threshold is zero and below the threshold the conductance is given by:

$$\sigma \sim (p - p_c)^{-s} \tag{6.15}$$

The exponent s has been studied in similar detail as t and consequently its values have been calculated to some accuracy with $s = 1.288\pm0.002$ in 2D and 0.73 ± 0.01 in 3D (Clerc et al, 1990). The exponent s has considerable importance for ac conductivity in a normal conductor-insulator mixture as we can consider the connectivity of ideal capacitors at very high frequencies to be similar to that of the superconductors.

So we wish to consider the case where h is small but not zero and see how this affects the over all conductivity. This is accomplished by writing the conductivity in terms of a *scaling function* not unlike that of equation (6.3). Such a relation has been proposed by many groups and is supported by numerical simulations. Following Clerc et al (1990), we write the conductivity with scaling function $\Phi_\pm$:

$$\sigma \sim (p - p_c)^t \Phi_\pm\left[h|p - p_c|^{-(s+t)}\right] \tag{6.16}$$

Where $\Phi_\pm$ is assumed to be a universal property of percolation systems varying only with the number of spatial dimensions of the problem. The '$\pm$' refers to different values below and above the critical point. First we notice that in the limiting case of $h \rightarrow 0$ that we recover the previous result for the ideal random resistor network. Since for most insulator conductor mixtures $h << 1$ it is usually safe to ignore the scaling function altogether for the dc response. When we consider the ac response of the system, however, we realize that h, as a complex number, need not be small at all, and in these cases the scaling function can be dominant at some frequency. Intuitively, we can understand this by considering that conduction will begin to be dominated by the unoccupied sites that are considered to be

capacitors which will conduct at high frequency. Therefore let us consider the 'RC' model where:

$$\sigma_1 = \frac{1}{R}$$

$$\sigma_2 = iC\omega$$

(6.17)

and R is the resistance of an indvidual connection, C the capacitance of a single unoccupied site, ω the applied frequency, and $i = (-1)^{1/2}$. Using the definition of h and letting $\omega_0 = 1/RC$:

$$h = \frac{i\omega}{\omega_0}$$

(6.18)

We can now use (6.16) and write the conductivity as a function of p and ω :

$$\sigma(p,\omega) \sim (p - p_c)^t \Phi_\pm \left[\frac{i\omega}{\omega_0} |p - p_c|^{-(s+t)} \right]$$

(6.19)

It has also been proposed that the form of $\Phi_\pm(x)$ in the limit of large argument is $\sim x^u$ where $u = t/(s+t)$. As $p \to p_c$ the argument of (6.19) diverges such that we can use the assymptotic form for analysis of the frequency response at threshold:

$$\sigma(p_c,\omega) \sim \left(\frac{i\omega}{\omega_0} \right)^u$$

(6.20)

where again we have a result than can be compared directly to experiment.

Related to the frequency dependence of the conductivity and also measureable by experiment is the dielectric constant. In discussions of dielectric properties of percolation models, the dielectric constant is usually defined by

$$\varepsilon(p,\omega) \propto \frac{\sigma(p,\omega)}{i\omega} \qquad (6.21)$$

which at the percolation threshold can then be written as:

$$\varepsilon(p_c,\omega) \propto \frac{1}{\omega_0}\left(\frac{i\omega}{\omega_0}\right)^{u-1} \qquad (6.22)$$

We can also use these relations to deduce the dc value of the dielectric constant by taking the low frequency limit of the real part of (6.21) with (6.19). With $\omega <<\omega_0$, we can expand scaling function and take only the zero and first order terms which then yields:

$$\varepsilon_0 \sim (p-p_c)^{-s} \qquad (6.23)$$

Which is a remarkable result which not only allows us to measure the exponent s without needing a superconductor mixture, but also means that conductor insulator mixtures near the percolation threshold can have an arbitrarily large dielectric constant.

This approach to ac properties based on the 'RC' model is not the only one. Most notably is the model of 'anomalous diffusion' which is an extension of the random walk/diffusion approach used to derive the exponent t above. Both anomalous diffusion and the RC model predict the same qualitative behavior: a power law frequency response for both dielectric constant and conductivity and a diverging dielectric constant at the percolation threshold. The details of the exponents, however, differ considerably between the two models as is to be expected since each model comes with its own set of assumptions about transport on percolation clusters. It is therefore at this point that real physical experiments have attracted considerable interest as we have two constrasting approaches with definite experimental predictions. In the experimental literature the dielectric constant and conductivity frequency dependence are then usually written independent of these approaches:

$$\sigma(p_c, \omega) \sim \omega^x$$
$$\varepsilon(p_c, \omega) \sim \omega^{-y}$$

(6.24)

where (6.21) implies $x + y = 1$.

Remarkably, experiments with a number of different systems in both two and three dimensions display the behavior of (6.24) (Laibowitz and Gefen, 1984; Song et al., 1986; Hundley and Zettl, 1988), dielectric constant divergence with s very close to its theoretical value (Grannan et al, 1981), and the relation $x + y = 1$, but the exact values of x and y do not particularly agree with either approach indicating perhaps that neither set of assumptions is altogether correct for real systems. Table 6.1 lists the theoretical predictions and experimental results in two and three dimensions, where the experiments were with gold thin films in two dimensions and teflon-carbon mixtures in three dimensions. The possibility that tunneling between disconnected clusters or parts of clusters is occuring has been suggested as an explanation for the deviation between experiment and theory (Sarychev and Brouers, 1994).

6.5 Nonlinear Current Voltage Characteristics

Nonlinear current-voltage (I-V) characteristics are a unique problem in percolation theory in the sense that theoretical analysis of nonlinear networks was performed in order to better understand certain types of percolation problems and the exponents that describe them before actual experimental observation of nonlinear characteristics in real systems was observed. The significant departure from the earlier theory of the newer observations has led to considerable interest in this area in the last two years. Theoretically several types of problems have been considered: nonlinear resistor networks where each connection is assumed to have a power law I-V characteristic (Meir et al, 1986; Kenkel and Straley, 1982; Straley and Kenkel, 1984; Aharony, 1987) also called the nonlinear random resistor network model (NLRRN), linear resistor networks with tunneling currents being allowed

Table 6.1

Dimension	Anomalous Diffusion[a]	Scaling Theory	Experiments
2	$x = 0.34$; $y = 0.66$	$x = 0.5$ $y = 0.5$	[b]$x = 0.95 \pm 0.05$ $y = 0.13 \pm 0.05$
3	$x = 0.58$ $y = 0.42$	$x = 0.72$ $y = 0.28$	[c]$x = 0.86 \pm 0.06$ $y = 0.12 \pm 0.04$

[a]Gefen, Aharony and Alexander (1983)
[b]Laibowitz and Gefen (1984)
[c]Song et al. (1986)

between dangling clusters (Bardhan and Chakrabarty, 1994; Gefen et al., 1986) also called the dynamic random resistor network model (DRRN), two component composites where one has a nonlinear susceptibility (Yu and Hui, 1994; Lee et al., 1995; Levy and Bergman, 1994), and superconductor-nonlinear conductor composites (Hui, 1990; Yu et al., 1994; Lee et al., 1995).

With the exception of the work from Bardhan and Chakrabarty (1994) and Gefen et al (1986) with DRRN, these are theories which have not been applied to real experiments but are more theoretical exercises in percolation and effective medium theory. The DRRN theory is candidate to describe the experimental results of the next chapter so we will discuss it at greater length here. One final theoretical interpretation in terms of space-charge-limited currents (SCLC) will be presented in the next chapter which is an entirely new approach that describes experimental results very well (Ball and Sauerbrey, 1996).

The DRRN theory was first proposed by Gefen et al. (1986) as an attempt to theoretically describe experimentally observed nonlinear I-V relations in gold thin films near the percolation threshold. Subsequently two other experimental systems have also exhibited nonlinear behavior--carbon-wax mixtures (Bardhan and Chakrabarty, 1994; Bardhan and Chakrabarty, 1992; Chakrabarty et al., 1991) and excimer-laser-irradiated polyimide (Ball et al., 1994). The physical conduction mechanism considered responsible

for nonlinear behavior is tunneling between nearby disconnected sites on so-called dangling

clusters (DCs). A dangling cluster is a potential conduction path that branches away from

the infinite cluster but never reattaches and cannot contribute to conduction in a classical

model. Such DCs may however have several 'points of close approach' (PCA) with the

conducting backbone itself or other DCs. Tunneling accross such PCAs would then be

similar to adding extra connections. That this gives rise to a nonlinear *I-V* relation is easy to

see. At a given applied voltage a certain class of PCAs where there is a separation distance

that is smaller than some tunneling length, conduction will occur. At higher voltages this

tunneling length can be longer and thus make a large class of PCAs contribute to

conduction. At some point, however, a high enough voltage should be reached that all

PCAs are conducting and the *I-V* relation should linearize. Experimentally, however, this

voltage may be so high that breakdown occurs at the PCAs with the smallest tunneling

lengths, creating a destructive non-reversible situation.

Before we describe the specific theoretical predictions let us quickly review what

the results of the experiments are and what quantities such a theory must describe. In gold

thin film experiments, Gefen et al. (1986) prepared a set of samples near the percolation

threshold and measured their I-V characteristics which were found to be linear for small

voltages and then at some voltage crossed over to nonlinear behavior. This crossover point

depends on the value of p of the thin films, but since the exact value of p is not easy to

measure the dependence of the crossover point (usually expressed as a crossover current I_c)

is shown as a function of the linear conductance which through (6.9) is implicitly a

function of p. So the measured value is a scaling exponent x (not the same as above) given

by the following:

$$I_c \sim \sigma_0^{\ x} \qquad (6.25)$$

Where σ_0 is the linear conductance which scales as (6.9), and the measured value of x was

1.47 ±0.1. One can also find x for the NLRRN model but the values of x found are always

less than 1 in clear disagreement with the measurement. Analysis with the DRRN is not so simple.

In qualitative terms the DRRN is rather successful but to be quantitative with such a theory is extremely difficult. Other theories such as the NLRRN have been studied mostly because solutions can be found, not because they correspond to an experimental observation. Here we will make some simple estimates of the results of the theory. To quantitatively analyze the theory one must use computer techniques such as small-cell renormalization (Gefen et al., 1986). First we consider a single loop of size ξ where would like to know the voltage drop accross an open end. This constitutes an upper bound since there should always be smaller loops and other channels in parallel. We can then write, following Gefen et al. (1986) the microscopic current on a block of the size ξ, $I(\xi)$, as function of the length ξ:

$$I(\xi) \sim \frac{I_{ex}}{\left(L/\xi\right)^{d-1}} \tag{6.26}$$

To write the voltage drop $\Delta V(\xi)$ we consider that $\sigma \sim \xi^{-t/v}$:

$$\Delta V(\xi) \sim \frac{I(\xi)}{\sigma(\xi)} \sim \frac{I_{ex}\xi^{d-1+t/v}}{L^{d-1}} \tag{6.27}$$

Where I_{ex} is the external (sample) current and d the ordinary spatial dimension. We then say that the critical current at which nonlinear behavior begins to dominate occurs when $\Delta V \sim V_0$, where V_0 is some critical voltage that allows the connection to become conducting.

$$I_c \sim \xi^{-(d-1+t/v)} \sim \sigma^{d-1+t/v}$$
$$x < d-1+v/t \tag{6.28}$$

which when evaluated with the known values of the exponents gives $x < 1.97$ in 2D and $x < 2.43$ in 3D. Clearly the two dimensional result is compatible with the experiments.

Results of a renormalization calculation (Gefen et al., 1986) yielded x=1.68 ±10% and

further analytical arguments suggested $x = 3/2$, all in two dimensions.

The work of Bardhan and Chakrabarty (1991, 1992, 1994) (henceforth BC) also

found nonlinear behavior close to the threshold but with different I-V characteristics. These

experiment were with carbon-wax mixtures which means a three dimensional picture must

be used. As the DRRN model seemed to have provided a suitable explanation for the thin

film behavior, the same picture was adopted for this case. The measured value of x=

1.38±0.18 is not in disagreement with (6.27) but it is surprising and, within the error

margin, the same value as for two dimensions. Such mixtures were also studied with ac

signals with the interesting result that there was no complex frequency dependence to the I-

V curves (Bardhan and Chakrabarty, 1992) which would normally be associated with

tunnelling effects indicating that the physical descrption of tunneling may not be

appropriate. With thin metal films there is independent evidence to suggest tunneling is an

important conduction mechanism as in the observation of a modified coulomb staircase

effect from multiple site tunneling with an STM (Young, 1995) and a complex temperature

dependence to the linear and nonlinear components (Ye et al., 1994).

In order to explain their results BC (1992,1994) performed a rather questionable

scaling function analysis related to the description above for the frequency response. They

assume the scaling function to be a function of three variables ω, p , and applied voltage V.

Where they studied the behavior of the scaling function for these variables separately. In

the more recent work of BC (1994) they compared the differential conductance dI/dV to the

frequency response and experimentally found "identical" scaling relations, though this has

been questioned in subsequent comments (Sen, 1995). We can understand their approach

by considering the general scaling law of (6.16) where for the RC model h became a

frequency variable. In the three variable appoach in the limit of low frequency, h is

assumed to have a voltage dependence. They claim that this voltage dependence of h is

from tunneling between DCs just as in the gold thin film work and also that this reflects the universal properties of the scaling function. Perhaps, given the opaqueness of BC's analysis, the obvious contradiction between conduction through DCs and the use of the universal scaling function for percolation has been missed.

BC claim their dI/dV measurements are a direct measure of the properties of the scaling function similar to experiments where changes in temperature altered the conductivity of the occupied sites. Using the temperature dependence of the conductance of one type of site, one changes the value of h directly as the temperature affects all sites equally. The DRRN model is a very different situation-- the change in conductivity with voltage comes from a sub-class of sites, specifically PCAs. As the definition of h is the unoccupied site conductivity divided by the occupied site conductivity ($h=\sigma_2/\sigma_1$), the h parameter only allows us to introduce properties of occupied and unoccupied sites (such as considering them to be capacitors as in the RC model or as temperature dependent resistors), however, it *does not* allow us to introduce properties of a *special class* of occupied or unoccupied sites. Tunneling through a particular group of PCAs which adds extra connections in the lattice is hardly the same geometrical problem. Perhaps *a* scaling function is involved but it clearly cannot be the same as for classical percolation.

Therefore we would conclude that theoretical understanding of nonlinear $I-V$ characteristics near the percolation threshold as observed in experiments is not well understood by existing theory, neither the DRRN model with its lack of specific predictions or the questionable use of the universal scaling function by Bardhan and Chakrabarty. Which is not to say that the assumption of tunneling through DCs should be considered incorrect so much as unproven, particularly in the three dimensional case.

6.6 Conclusion

In percolation theory we have a powerful tool for exploring the properties of strongly disordered systems. Fractal geometry and power law expressions provide accurate descriptions of cluster geometries, but difficulties are found when measureable physical properties are considered, notably, electrical conduction. Here we have concentrated on the theory as a model for electrical properties of binary disordered systems such as conductor-insulator mixtures and found that these systems display several remarkable properties such as a diverging dielectric constant, power law frequency response, and nonlinear I-V relations in mixtures of linear elements--all of which have been observed experimentally in both two and three dimensions. Varied theoretical approaches such as anomalous diffusion and scaling functions make detailed predictions for real systems such that actual experiments now play an important role in understanding fundamental aspects of percolation theory

CHAPTER SEVEN

CURRENT INJECTION NEAR THE PERCOLATION THRESHOLD

7.1 Introduction

In recent years there have been several theoretical and experimental studies that treat the nonlinear behavior of percolation systems. On the theoretical side a number of models have appeared describing composites of nonlinear media (Lee et al., 1985; Yu et al., 1994; Levy et al., 1994; Yu et al., 1994), dilute nonlinear random resistor networks (Meir et al., 1986; Kenkel and Straley, 1982), and tunneling currents between disconnected sites (Gefen et al., 1986; Chakrabarty et al., 1991; Bardhan et al., 1992; 1994; Sarychev and Brourers, 1994). Several outstanding problems remain and one of the most interesting is the observation of nonlinear current-voltage characteristics in many systems.

Many experimental systems associated with percolation descriptions exhibit nonlinear current-voltage (I-V) relations near the percolation threshold, including thin metal films (Gefen et al., 1986; Young et al., 1994), carbon wax composites (Bardhan et al., 1992; 1994, Chakrabarty, 1991), and excimer laser irradiated polyimide (Ball et al., 1994).

All of these systems conduct ohmically for low voltages and currents and cross over to nonlinear behavior at a critical current I_c. The crossover current is dependent on the conducting volume fraction p and therefore implicitly on the linear conductance. Scaling exponents for this crossover phenomenon have been measured for thin gold films and carbon-wax mixtures with remarkably similar results, though the form of the I-V characteristics are very different. The exact form of the I-V relations for the carbon-wax system are somewhat ambiguous and power law and polynomial expressions have both been used. In this chapter, the I-V relations and the crossover exponent are measured for excimer laser irradiated polyimide.

7.2.1 Excimer-Laser Irradiated Polyimide as a Percolation System

The percolation phenomenon in excimer laser irradiated polyimide is a transition where KrF excimer laser pulses of fluence greater than 20 mJ/cm^2 induce a conductivity change in a thin surface layer of the polymer. The interaction of the intense laser pulse with the polymer decomposes portions of a thin surface layer (about 1/2 to 2 μm in thickness) into small carbon clusters of about 50 nm diameter. These carbon clusters are electrically conducting and successive laser shots increase the density of these clusters until a critical point is reached and conduction over macroscopic areas is observed. The relationship between the increasing carbon cluster density and a continuum percolation model is easy to see. As discussed in the last chapter the assumptions of percolation theory will be met if conducting particles, in this case carbon clusters, are distributed in an insulating medium in a spatially random fashion.

The percolation threshold and conductivity critical exponent for this system have been studied previously with very good agreement with the percolation theory for three dimensions (Ball et al., 1994a, 1994b). In these experiments the electrical conductivity of the polymer was monitored *in situ* while laser processing proceeded with measurements on a shot to shot basis. The results of such a measurement are shown in figure 7.1, where
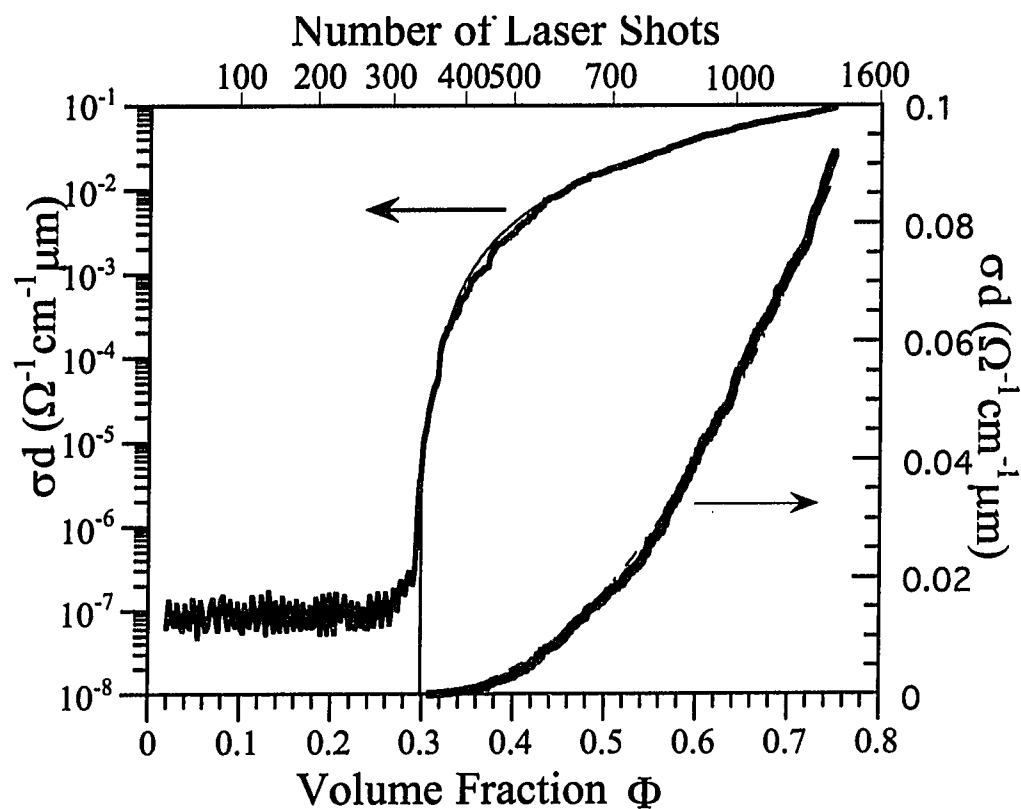
Fig. 7.1. Conductivity as a function of the number of laser shots and calculated volume fraction. The theoretical curves are shown for t = 2.0 and an excellent fit is found on both a linear and logarithmic scale (taken from Ball et al., 1994).

conductivity is shown as a function of the number of laser shots. The theoretical curve is from equation (6.9) and clearly fits the data with exacting precision. The fit in the region just at the threshold is not as good and is the result of two phenomena: i) nonlinear I-V characteristics and ii) the properties of a two component system where the resistance of the medium is nonzero.

As discussed in chapter 2, the conduction mechanism has been investigated through the temperature dependence of the conductivity. The result is a $\exp\{(T/T_0)\}^{1/4}$ which is in agreement with Mott's law for three dimensional variable range hopping (VRH) conduction. This type of electrical conduction is closely related to the idea of percolation and is expected in a system with strongly localised, spatially disordered sites. The observation of VRH conduction confirms the existence of localized conducting sites and three dimensional conduction. The thickness of the layer, which is more than 20 times the diameter of the cluster size, is sufficient for three dimensional behavior to be dominant even though the length and width of the samples are of macroscopic size. The three dimensional nature of the VRH strongly supports this three dimensional view.

There are two primary advantages for using laser processed polyimide for the study of percolation: (i) the semicontinuous nature of the laser processing allows for the study of properties on a single sample for hundreds of different values of p. (ii) the opportunity for *in situ* monitoring of the conductivity allows for the preparation of samples much closer to the percolation threshold than other systems with sample resistance controllable over seven orders of magnitude from 10 kΩ to more than 100 GΩ in these experiments. The nonlinearity of these laser processed samples at such high resistances is also much more pronounced, providing for the measurement of the cross over behavior much more accurately and over many more orders of magnitude in resistance than other systems. Laser processed polyimide is particularly interesting as the method of achieving spatial disorder is fundamentally different than conductor-insulator mixtures.

7.3 Experimental Method and Results.

Samples were obtained by irradiating commercially available 75 μm Kapton™ polyimide films from DuPont corporation with the output of a Lambda Physik LPX 105i KrF excimer laser operating at 248 nm (pulse width of 15 ns) at fluences from 30-45 mJ/cm^2. To insure homogeneous irradiation, a small, homogeneous part of the beam was expanded with a cylindrical lens, and the sample was rotated within the beam. A constant flow of nitrogen gas was maintained over the sample surface during irradiation which has been found to produce better surface stability and prevent oxidation, but is not necessary in order to observe the metal-insulator transition. Contacts to the sample were made such that the resistance could be monitored during irradiation. These contacts consist of previously irradiated, conducting strips separated by a fixed distance (about 5 mm), which are then coated with colloidal silver paint. The silver has been verified to form an ohmic contact with the fully conducting (far from threshold) irradiated polymer (Feurer et al., 1993). Such contacts are ideal for measurement of the metal insulator transition since the sample area is in contact only with similarly treated polymer foil and since they are present to the same depth as the surface layer under study. The I-V characteristics were measured with a computer controlled Keithley 6517 electrometer/high resistance system by the Forced Voltage Measured Current method. The measurements exhibited no hysteresis and were both symmetric and reproducible, indicating Joule heating and breakdown between disconnected sites were not significant.

Two current-voltage (I-V) characteristics are shown in Fig.7.2. The first is a sample very near threshold displaying a very strong nonlinear behavior, the second is far from threshold where essentially linear behavior dominates. More than 50 samples have been prepared at different points in the transition and for many different experimental cases (variations in laser fluence, repetition rate etc.) and all I-V characteristics could be fitted to the following polynomial equation with linear correlation coefficients greater than 0.99985,
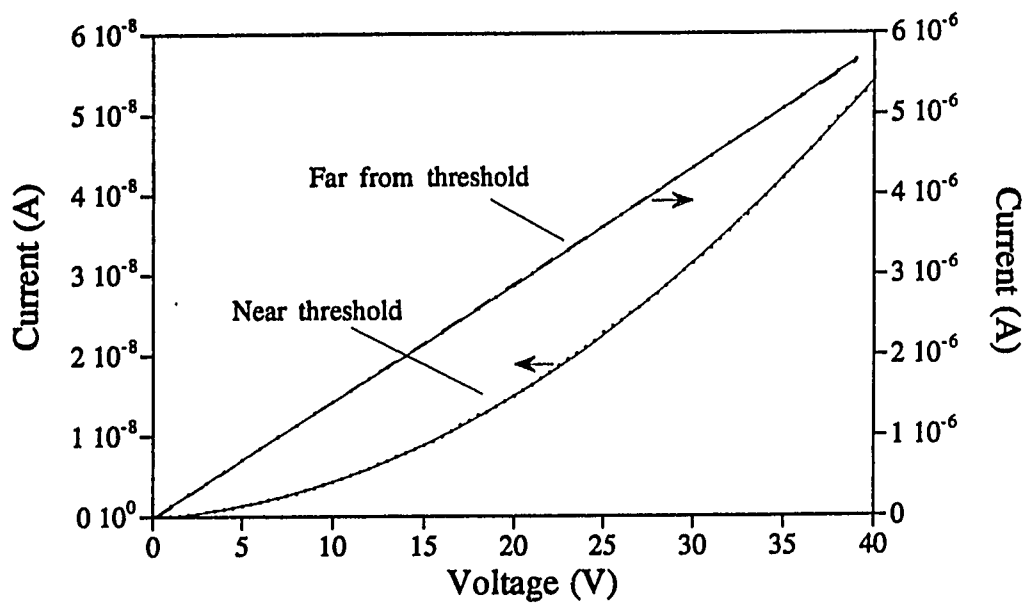
152

Fig. 7.2. I-V curves for two samples, one near the percolation threshold and one farther from the threshold. The sample near threshold exhibits a strong nonlinearity which follows equation (7.1), drawn curve, to exacting accuracy.

$$I = \Sigma_1 V + \Sigma_2 V^2 sgn(V) \qquad (7.1)$$

where the coefficients Σ_1 and Σ_2 were a function of the number of laser shots which is in turn directly related to the conductor concentration p. We have also performed *in situ* measurements (described below) where thirty or more I-V measurements could be taken on a single sample during processing, bringing the total number of measurements in agreement with (1) to more than 500. In the characteristic near threshold the form of the curve is clearly that of (1) where a least squares fit to (1) is shown in the figure. The exponent of the nonlinear term in (1) was also fitted as a free parameter with the result of 2.01. Similar fits for 15 samples near threshold where the nonlinearity is strongest give 1.99 ± 0.06. The value of the exponent of the nonlinear term has significant consequences for proposed theoretical descriptions of these results. The second curve was taken from a sample far from threshold where essentially linear behavior is observed. In the figure both a linear fit and a fit to equation (1) are shown where (1) provides only slightly better agreement with the data.

In order to study the crossover from linear to nonlinear behavior, each I-V relation was then fit to (1) using a least squares method and the values for Σ_1 and Σ_2 were extracted. Defining the crossover point as was done by Chakrabarty et al. (1991) to be when the two terms on the right hand side of (1) are equal then the crossover current I_c can be written as:

$$I_c \sim \frac{\Sigma_1^2}{\Sigma_2} \sim \Sigma_1^x \qquad (7.2)$$

A discussed in chapter 6, equation (2) is the preferred manner in which to express the crossover behavior since one avoids using the explicit p dependence which would introduce considerable error from the uncertainty of p and p_c.. In Fig. 7.3, I_c is shown as a function of Σ_1 on a log log scale for samples prepared at a fluence of 42 mJ/cm^2, though
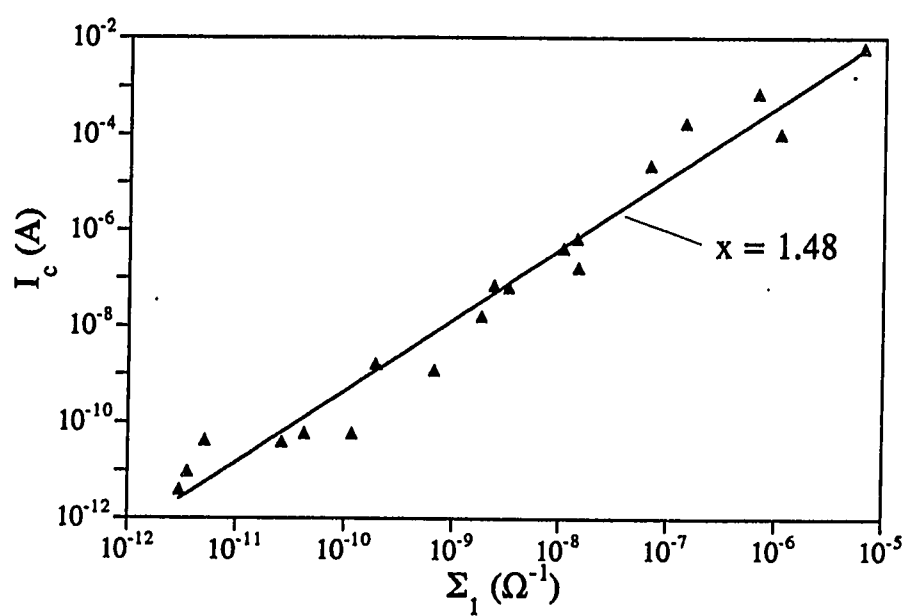
Fig. 7.3 Crossover current as a function of linear conductance where measurements were taken from samples prepared with separate samples.

the exact fluence value had no measurable effect on I_c. A power law fit yields $x = 1.49 \pm$ .19. The scaling of the crossover current in carbon wax composites in three dimensions yielded $x = 1.38 \pm 0.06$ and 1.41 ± 0.18 (Chakrabarty et al., 1991) while for thin gold films a value of 1.47 ± 0.10 (Gefen et al., 1986) was found. Therefore all of these systems yield the same value to within the errors of the measurements despite the two-dimensional nature of the gold films.

The I-V relations could also be determined during laser processing where the processing was paused at intervals and the I-V relation found. Such a method allows us to follow changes in the I-V characteristic on a single sample while p is changed incrementally with continued laser irradiation. In Fig. 7.4 the crossover current is shown as a function of linear conductance just as in Fig. 7.3 where the laser processing was paused for measurement every ten laser shots. The scatter to the data here is much less than in Fig. 7.3 even though the accuracy of the fit of each curve is less than the precision measurements on individual samples (In the *in situ* measurements only 12 points are measured for each curve.). For the data shown in the figure the crossover exponent is found to be $x =$ 1.32 ± 0.05. However, subsequent *in situ* measurements yielded varying values of the exponent from 1.27 to 1.55 with similar margins of error. Comparing these results to the data of Fig. 7.3 we conclude that the exact value of the exponent is different for each sample which is then the reason for the scatter in the data of Fig. 7.3.

These experiments also allowed the determination of the explicit dependence of Σ_1 and Σ_2 on p, though the accuracy of each value is considerably less than those of Fig. 7.3 where measurements were made with a larger number of data points in a shielded test fixture. The result is shown in Fig. 7.5 for the same measurement as Fig. 7.4 where Σ_1 and Σ_2 are shown as a function of both the number of laser shots, n, and conducting volume fraction, p, which is related to n through the relation (Ball, 1994; Feurer et al., 1993),
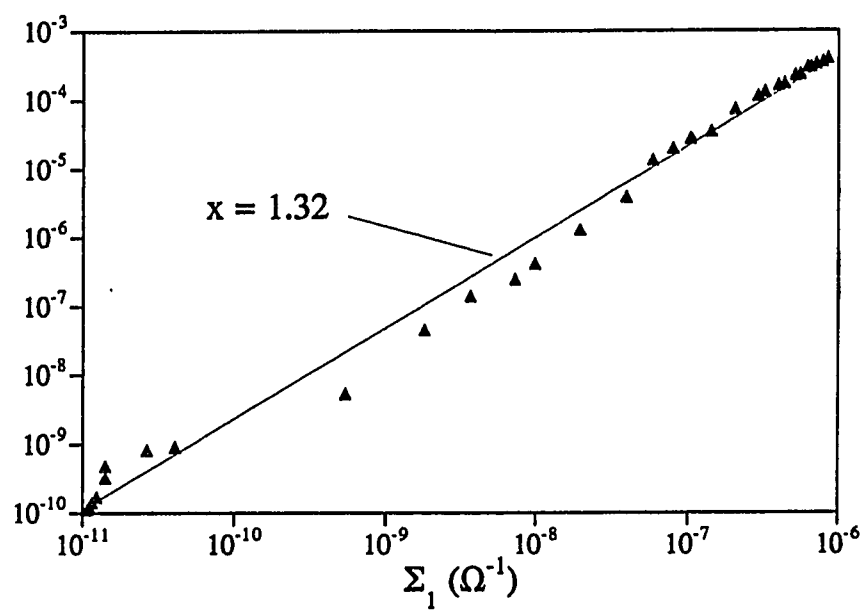
Fig. 7.4. Crossover current as a function of linear conductance where measurements are form a single sample.
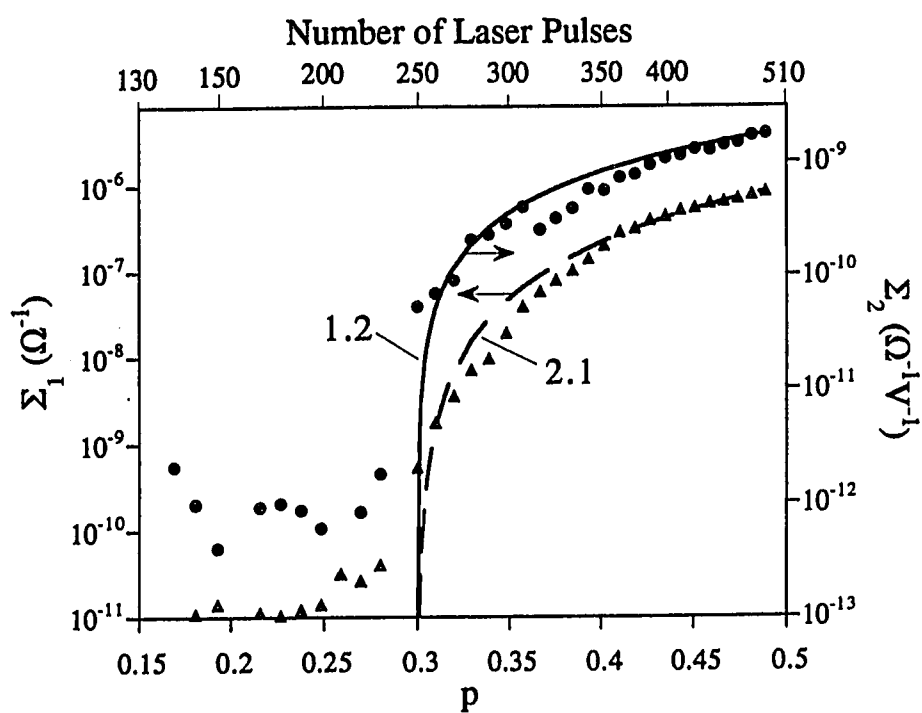
Fig. 7.5. Linear and nonlinear conductance as defined in equation (7.1) are shown as a function of the number laser shots and *p* where *in situ* measurements were from the same experiment as the data in Fig. 4.

$$p(n) = 1 - exp(-\eta n) \qquad\qquad (73)$$

where η is found from the measured percolation threshold of $p_c = 0.3$ andthe measured critical number of laser pulses for each experiment. The value of $p_c = 0.3$ has been measured independently for this system previously (Feurer et al., 1993). In figure 3 we find that $\Sigma_1 \sim (p - p_c)^t$ scales with an exponent of $t = 2.1 \pm 0.2$, in agreement with previous results (Ball et al., 1994) and that $\Sigma_2 \sim (p - p_c)^\alpha$ scales with an exponent of $\alpha = 1.2 \pm 0.2$. Somewhat different values are obtained if the linear and nonlinear parts are allowed to have a slightly different threshold and this is also reflected in the error margins. Two points very near the threshold were not measurable with the electrometer due to large fluctuations in current which was typical of all of these experiments and may reflect the critical fluctuations at the critical point of the metal-insulator phase transition (Bunde and Havlin, 1991).

7.4 SCLC in percolation systems

As discussed in chapter 6, two theoretical approaches to describe this phenomenon have been considered, the nonlinear random resistor network model (NLRRN) and the dynamic random resistor network model (DRRN). The first is based on the assumption that each connection in the network obeys a power law I-V characteristic. This model lends itself to theoretical analysis and specific predictions which can be applied to experiments. The results for the crossover exponent of the NLRRN model and experiments are in clear disagreement for both two and three dimensions and one then concludes that the nonlinearities observed are not from the nonlinearity of individual sites. The dynamic model is based on the idea that near the percolation threshold high fields develop across sites that are classically disconnected but in close proximity to one another. Conduction across these dangling clusters results from tunneling or some other phenomenon in response to the high field. The predictions of this model are less specific than the NLRRN model but are consistent with the experimental results in two dimensions if a number of assumptions are made. In particular the DRRN model as presented in makes *no prediction*

of the form of the *I-V* characteristic, only the scaling of the crossover point. Bardhan and

Charkrabarty (1994) extended the predictions of the DRRN model through a finite scaling

analysis which was compared to ac measurements of the differential conductance dI/dV and

its derivative d^2I/dV^2 on carbon-wax samples. They determined that the form of the 'excess

conductance' was a power law. Further, the scaling was found to be the same for both

frequency and voltage. As was pointed out in chapter 6, the analysis of Bardhan and

Chakrabarty is questionable in its methods and conclusion. Implicit in the work of Gefen et

al. (1986) and Bardhan and Chakrabarty (1994) is that the conduction mechanism for the

nonlinearity is tunneling between dangling clusters on the incipient percolating cluster. In

the case of thin gold films, there is independent evidence (observation of the Coulomb

staircase with an STM)(Young et al., 1995) to suggest tunneling is occurring. However, in

the case of the carbon-wax composites there is evidence that the assumption of tunneling

may not be correct based on the lack of complex structure in the frequency response that is

normally associated with tunneling as pointed out by Bardhan and Chakrabarty (1992).

Here, an alternative model is proposed, based on a different mechanism than

tunneling, that describes both the form of the *I-V* characteristic and the crossover behavior

in a very simple way. Typically in percolation analysis at values $p < p_c$ the system is

considered an insulator and at values $p > p_c$ the system is considered a conducting network

of discrete real (random resistors models) or complex (R-C models) conductances. The

behavior in the region around p_c is given by power law expressions that follow from the

self-similar nature of the geometry at the critical point. In the critical region the system

retains properties of both a conductor and an insulator while exhibiting properties only

associated with the critical point such as dielectric constant enhancement. It is from this

view of the critical region as having both insulating and conducting properties that we

consider what role charge injection phenomena normally associated with insulators play for

the conduction in the critical region. Such a picture deviates from the usual description of

the system as an electrical network of independent discrete components by considering the effect of the charge distribution in the system as a whole.

Space charge limited currents are a natural consequence of the band theory of solids and were predicted by Mott and Gurney (1940) in the early development of the quantum theory of insulators. Experimental observation of such currents was first verified rigorously in a series of experiments by Rose and Smith (1955a;1955b;1955c). Space charge currents in insulators occur when carriers are injected from an ohmic contact into the conduction band of an insulator faster than the low mobility can transport them resulting in a deviation from Ohm's law. That deviation is of the same form as in equation (1). In a percolation experiment the situation is in many ways analogous to that analyzed by Rose: an ohmic contact allows charge to enter the sample faster than the system can transport such charge. The charge injected into an insulator from an ohmic contact is proportional to the voltage:

$$Q = CV, \tag{7.4}$$

where C is proportional to the capacitance of the sample/contact configuration. The current due to this injected charge is then given by

$$I = Q/\tau, \tag{7.5}$$

where τ is the transit time between the two electrodes. τ is given in terms of the sample length, d, the mobility, μ, and the electric field, E :

$$\tau = \frac{d}{E\mu} \tag{7.6}$$

In the case of a homogeneous insulator the current voltage relation is then obtained by substituting (7.4) and (7.6) into (7.5),

$$I = \frac{C\mu EV}{d} = \frac{C\mu V^2}{d^2} \tag{7.7}$$

The current given in (7.7) can be added to the ohmic current which comes from the normal intrinsic (non-injected) charge density to give the total current according to (7.1) with

$$\Sigma_2 \sim C\mu$$

$$\Sigma_1 \sim n_i e\mu . \tag{7.8}$$

where n_i is the intrinsic charge density and e elementary charge. It is suggestive that the nonlinear component is determined by the capacitance which, for a percolation system, diverges at the critical point indicating that the injected charge becomes large near the threshold.

An SCLC current on a percolation cluster as a model for a nonlinear I-V characteristing is essentially saying that the excess conductance is coming not from a change in connectivity properties of the lattice but from an inhomogeneous distribution of charge throughout the system which is the result of a very low mobility and the pool of charge carriers available at an ohmic contact. It should be made clear that this is the charge distribution on the conducting backbone of the percolation cluster and that we are not discussing possible charge injection into the insulating sites. These carriers are free to enter the system as no energy barrier exists at the contact and these carriers can contibute to conduction. By considering how many such carriers enter the percolating cluster we can describe how this effect influences the current voltage relation and how the effect should scale with increasing mobility, ie, increasing p.

For the simple linear random resistor network the conductivity follows a power law as discussed in chapter 6 $\sigma \sim n_i e\mu \sim (p\text{-}p_c)^t$. Following Havlin and Bunde (1991), the effective macroscopic charge density follows the number of sites on the percolating cluster

$n_i \sim (p\text{-}p_c)^\beta$ such that we can write the effective mobility which will apply to both the intrinsic charge and the injected charge:

$$\mu \sim (p - p_c)^{t-\beta} \quad (p > p_c). \tag{7.9}$$

As (7.9) describes the macroscopic behavior of the whole system, the transit time in (7.7) is inversely proportional to the applied voltage, i.e, $E = V/d$. In order to write the complete $I\text{-}V$ relation, we then consider the current from the intrinsic charge density n_i and the injected charge q_{inj}. The total injected charge is given by (7.4) where $C \sim (p\text{-}p_c)^{-s}$, but here we must consider only the fraction of the total injected charge which is on the percolating cluster and may contribute to the conductivity. This fraction also scales with number of sites on the percolating cluster:

$$q_{inj} \sim \left(p - p_c\right)^{\beta-s} \tag{7.10}$$

Combining relations (7.1), (7.8), (7.9), and (7.10) we can then write the $I\text{-}V$ relation (7.1) in terms of a linear part due to the intrinsic charge and a nonlinear part due to the injected charge,

$$I = k_1(p - p_c)^t V + k_2(p - p_c)^{t-s} V^2 sgn(V) \tag{7.11}$$

where k_1 and k_2 are constants. Using (7.2) and the well known values of $s = 0.73 \pm 0.01$ and $t = 1.9 \pm 0.1$ in three dimensions (Clerc et al., 1990) we find

$$x = \frac{t+s}{t} = 1.38 \pm 0.07 \tag{7.12}$$

Which is in agreement with the experimental results for excimer laser irradiated polyimide and carbon-wax composites. The value obtained in two dimensions where t and s are equal of $x = 2.0$ is not at all in agreement with observations with gold films, but since the gold thin films have produced an entirely different $I\text{-}V$ characteristic and other studies have experimentally shown the importance of tunneling currents independently, these results

clearly should not be applied to these experiments. We also note the coincidence that x in this analysis is $1/u$ where u is the exponent of the universal scaling function in the limit of large argument (Clerc et al., 1990).

We can also compare (7.11) to the results of Fig. 4 where the dependence of the individual terms are measured explicitly as a function of p. Utilizing values for the exponents listed by Clerc et al. (1990), we find good agreement between theory and experiment as $t - s = 1.17 \pm 0.11$ compared to the measured value of $\alpha \sim 1.2 \pm 0.2$ and also $t = 1.9 \pm 0.1$ is clearly in agreement with the measurement of $t = 2.1 \pm 0.2$.

We also note that this model is rather independent of the microscopic conduction mechanism. It is even possible that the injected charge may have an entirely different conduction mechanism than the intrinsic charge density and recover the same result as the change in conduction with p for either is governed only by (7.9). We can also see that the effect in percolation systems involving true metals may not display a very strong effect since the charge density in the conduction band is very large and would dominate the conduction even close to the threshold.

Equation (7.11) thus describes the measured I-V curves and crossover phenomenon in excimer laser irradiated polyimide very well. Such a relation also describes the results obtained with carbon-wax mixtures though the agreement of equation (7.1) with differential conductance measurement of Bardhan and Chakrabarty (1994) requires further clarification as the authors state that their measurements are incompatible with the polynomial expression (7.1) for the I-V characteristic. The first measurements of the I-V characteristics of these samples were initially fit to (7.1) with success in the original work with the carbon wax system (Chakrabarty et al., 1991) but (7.1) was later discounted based on measurements of dI/dV and d^2I/dV^2. Specifically $d^2I/dV^2 = 0$ for $V = 0$. The second derivative of a second order polynomial is naturally a constant, seemingly in direct

contradiction to the measurement. However, (7.1) is not a true polynomial. Taking the derivatives of (7.1),

$$\frac{dI}{dV} = \Sigma_1 + 2\Sigma_2 V sgn(V)$$

$$\frac{d^2 I}{dV^2} = 2\Sigma_2 sgn(V)$$

(7.13)

we see that the second derivative exhibits a discontinuity at $V=0$ due to the change in sign. Therefore formally $d^2I/dV^2 = 0$ at $V=0$ and any measurement of d^2I/dV^2 about a small amplitude will be 0 at $V=0$. In order to compare this result with data presented by Bardhan and Chakrabarty (1994) more clearly we also consider the ratio of the two derivatives with V normalized to $V'=V/V_c$ where $V_c = \Sigma_1/\Sigma_2$:

$$\frac{d^2I/dV^2}{dI/dV} = \frac{2}{V_c}\left[\frac{sgn(V')}{1+2V'sgn(V')}\right].$$

(7.14)

Equation (7.14) is shown in Fig. 7.6 along with a sketch of the form of the measurements. When one considers the noise and finite amplitude always present in such an ac measurement, the data are consistent with the pseudo-polynomial form of equation (1). As (14) is determined only by V_c, all data should fall on the same curve when V is scaled to V/V_c as is displayed in the figure, which is the same as the prediction of the Bardhan and Chakrabarty's scaling theory, though the position of the peak is a function of the measurement method.

7.5 Conclusion

This new theory based on injected currents successfully describes both the form of the I-V characteristic and the scaling of the crossover point. However, perhaps the most important feature of this analysis is that it should be possible to verify if a space charge current is indeed present independently of the I-V relations themselves. One method used in
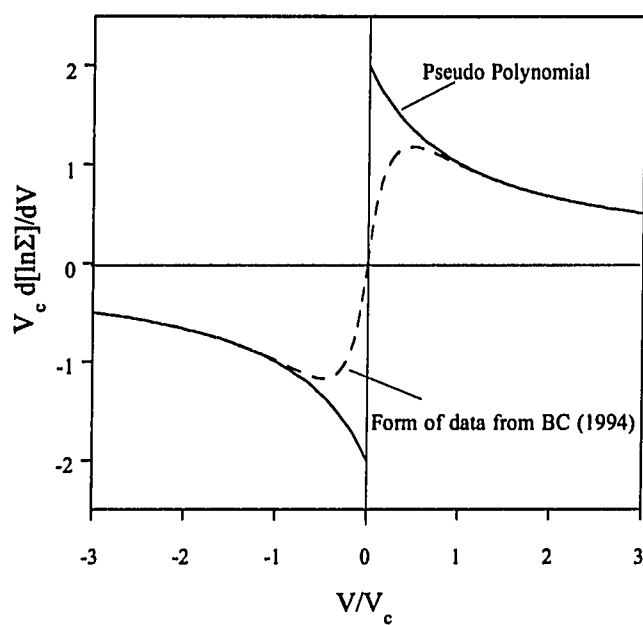
Fig 7.6. A plot of equation (7.14) is shown along with a rough sketch of the form of the data of Bardhan and Chakrabarty (1994) for carbon wax mixtures.

studies of insulators is to observe the current transient, though any such measurement would likely require a more sophisticated analysis than that presented here in order to interpret the results, notably requiring knowledge of the charge distribution on the percolating cluster.

To summarize, the *I-V* characteristics of excimer laser processed polyimide have been studied. The form of the characteristic was determined to be a second order polynomial to such accuracy as to exclude a power law interpretation of the data. We have studied the scaling behavior of the crossover current and found general agreement with the results of other percolation systems. Finally we have derived both the form of the *I-V* characteristics and the scaling from applying the analysis of space charge currents to the case of the percolation metal-insulator transition and found good agreement between the model and the experimental data presented here as well as for other three dimensional systems.

CHAPTER EIGHT

CONCLUSIONS AND NEW DIRECTIONS

The work described here has focused on three aspects of laser processing of polyimide: a model experimental system for percolation theory, applications to electronic packaging and metallization, and laser ablation. The results of this work have brought up many interesting questions as well as exciting opportunities for significant new applications. In this chapter we will review from a general standpoint the significance of the results that have been presented in the preceding chapters and highlight areas of future research and applications.

In terms of laser ablation, the key innovation uncovered by this work is the complexity of multiple fluence and multiple pulse processing. The fact that ablation properties can be not only be affected but dominated by pretreatments at different fluences opens up considerable opportunities for applications. First among these is the use of the

laser controlled surface for selective copper deposition. It is significant that partial ablation, decomposition, and conductivity modification occur at a single fluence without ablating deeper and deeper into the film effectively creating a fluence defined surface that provides substantially enhanced adhesion of the copper layers. Combining these significant results with micromachining of the surface, planar interconnections should be possible where the interconnection is first etched into the surface at high fluence (> 260 mJ/cm^2) and then irradiated at a lower fluence for conductivity modification and subsequent copper plating. The resolution of such a process should be investigated to see if applications are limited to packaging scale (10 µm) interconnections.

Further study of the surface roughness produced by fluences near threshold is also warranted. A better understanding of the geometric properties of the surface in terms of self affine geometry and the relation between chemical transformation and geometric transformation of the surface would be an important step in understanding more about multiple shot effects in laser processing of materials. The effect of nitrogen gas on surface roughness has also not been investigated thoroughly and may be a further way to control the laser-processed surface.

The change in reflectivity of the polyimide surface during irradiation was shown in chapter 4 to be from a transient refractive index. However, the exact mechanism behind the phenomenon has not been established. Three mechanisms were suggested: saturation of the ground state, creation of an electron density gradient of degrading or ablating material, or a phase change. Any such explanation must account for not only the transient refractive index change but also a strong decrease in scattering over the same time span. Further research along these lines is warranted since a full understanding of the effect may lead to a non-contact diagnostic technique for monitoring ablation processes.

Perhaps the largest number of interesting questions was generated by the discussion of SCLC in laser treated films near the threshold. This work is very significant in that not

only does it provide a far more plausible description of a wide class of experimental results, it draws attention to the weaknesses of circuit models for real systems and the need to treat charge distributions and contacts in a realistic manner. The significance of this issue is considerable, implying that the majority of the theoretical work performed on nonlinear percolation networks is irrelevant for real systems.

Several interesting experiments are suggested by the space charge current model. First, a determination of the temperature dependence of the linear and nonlinear terms near threshold would be of great interest in determining a better understanding of what SCLC means in the context of a VRH conduction mechanism. This is an interesting question since, in a VRH model, conduction does not take place in the conduction band where conduction in SCLC models is typically assumed to be.

Second, the magnitude of the linear and nonlinear coefficients of the I-V relation in the SCLC model have geometric dependences which were largely neglected in the analysis in chapter 7. As one changes sample dimensions the values of these coefficients should change. This would serve as an important and relatively simple check on the SCLC model. It might even have practical application as the nonlinear I-V relation could be tailored by selecting sample size.

Third, one could attempt to measure the space charge transient. This measurement would be a particularly direct way of looking at the SCL currents and would provide a measurement of the transit time for the electrons to go across the sample. Measurement of a current transient in such an extremely high impedance sample is a considerable technical difficulty, but if one could observe the transient there should be a peak in the current corresponding to the transit time across the sample, a time that is inversely proportional to applied voltage. Since the charge contributing to SCLC must be injected from one side of the sample it is easy to understand that the enhanced current will not reach the opposite sample side until after the transit time. A measurement of transit time as a function of

concentration p would be a direct measure of the pathlength of the electrons through the system and could be used to study many types of scaling relations in percolation theory.

Fourth, dielectric enhancement should be demonstrated directly. This prediction of the percolation model, verified in other percolation systems, may have tremendous technological applications. In multi-chip modules, for example, one key problem is the introduction of discrete components into the circuit. Most important of these components and the most difficult to realize in a cost effective manner are capacitors. If laser processing of polyimide, which is already in place in manufacturing, could be used to make high dielectric constant material out of the dielectric the problem would be solved in an extremely cost effective manner. Naturally laser induced conductivity can be used make resistors as well and when combined with the metallization technology developed in chapter 5 constitutes a total manufacturing process centered on one tool, the excimer laser.

Demonstration of dielectric enhancement at the threshold would lead to samples where the frequency dependence of the dielectric constant and conductivity could be investigated. As discussed in chapter 6 the values of the scaling exponents for the few experiments that exist are in disagreement with candidate theories and a new measurement from a new system would be of value in resolving the question.

References

A. Aharony, "Multifractality on Percolation Clusters". in *Time Dependent Effects in Disordered Materials*. Eds. R. Pynn and T.Riste. (New York: Plenum Press, 1987)

D. H. Auston, C.M. Surko, T.N.C. Venkatesan, R.E. Slusher, and J.A. Golovchenko, "Time Resolved Reflectivity of Ion-Implanted Silicon During Laser Annealing", *Applied Physics Letters* **33**, 437 (1978)

P. Baeri, S. U. Campisano, G. Foti, and E. Rimini, "A Melting Model for Pulsing Laser Annealing of Implanted Semiconductors", *Journal of Applied Physics* **50**, 788 (1979)

Z. Ball, H. M. Phillips, D. L. Callahan, and R. Sauerbrey, "Percolative Metal-Insulator Transition in Excimer Laser Irradiated Polyimide", *Physical Review Letters* **73**, 2099 (1994)

Z. Ball, "Percolative Metal-Insulator Transition in Excimer Laser Irradiated Polyimide", M.S. Thesis, Rice University, (1994).

Z. Ball, B. Hopp, M. Csete, F. Ignácz, B. Rácz, R. Sauerbrey, and G. Szabó, "Transient Optical Properties of Excimer Laser Irradiated Polyimide I: Transient Refractive Index", *Applied Physics A* **61**, 547 (1995)

Z. Ball, B. Hopp, M. Csete, F. Ignácz, B. Rácz, G. Szabó, and R. Sauerbrey "Transient
Optical Properties of Excimer Laser Irradiated Polyimide II: Carbon Cluster
Scattering," *Applied Physics A* **61**, 575 (1995)

Z. Ball, T. Feurer, D.L. Callahan, and R. Sauerbrey, "Thermal and Mechanical Coupling
Between Successive Pulses in Excimer Laser Ablation of Polyimide", *Applied
Physics A* (1996) (in press).

Z. Ball and R. Sauerbrey, "Current Injection Near the Percolation Metal-Insulator
Transition", (1996) submitted to *Physical Review Letters*.

K. K. Bardhan and R. K. Chakrabarty, "Identical Scaling Behavior of dc and ac Response
Near the Percolation Threshold in Conductor-Insulator Mixtures", *Physical Review
Letters* **72**, 1068 (1994)

K. K. Bardhan and R. K. Chakrabarty, *Physical Review Letters* **74**, 1694 (1995)

K. K. Bardhan and R. K. Chakrabarty, "Nonlinear ac Response near the Percolation
Threshold and Three-Variable Scaling", *Physical Review Letters* **69**, 2559 (1992)

D. Bäuerle, *Chemical Processing with Lasers* (Springer, Berlin, 1986)

J. Bentley, H.M. Phillips, D.L. Callahan, and R. Sauerbrey. 1993. "Electron Energy-Loss
Spectrometry of Laser-Irradiated Kapton Polyimide". *Proceedings of the 51st
Annual Meeting of the Microscopy Society of America.*

J. Bokor, A.R. Neureuther, and W.G. Oldham, "Advanced Lithography for ULSI", *Semiconductor International*, January, 1996, p.11.

Z. Bor, B. Rácz, G. Szabó, D. Xenakis, C. Kalpouzos, C. Fotakis, "Femtosecond Transient Reflection from Polymer Surfaces During Femtosecond UV Photoablation", *Applied Physics A* **60**, 365 (1995)

M. Born and E. Wolf, *Principles of Optics*, Sixth Edition, (Oxford, Oxford Press, 1980)

I. W. Boyd, *Laser Processing of Thin Films and Microstructures* (Springer, Berlin, 1987)

A. Brezini and N. Zekri, "X-Ray Photoelectron Spectroscopy Analysis of Polyimide Films Modified by Ultraviolet Pulsed Laser Radiation at 193 nm", *Journal of Applied Physics* **75**, 2015 (1994)

A. Bunde and S. Havlin, *Fractals and Disordered Systems* (Springer, Berlin, 1991)

R. Carluccio, J. Stoemenos, G. Fortunato, D.B. Meakin, M. Bianconi, "Microstructure of Polycrystalline SIlicon Films Obtained by Combined Furnace and Laser Annealing", *Applied Physics Letters* **66**, 1394 (1995)

R. K. Chakrabarty, K.K. Bardhan, and A. Basu, "Nonlinear I-V Characteristics Near the Percolation Threshold", *Physical Review B* **44**, 6773 (1991)

R. B. Chester and J.E. Geusie in *Laser Handbook* Vol. 1, ed. by F. T. Arechi and
E.O. Schulz-Dubois (North Holland, Amsterdam, 1972), p. 325

C.-C. Cho, D. M. Smith, and J. Anderson, *Materials Chemistry and Physics* **42**, 91
(1995)

M. K. Chun and K. Rose., "Interaction of High-Intensity Laser Beams with Metals",
Journal of Applied Physics **41**, 614 (1970)

J.P. Clerc, G. Giraud, J.M. Laugier, and J.M. Luck, "AC Conduction in Binary
Disordered Systems", *Advances in Physics* **39**, 191 (1990)

R. J. Creswick, H. A. Farach, C. P. Poole, Jr., *Introduction to Renormalization Group*
Methods in Physics (New York, John Wiley, 1992)

C. A. Deckert, "Electroless Copper Plating: A Review Part I", *Plating and Surface*
Finishing, February, 1995, pp. 48-64.

T.F. Deutsch, D.J. Ehrlich, R.M. Osgood, Jr. and Z.L. Liau, "Ohmic Contact Formation
on InP by Pulsed Laser Photochemical Doping", *Applied Physics Letters* **36**, 847
(1980)

T.F. Deutsch, J.C.C. Fan, G.W. Turner, R.L. Chapman, D.J. Ehrlich, R.M. Osgood,
Jr., " Efficient Si Solar Cells by Laser Photochemical Doping", *Applied Physics,*
Letters **38**, 144 (1981)

T.F. Deutsch, J.C.C. Fan, G.W. Turner, R.L. Chapman, R.P.Gale, "Efficient GaAs
Solar Cells Formed by UV Laser Chemical Doping", *Applied Physics Letters.* **40**,
722 (1982)

D. Deirmendjian, *Electromagnetic Scattering on Spherical Polydispersions.* (Elsevier, New
York , 1969) p.34.

J. T. Dickinson, L.C. Jensen, R.L. Webb, M.L. Dawes, and S.C. Langford,
"Mechanisms of Excimer Laser Ablation of Wide Band Gapo Materials: The Role of
Defects in Single Crystal MgO", *MRS Proceedings* **285**, 131 (1993)

A.G. Doukas, A.D. Zweig, J.K. Frisoli, R. Birngruber, and T.F. Deutsch, *Appl.
Phys. B* **53**, 237 (1991).

H. M. van Driel, J. E. Sipe, J.F. Young, "Laser-Induced Periodic Surface Structure on
Solids: A Universal Phenomenon", *Physical Review Letters* **49**, 1955 (1982)

N. Duhamel and B. Loisel, *Solid State Phenomena* **37-38**, 535 (1994)

Kapton^{TM}: Summary of Properties (Dupont Corporation)

P.E. Dyer and J. Sidhu, "Excimer Laser Ablation and Thermal Coupling Efficiency to
Polymer Films", *Journal of Applied Physics* **57**, 1420 (1985)

P.E. Dyer and R. Srinivasan, *Applied Physics Letters* **48**, 445 (1986).

M. N. Ediger and G. H. Pettit, "Time-Resolved Reflectivity of ArF Laser-Irradiated Polyimide", *Journal of Applied Physics* **71**, 3510 (1992)

M. N. Ediger, G. H. Pettit, and R. Sauerbrey, "Diffuse Reflectivity Measurements of Polyimide During Argon Fluoride Excimer Laser Ablation", *Journal of Applied Physics* **74**, 6982 (1993)

K. M. A. El-Kader, J. Oswald, J. Kocka, V. Cháb, "Formation of Luminescent Silicon by Laser Annealing of a-Si:H", *Applied Physics Letters* **64**, 2555 (1994)

T. Feurer, R. Sauerbrey, M. C. Smayling, and B.J. Story, "Ultraviolet-Laser-Induced Permanent Electrical Conductivity in Polyimide", *Applied Physics A* **56**: 275 (1993).

T. Feurer, S. Wahl, and H. Langhoff, "Modification of Polyimide Surfaces Using Intense Proton Pulses", *Journal of Applied Physics* **74**, 3523 (1993)

N. P. Furzikov, "Approximate Theory of Highly Absorbing Polymer Ablation by Nanosecond Laser Pulses", *Applied Physics Letters* **56**, 1638 (1990)

Y. Gefen, W.-H. Shih, R. B. Laibowitz and J. M. Viggiano, "Nonlinear Behavior near the Percolation Metal-Insulator Transition", *Physical Review Letters* **57**, 3097 (1986)

Y. Gefen, A. Aharony, and S. Alexander, "Anomalous Diffusion on Percolating Clusters", *Physical Review Letters* **50**, 77 (1982)

V.L. Ginsburg, *The Propogation of Electromagnetic Waves in Plasmas* (Pergamon, New York, 1970)

G. Gorodetsky, T.G. Kazyaka, R.L. Melcher, and R. Srinivasan, *Applied Physics Letters* **46**, 828 (1985).

J.-F. Gouyet, M. Rosso, and B. Sapoval in *Fractals and Disordered Systems* eds. A. Bunde and S. Havlin (Springer, Berlin, Heidelberg, 1991) p.229.

D. M. Grannan, J. C. Garland, and D. B. Tanner, "Critical Behavior of the Dielectric Constant of a Random Composite near the Percolation Threshold", *Physical Review Letters* **46**, 375 (1981)

H. Haferkamp, M. Marquering, H. Ebsen, "Alloying of Copper Surfaces with a Pulsed Nd:YAG Laser, *SPIE Proceedings* **2207**, 690 (1994)

R. F. Haglund Jr. and R. Kelly, *Matematisk-fysiske Meddelelser* **43**, 527 (1993)

D. W. Hahn, G. H. Pettit, and M. N. Ediger, "Optical Properties of Polyimide During ArF Excimer Laser Ablation", *Journal of Applied Physics* **76**, 1830 (1994)

B.I. Halperin, Shechao Feng, and P.N. Sen, "Differences between Lattice and Continuum Transport Exponents", *Physical Review Letters* **54**: 2391 (1985)

J. Heitz, E. Arenholz, D. Bäuerle, R. Sauerbrey, H. M. Phillips, "Femtosecond Excimer-Laser-Induced Structure Formation on Polymers", *Applied Physics A* **59**, 289 (1994)

P. M. Hui "Enhancement of Nonlinear Effects in percolating Nonlinear Resistor Networks", *Physical Review B* **41**, 1673 (1990)

P. M. Hui, "Crossover Electric Field in Percolating Perfect-Conductor--Nonlinear-Normal-Metal Composites", *Physical Review B* **49**, 15344 (1994)

K. Jain, *Excimer Laser Lithography*, (SPIE, Bellingham, 1990)

M. Jyumonji, K. Sugioka, H. Takai, and H. Tashiro, and K. Toyoda, "Mechanism of Silicon Implant-Deposition for Surface Modification of Stainless Steel 304 Using KrF-Excimer Laser", *Applied Physics A* **60**, 41 (1995)

S. W. Kenkel and J. P. Straley "Percolation Theory of Nonlinear Circuit Elements", *Physical Review Letters* **49**: 767 (1982)

L. B. Kiss and P. Svedlindh, "New Noise Exponents in Random Conductor-Superconductor and Conductor-Insulator Mixtures", *Physical Review Letters* **71**, 2817 (1993)

P. Klopotek, B. Burghardt, and W. Mückenheim, *J. Phys. E.* **20**, 1269 (1987).

F. Kokai, H. Saito, T. Fujioka, "X-Ray Photoelectron Spectroscopy Analysis of on

    Modified Polyimide Surfaces After Ablation with a KrF Excimer Laser", *Journal of*

    Applied Physics **66**, 3252 (1989)

G. Koren and J.T.C. Yeh, *Journal of Applied Physics* **56**, 2120 (1984)

W.L. Kruer, *The Physics of Laser Plasma Interaction* (Addison-Wesley, New York, 1988)

H. Kumagi, K. Toyoda, H. Machida, and S. Tanaka, *Applied Physics Letters.* **59**, 2974

    (1991)

S. Küper, J. Brannon, and K. Brannon, "Threshold Behavior in Polyimide Photoablation:

    Single-Shot Rate Measurements and Surface-Temperature Modeling", *Applied*

    Physics A. **56**, 43 (1993)

D. L. Kwong and D. M. Kim, "Pulsed Laser Heating of Silicon: The Coupling of Optical

    Absorption and Thermal Conduction During Irradiation", *Journal of Applied*

    Physics **54**, 366 (1983)

R. B. Laibowitz and Y. Gefen, "Dynamic Scaling near the Percolation Threshold in Thin

    Au Films", *Physical Review Letters* **53**, 380 (1984)

B. Lacour, H. Brunet, H. Besaucele, C. Gagnol, B. Vincent, *SPIE Proc. Vol. 2206*, 41

    (1994)

J.R. Lankard Sr. and G. Wolbold, "Excimer Laser Ablation in a Manufacturing Facility", *Applied Physics A* **54**, 355 (1992)

S. Lazare and V. Granier, *Laser Chem.* **10**, 25 (1989)

H.C. Lee, W.H. Siu, and K.W. Yu, "Percolation Effects in Two-Compnent Strongly Nonlinear Composites: Universal Scaling Behavior", *Physical Review B* **52**, 4217 (1995)

I. N. Levine, *Molecular Spectroscopy* (Wiley, New York, 1975) pp. 296-314

O. Levy and D. J. Bergman, "Critical Behavior of the Weakly Nonlinear Conductivity and Flicker Noise of Two-Component Composites", *Physical Review B* **50**, 3652 (1994)

A.M. Lyons, "Electrically Conductive Adhesives: Effect of Particle Composition and Size Distribution", *Polymer Engineering and Science* **31**, 445 (1991)

Excyclopedia of Polymer Science and Engineering, H. F. Marki, N. M. Bikales, C. G. Overberger, and G. Menges editors, Vol. 16, p. 585

L. J. Matienzo, J.A. Zimmerman, and F.D. Egitto, "Surface Modification of Fluoropolymers with Vacuum Ultraviolet Irradiation", *Journal of Vacuum Science Technology A* **12**, 2662 (1994)

P.W. Miloni, J. H. Eberly, *Lasers* (Wiley, New York, 1988) pp. 56-58.

Y. Meir, R. Blumenfeld, A. Aharony, and A. B. Harris, "Series Analysis of Randomly Diluted Nonlinear Resistor Networks", *Physical Review B* **34**, 3424 (1986)

N.F. Mott and R. W. Gurney, *Electronic Processes in Ionic Crystals* (Oxford University Press, London, 1940) pp. 168-173

M. Nakase, "Recent Progress in KrF Excimer Laser Lithography", *IEICE Trans. Electron.*, **E76-C**, 26 (1993)

H. Niino and A. Yabe, "Surface Modification and Metallization of Fluorocarbon Polymers by Excimer Laser Processing", *Applied Physics Letters* **63**, 3527 (1993)

M. Okoshi, M. Murahara, and K. Toyoda, "Photochemical Modification of Polytetrafluoroethylene in Oleopholic Property using an ArF Excimer Laser", *Journal of Materials Research* **7**, 1912 (1992)

G. Parakevopoulos, D. L. Singleton, R. S. Irwin, and R. S. Taylor, *Journal of Applied Physics* **70**, 1938 (1991).

M.J. Patterson, J.L. Margrave, R.H. Hauge, Z.Ball, and R. Sauerbrey, *Proceedings of the Electrochemical Society: Diamond Materials IV*, **95-5** (1995).

G. H. Pettit and R. Sauerbrey, *Applied Physics Letters* **58**, 793 (1991)

G.H. Pettit, M. N. Ediger, D. W. Hahn, B. E. Brinson, and R. Sauerbrey, "Transmission of Polyimide During Pulsed Ultraviolet Laser Irradiation", *Applied Physics A* **58**, 573 (1994)

H.R. Philip, H.S. Cole, Y.S. Liu, and T.A. Sitnik, "Absorption of Some Polymers in the Region 170 nm-250 nm" *Applied Physics Letters* **48**, 192 (1986)

H. M. Phillips, T. Feurer, D.L. Callahan, and R. Sauerbrey, "Excimer Laser Induced Electrical Conductivity in Polymers", *MRS Proc. No. 285*, 175 (1992)

H. M. Phillips, S. Wahl, R. Sauerbrey, "Submicron Electrically Conducting Wires Produced in Polyimide by Ultraviolet Laser Irradiation", *Applied Physics Letters* **62**, 2572 (1993)

P.P. Pronko, S.K. Dutta, D. Du, R.K. Singh, *Journal of Applied Physics* **78**, 6233 (1995)

A. Rose, "Space Charge Currents in Solids", *Physical Review* **97**, 1538 (1955)

M. Rothschild, A. R. Forte, M. W. Horn, R. R. Kunz, S. C. Palmateer, and J. H. C. Sedlacek, "193 nm Lithography", *IEEE J. of Selectred Topics in Quantum Electronics* **1**, 916 (1995).

T. Sameshima, *Solid State Phenomena* **37-38**, 269 (1994)

R. Sauerbrey, J. Fure, S.P. LeBlanc, B. van Wonterghem, U. Teubner, and F. P. Schäfer, *Physics of Plasmas* **1**, 1635 (1994).

R. Sauerbrey and Z. Ball, "Threshold condition and optimum output coupling for a pulsed laser",*Optics Communications* <u>95</u>, 153 (1993).

R. Sauerbrey and Z. Ball, "Surface Modification with Lasers" in *Laser Ablation and Desorption* ed. by R. F. Haglund and J. C. Miller (Academic Press) *forthcoming*.

A. K. Sarychev and F. Brouers, "New Scaling for ac Properties of Percolating Composite Materials", *Physical Review Letters* **73**, 2895 (1994)

M. Sasago, M. Endo, Y. Tabui, S. Kobayashi, T. Koizumi, T. Matsuo, K. Yamashita, N. Nomura, "Quarter Micron KrF Excimer Laser Lithography", *IEICE Trans. Electron.*, **E76-C**, 582 (1993)

A. K. Sen, *Physical Review Letters* **74**, 1693 (1995)

B.I. Shklovskii and A.L. Efros, *Electronic Properties of Doped Semiconductors.* (New York: Springer-Verlag, 1984)

A. Shiltz, "A Review of Planar Techniques for Multichip Modules", *IEEE Transactions on Components, Hybrids, and Manufacturing Technology* **15**, 236 (1992)

M. Schumann, R. Sauerbrey, M. C. Smayling, and B. J. Story, "Permanent Increase of
the Electrical Conductivity of Polymers Induced by Ultraviolet Laser Radiation",
Applied Physics Letters **58**, 428 (1991)

P. Simon, *Applied Physics B.* **48**, 253 (1989)

P. Singer, "New Interconnect Materials: Chasing the Promise of Faster Chips",
Semiconductor International, November, 1994, pp. 52-56

D. L. Singleton, G. Paraskevopoulos, and R.S. Taylor, *Applied Physics B* **50**, 227
(1990)

J. Sipe, J.F. Preston, H. M. van Driel, "Laser Induced Periodic Surface Structures I:
Theory",*Physical Review B* **27**, 1141 (1983)

R. W. Smith, *Physical Review* **97**, 1525 (1955)

R. W. Smith and A. Rose, *Phyiscal Review* **97**, 1531 (1955)

Y. Song, T. W. Noh, S.-I. Lee, and J. R. Gaines, "Experimental Study of Three
Dimensional ac Conductivity and Dielectric Constant of a Conductor Insulator
Composite near the Percolation Treshold", *Physical Review B* **33**, 904 (1986)

R. Srinivasan and B. Braren, "Ultraviolet Laser Ablation of Organic Polymers", *Chem.*
Rev. **89**, 1303 (1989)

J. P. Straley and S. W. Kenkel, "Percolation Theory for Nonlinear Conductors", *Physical Review B* **29**, 6299 (1984)

D. B. Tuckerman, A.H. Weisberg, "Laser Planarization", *Solid State Technology* **29**, 129 (1986)

T.N.C. Venkatesan, J. A. Golovchenko, J. M. Poate, P. Cowan, and G. K. Celler, "Dose Dependence in the Laser Annealing of Arsenic-Implanted Silicon", *Applied Physics Letters* **33**, 429 (1978)

C.T. Walters and A. H. Clauer, "Transient Reflectivity Behavior of Pure Aluminum at 10.6 μm, *Applied Physics Letters* **33**, 713 (1978)

T.F. Young, W.C. Kuo, I.M. Jiang, T.C. Chang, and C.Y. Chang, " The Novel Nonlinear dc Response of Ag Thin Films Deposited on Porous Silicon: a Fractal Model Explanation", *Physica A* **221**, 380 (1995).

Handbook of Chemistry and Physics 70th Edition, R. C. Weast, D. R. Lide, M. J. Astle, and W. H. Beyer editors (Boca Raton, Florida: CRC Press, 1989)

S. Wolf, "Silicon Processing for the VLSI Era, Volume Two: Process Integration, (Sunset Beach, CA, Lattice Press, 1990)

G.-X. Ye, J.-S. Wang, Y.-Q. Xu, Z.-K. Jiao, Q.-R. Zhang, "Evidence of Anomalous Hopping and Tunneling Effects on the Conductivity of a Fractal Pt-film System", *Physical Review B* **50**, 13163 (1994)

K. W. Yu, Y.C. Chu, and E. M. Y. Chan, "Effective Medium Theory for Two-Component Nonlinear Composites", *Physical Review B* **50**, 7984 (1994)

K. W. Yu and P.M. Hui, "Percolation Effects in Two-Component Nonlinear Composites: Crossover from Linear to Nonlinear Behavior", *Physical Review B* **50**, 13327 (1994)

R. Zallen, *The Physics of Amorphous Solids* (New York, John Wiley and Sons, 1983)

S. K. Zhang, K. Sugioka, J. Fan, K. Toyoda, and S.C. Zou, " Studies on Excimer Laser Doping of GaAs Using Sulphur Adsorbate as Dopant Source", *Applied Physics A* **58**, 191 (1994)

A. D. Zweig, V. Venugopalan, and T.F. Deutsch, *J.ournal of Applied Physics* **74**, 4181 (1993)

B. Zysset, J.G. Fujimoto, and T. F. Deutsch, *Applied Physics B* **48**, 139 (1989)